

**Copyright**  
**By**  
**Tanya Lüthi**  
**2005**

**Factors Affecting Bond and Friction Losses in Multi-Strand Post-Tensioning Tendons Including the Effect of Emulsifiable Oils**

by

**Tanya Lüthi, B.A.**

**Thesis**

Presented to the Faculty of the Graduate School of

The University of Texas at Austin

in Partial Fulfillment

of the Requirements

for the Degree of

**Master of Science in Engineering**

**The University of Texas at Austin**

**May 2005**

**Factors Affecting Bond and Friction Losses in Multi-Strand Post-Tensioning Tendons Including the Effect of Emulsifiable Oils**

**APPROVED BY  
SUPERVISING COMMITTEE:**

---

**John E. Breen, Supervisor**

---

**Sharon L. Wood**

*to my parents*

## **Acknowledgements**

My most sincere thanks belong to Dr. John Breen, for believing that someone with a bachelor's degree in politics could become a successful engineer and for guiding me through my years at the University of Texas. He has been a role model for me not only because of his expertise, but because of his ability to share that expertise with such unparalleled enthusiasm, humor, and kindness. It has been both an honor and a pleasure to work with him.

I would also like to thank my research partners, Juan José Icaza and Jeff Diephuis. Their hard work getting this project off the ground made my job an easy one. Special thanks to Jeff for his lasting friendship and support.

I thank my other friends at the Ferguson Structural Engineering Laboratory, particularly my undergraduate assistant, Kyle Steuck, and Mike Brown, without whom I probably never would have had working electronic equipment.

Special thanks to the staff at the Ferguson Lab for all their assistance: Mike Bell, Dennis Phillip, Blake Stasney, Hortensia Peoples, Barbara Howard, Regina Forward, and Michelle Santos.

I wish to thank Dr. Sharon Wood for her valuable input in the revision of this document.

I also wish to thank Dr. Hillary Hart; I had the good fortune to work for her as a teaching assistant when I first came to the University. I have greatly appreciated her advice and friendship over these past two years.

I gratefully acknowledge the Texas Department of Transportation and the Federal Highway Administration, whose funding made this work possible.

Finally, I would like to thank my parents, Ernst and Rosalie, and my brother, Eric, for their unwavering love and support.

**Tanya Lüthi**

**May 2005**

# **Factors Affecting Bond and Friction Losses in Multi-Strand Post-Tensioning Tendons Including the Effect of Emulsifiable Oils**

Tanya Lüthi, M.S.E.

The University of Texas at Austin, 2005

SUPERVISOR: John E. Breen

Emulsifiable oils are often used in post-tensioned construction to reduce friction losses and to provide temporary corrosion protection for tendons during the period of time between stressing and grouting. In the past, oils were flushed from the ducts with water prior to grouting. This practice often led to voids in the grout and created environmental problems related to the disposal of the flushing water.

This thesis addresses the effect of emulsifiable oils on corrosion, bond, and friction losses and is a summary of work done by multiple researchers at Pennsylvania State University and The University of Texas at Austin. Based on

preliminary corrosion and pullout tests at Pennsylvania State University, two oils were chosen for large-scale bond and friction tests at The University of Texas at Austin. Large-scale tests investigated the effects of duct type and oil on bond and friction losses.

Overall bond test results indicate that corrugated galvanized ducts provide better development than corrugated HDPE ducts. Rigid steel pipes performed poorly due to failure at the duct-concrete interface, indicating the need for shear studs or connectors to provide better anchorage for smooth steel deviator pipes. Even though such studs anchor the pipe effectively, the plane of failure changed to the inside of the pipe-grout interface, and bond results were substantially below those for corrugated ducts.

Bond test results also indicate that the strength of post-tensioned specimens with oiled tendons is similar to or better than the strength of specimens with unoiled tendons. Specimens with oiled tendons did experience large amounts of slip in comparison to specimens with unoiled tendons. However, because service load level cracking often will not occur in precast segmental structures and can easily be controlled with additional mild steel in cast-in-place post-tensioned applications, slip behavior is less important than strength.

Overall friction test results indicate that current design values for the coefficient of friction for steel pipes and galvanized ducts are accurate. However, the coefficient of friction for HDPE ducts measured from this test program was significantly less than the value recommended by AASTHO.



Friction tests also indicate that lubrication reduces the friction coefficient on the order of 15% if the tendon is stressed when the oil is fresh. Friction loss reductions were significant in rigid steel pipes and HDPE ducts but were relatively insignificant in galvanized steel ducts.

## Table of Contents

<b>CHAPTER 1 INTRODUCTION .....</b>	<b>1</b>
1.1 Background.....	1
1.2 Project Scope and Objectives .....	2
1.3 Thesis Scope .....	3
<b>CHAPTER 2 BACKGROUND INFORMATION AND LITERATURE REVIEW.....</b>	<b>5</b>
2.1 Bond in Post-tensioned Concrete.....	5
2.1.1 Previous Single-Strand Bond Research .....	6
2.1.2 Previous Multi-Strand Bond Research .....	8
2.1.3 Limitations of Previous Bond Research .....	13
2.2 Friction Losses in Post-tensioned Concrete.....	13
2.2.1 Previous Friction Research .....	16
2.2.2 Limitations of Previous Friction Research .....	18
<b>CHAPTER 3 PRELIMINARY CORROSION AND PULLOUT TESTS .....</b>	<b>19</b>
3.1 Introduction.....	19
3.2 Selection of Oils.....	19
3.3 Long-Term Corrosion Tests .....	23
3.3.1 Description of Specimens .....	23
3.3.2 Test Setup and Procedure.....	25
3.3.3 Test Results .....	26

3.4	Single-Strand Pullout Tests .....	27
3.4.1	Description of Specimens .....	28
3.4.2	Test Setup and Procedure.....	29
3.4.3	Test Results .....	31
3.5	Selection of Oils for Large-Scale Tests.....	33
 <b>CHAPTER 4 LARGE-SCALE EXPERIMENTAL PROGRAM .....</b>		<b>34</b>
4.1	Introduction.....	34
4.2	Common Variables.....	34
4.3	Materials .....	35
4.3.1	Oils .....	36
4.3.2	Prestressing Strand .....	36
4.3.3	Ducts .....	36
4.3.4	Mild Steel.....	37
4.3.5	Post-Tensioning Hardware.....	37
4.3.6	Concrete .....	38
4.3.7	Grout (Bond Tests Only) .....	38
4.3.8	Concrete Debonder (Friction Tests Only) .....	38
4.4	Bond Tests .....	38
4.4.1	Additional Variables.....	39
4.4.2	Description of Specimens .....	40
4.4.3	Description of Tests.....	44
4.5	Friction Tests .....	48
4.5.1	Additional Variables.....	48
4.5.2	Description of Specimens .....	49
4.5.3	Description of Tests.....	55

<b>CHAPTER 5 LARGE-SCALE TEST RESULTS .....</b>	<b>59</b>
5.1 Introduction.....	59
5.2 Bond Tests .....	59
5.2.1 Steel Pipe Specimens.....	63
5.2.2 Galvanized Duct Specimens .....	80
5.2.3 HDPE Duct Specimens.....	105
5.3 Friction Tests .....	130
5.3.1 Steel Pipe Specimens.....	131
5.3.2 Galvanized Duct Specimens .....	136
5.3.3 HDPE Duct Specimens.....	140
5.3.4 Duct Damage.....	145
<b>CHAPTER 6 COMPARISON OF BEHAVIOR AND EFFECT OF VARIABLES.....</b>	<b>151</b>
6.1 Introduction.....	151
6.2 Corrosion Tests .....	151
6.3 Bond Tests .....	153
6.3.1 Comparisons among Duct Types .....	154
6.3.2 Comparisons among Strand Surface Conditions.....	157
6.4 Friction Tests .....	169
6.4.1 Comparisons among Radii of Curvature and Duct Types .....	170
6.4.2 Comparisons among Strand Surface Conditions.....	173
6.4.3 Comparison of Results with Current Design Values and Previous Research.....	178
6.4.4 Duct Damage.....	180
6.4.5 Example of Practical Implications .....	181

<b>CHAPTER 7 SUMMARY AND CONCLUSIONS.....</b>	<b>185</b>
7.1 Summary of Project Objectives and Test Program.....	185
7.2 Corrosion Test Conclusions.....	186
7.3 Bond Test Conclusions.....	187
7.4 Friction Test Conclusions.....	189
7.5 Recommendations.....	191
7.6 Suggestions for Future Research .....	192
<b>APPENDIX A.....</b>	<b>193</b>
<b>REFERENCES .....</b>	<b>198</b>
<b>VITA.....</b>	<b>203</b>

## List of Tables

Table 2-1 Friction and Wobble Coefficients (ACI 318-02).....	15
Table 2-2 Friction and Wobble Coefficients (AASHTO 1999, 2002).....	15
Table 2-3 Friction and Wobble Coefficients (PTI 1990).....	16
Table 2-4 Reductions in Friction Coefficient, Tran and Davis (Davis et al. 1993) .....	18
Table 3-1 Oil List and Product Description (Descriptions Provided by Manufacturers).....	20
Table 3-2 Summary of Corrosion Specimens .....	25
Table 3-3 Rating System for Corrosion Tests .....	26
Table 3-4 Summary of Pullout Specimens.....	28
Table 5-1 Bond Specimen Summary .....	61
Table 6-1 Rating System for Corrosion Tests .....	152
Table 6-2 Corrosion Test Results, Trukut NC205 and NoxRust 703D .....	153
Table 6-3 Comparison of Friction Coefficients to Recommended Values .....	179
Table 6-4 Reduction in Friction Coefficients Compared to Previous Research .	180
Table A-1 Bond Test Results .....	193
Table A-2 Friction Test Results – Average Total Load Loss, Kip .....	195
Table A-3 Friction Test Results – Average Percent Load Loss (Curvature Friction Only).....	196
Table A-4 Friction Test Results – Average Friction Coefficient .....	197

## List of Figures

Figure 2-1 Hoyer Effect (Diephuis 2004) .....	6
Figure 2-2 Wobble Friction Losses (Collins and Mitchell 1997).....	15
Figure 3-1 Corrosion Test Specimens.....	24
Figure 3-2 Final Corrosion Test Results .....	27
Figure 3-3 Pullout Test Specimens (Salcedo 2003).....	29
Figure 3-4 Pullout Test Frame (Salcedo 2003) .....	30
Figure 3-5 Pullout Test Frame Close-Up (Salcedo 2003).....	30
Figure 3-6 Mechanical Restraint Device Close-Up (Salcedo 2003) .....	30
Figure 3-7 Pullout Test Results, All Oils .....	32
Figure 3-8 Pullout Test Results, Selected Oils with Corrosion Ratings $\square$ 4 .....	32
Figure 4-1 Ducts (Icaza 2004).....	35
Figure 4-2 Post-Tensioning Hardware (Diephuis 2004).....	37
Figure 4-3 Bond Specimen Elevation and Cross-Section .....	40
Figure 4-4 Bond Specimen Reinforcement Layout .....	41
Figure 4-5 Assembled Specimen Cage, Duct, and Formwork .....	42
Figure 4-6 Specimen Ready for Installation of Tendon.....	43
Figure 4-7 Oil Application .....	43
Figure 4-8 Sealing of Duct Ends .....	44
Figure 4-9 Complete Prestressing Setup .....	44
Figure 4-10 Bond Specimen Ready for Testing .....	45
Figure 4-11 Live End Linear Potentiometer Placement.....	46
Figure 4-12 Dead End Linear Potentiometer Placement .....	46
Figure 4-13 Placement of Duct and Casting of Removable Part (Icaza 2004) .....	50
Figure 4-14 Permanent Reaction Beam Cross-Section (Icaza 2004) .....	51
Figure 4-15 Plan View of Beams (Icaza 2004) .....	52
Figure 4-16 Complete Beam Cross-Section Schematic (Icaza 2004).....	53
Figure 4-17 Complete Beam Cross-Section.....	54
Figure 4-18 Friction Test Setup (Icaza 2004) .....	55
Figure 4-19 Friction Test Live End Detail .....	56
Figure 4-20 Friction Test Dead End Detail .....	57
Figure 5-1 Live End Load-Displacement and Dead End Load-Slip Behavior for Specimen 0-SP-7.5°-1 .....	64
Figure 5-2 Dead End Load-Slip Response for Specimen 0-SP-7.5°-1, Amplified Scale .....	64
Figure 5-3 Live End of Specimen 0-SP-7.5°-1 after Testing .....	65
Figure 5-4 Live End Load-Displacement and Dead End Load-Slip Behavior for Specimen 0-SP-7.5°-2 .....	66

Figure 5-5 Dead End Load Slip Response for Specimen 0-SP-7.5°-2, Amplified Scale .....	66
Figure 5-6 Live End of Specimen 0-SP-7.5°-2 after Testing .....	67
Figure 5-7 Live End Load-Displacement and Dead End Load-Slip Response for Specimen 0-SP-7.5°-3 .....	68
Figure 5-8 Dead End Load-Slip Response for Specimen 0-SP-7.5°-3, Amplified Scale .....	69
Figure 5-9 Live End Load-Displacement and Dead End Load-Slip Response for Specimen 0-SP-7.5°-4 .....	70
Figure 5-10 Dead End Load-Slip Response for Specimen 0-SP-7.5°-4, Amplified Scale .....	70
Figure 5-11 Live End Load-Displacement and Dead End Load-Slip Response for Specimen 1-SP-7.5°-1 .....	72
Figure 5-12 Dead End Load-Slip Response for Specimen 1-SP-7.5°-1, Amplified Scale .....	72
Figure 5-13 Live End of Specimen 1-SP-7.5°-1 after Testing .....	73
Figure 5-14 Live End Load-Displacement and Dead End Load-Slip Response for Specimen 1-SP-7.5°-2 .....	74
Figure 5-15 Dead End Load-Slip Response for Specimen 1-SP-7.5°-2, Amplified Scale .....	75
Figure 5-16 Live End of Specimen 1-SP-7.5°-2 after Testing .....	75
Figure 5-17 Live End Load-Displacement and Dead End Load-Slip Response for Specimen 2-SP-7.5°-1 .....	76
Figure 5-18 Dead End Load-Slip Response for Specimen 2-SP-7.5°-1, Amplified Scale .....	77
Figure 5-19 Live End of Specimen 2-SP-7.5°-1 after Testing .....	77
Figure 5-20 Live End Load-Displacement and Dead End Load-Slip Response for 2-SP-7.5°-2.....	78
Figure 5-21 Dead End Load-Slip Response for Specimen 2-SP-7.5°-2, Amplified Scale .....	79
Figure 5-22 Live End of Specimen 2-SP-7.5°-2 after Testing .....	79
Figure 5-23 Live End Load-Displacement and Dead End Load-Slip Response for Specimen 0-GD-7.5°-1 .....	81
Figure 5-24 Dead End Load-Slip Response for Specimen 0-GD-7.5°-1, Amplified Scale .....	82
Figure 5-25 Profile of Specimen 0-GD-7.5°-1 after Testing.....	82
Figure 5-26 Live End Load-Displacement and Dead End Load-Slip Response for Specimen 0-GD-7.5°-2 .....	84
Figure 5-27 Dead End Load-Slip Response for Specimen 0-GD-7.5°-2, Amplified Scale .....	84



Figure 5-28 Photo of Specimen 0-GD-7.5°-2 after Testing .....	85
Figure 5-29 Live End Load-Displacement and Dead End Load-Slip Response for Specimen 0-GD-7.5°-3 .....	86
Figure 5-30 Dead End Load-Slip Response for Specimen 0-GD-7.5°-3, Amplified Scale .....	87
Figure 5-31 Profile of Specimen 0-GD-7.5°-3 after Testing .....	87
Figure 5-32 Live End Load-Displacement and Dead End Load-Slip Response for Specimen 1-GD-7.5°-1 .....	89
Figure 5-33 Dead End Load-Slip Response for Specimen 1-GD-7.5°-1, Amplified Scale .....	89
Figure 5-34 Profile of Specimen 1-GD-7.5°-1 after Testing .....	90
Figure 5-35 Live End Load-Displacement and Dead End Load-Slip Response for Specimen 1-GD-7.5°-2 .....	91
Figure 5-36 Dead End Load-Slip Response for Specimen 1-GD-7.5°-2, Amplified Scale .....	92
Figure 5-37 Profile of Specimen 1-GD-7.5°-2 after Testing .....	92
Figure 5-38 Live End Load-Displacement and Dead End Load-Slip Response for Specimen 2-GD-7.5°-1 .....	93
Figure 5-39 Dead End Load-Slip Response for Specimen 2-GD-7.5°-1, Amplified Scale .....	94
Figure 5-40 Profile of Specimen 2-GD-7.5°-1 after Testing .....	94
Figure 5-41 Live End and Top of Specimen 2-GD-7.5°-1 after Testing .....	95
Figure 5-42 Live End Load-Displacement and Dead End Load-Slip Response for Specimen 2-GD-7.5°-2 .....	96
Figure 5-43 Dead End Load-Slip Response for Specimen 2-GD-7.5°-2, Amplified Scale .....	96
Figure 5-44 Live End Load-Displacement and Dead End Load-Slip Response for Specimen 2-GD-7.5°-3 .....	97
Figure 5-45 Dead End Load-Slip Response for Specimen 2-GD-7.5°-3, Amplified Scale .....	98
Figure 5-46 Photo of Specimen 2-GD-7.5°-3 after Testing .....	98
Figure 5-47 Live End Load-Displacement and Dead End Load-Slip Response for Specimen 2-GD-7.5°-4 .....	99
Figure 5-48 Dead End Load-Slip Response for Specimen 2-GD-7.5°-4, Amplified Scale .....	100
Figure 5-49 Profile of Specimen 2-GD-7.5°-4 after Testing .....	100
Figure 5-50 Live End Load-Displacement and Dead End Load-Slip Response for Specimen 1*-GD-7.5°-1 .....	102
Figure 5-51 Dead End Load-Slip Response for Specimen 1*-GD-7.5°-1, Amplified Scale .....	102

Figure 5-52 Profile of Specimen 1*-GD-7.5°-1 after Testing.....	103
Figure 5-53 Live End Load-Displacement and Dead End Load-Slip Response for Specimen 1*-GD-7.5°-2 .....	104
Figure 5-54 Dead End Load-Slip Response for Specimen 1*-GD-7.5°-2, Amplified Scale .....	104
Figure 5-55 Live End Load-Displacement and Dead End Load-Slip Response for Specimen 0-HD-7.5°-1 .....	106
Figure 5-56 Dead End Load-Slip Response for Specimen 0-HD-7.5°-1, Amplified Scale .....	107
Figure 5-57 Live End Load-Displacement and Dead End Load-Slip Response for Specimen 0-HD-7.5°-2 .....	108
Figure 5-58 Dead End Load-Slip Response for Specimen 0-HD-7.5°-2, Amplified Scale .....	109
Figure 5-59 Dead End of Specimen 0-HD-7.5°-2 after Testing .....	109
Figure 5-60 Live End Load-Displacement and Dead End Load-Slip Response for Specimen 0-HD-7.5°-3 .....	111
Figure 5-61 Dead End Load-Slip Response for Specimen 0-HD-7.5°-3, Amplified Scale .....	111
Figure 5-62 Profile of Specimen 0-HD-7.5°-3 after Testing.....	112
Figure 5-63 Profile 2 of Specimen 0-HD-7.5°-3 after Testing.....	112
Figure 5-64 Live End Load-Displacement and Dead End Load-Slip Response for Specimen 1-HD-7.5°-1 .....	114
Figure 5-65 Dead End Load-Slip Response for Specimen 1-HD-7.5°-1, Amplified Scale .....	114
Figure 5-66 Profile of Specimen 1-HD-7.5°-1 after Testing.....	115
Figure 5-67 Live End Load-Displacement and Dead End Load-Slip Response for Specimen 1-HD-7.5°-2 .....	116
Figure 5-68 Dead End Load-Slip Response for Specimen 1-HD-7.5°-2, Amplified Scale .....	117
Figure 5-69 Photo of Specimen 1-HD-7.5°-2 after Testing .....	117
Figure 5-70 Live End Load-Displacement and Dead End Load-Slip Response for Specimen 2-HD-7.5°-1 .....	119
Figure 5-71 Dead End Load-Slip Response for Specimen 2-HD-7.5°-1, Amplified Scale .....	119
Figure 5-72 Profile of Specimen 2-HD-7.5°-1 after Testing.....	120
Figure 5-73 Live End Load-Displacement and Dead End Load-Slip Response for Specimen 2-HD-7.5°-2 .....	121
Figure 5-74 Dead End Load-Slip Response for Specimen 2-HD-7.5°-2, Amplified Scale .....	122
Figure 5-75 Photo of Specimen 2-HD-7.5°-2 after Testing .....	122

Figure 5-76 Live End Load-Displacement and Dead End Load-Slip Response for Specimen 2-HD-7.5°-3 .....	124
Figure 5-77 Dead End Load-Slip Response for Specimen 2-HD-7.5°-3, Amplified Scale .....	124
Figure 5-78 Photo of Specimen 2-HD-7.5°-3 after Testing .....	125
Figure 5-79 Live End Load-Displacement and Dead End Load-Slip Response for Specimen 1*-HD-7.5°-1 .....	126
Figure 5-80 Dead End Load-Slip Response for Specimen 1*-HD-7.5°-1, Amplified Scale .....	127
Figure 5-81 Photo of Specimen 1*-HD-7.5°-1 After Testing .....	127
Figure 5-82 Live End Load-Displacement and Dead End Load-Slip Response for Specimen 1*-HD-7.5°-2 .....	128
Figure 5-83 Dead End Load-Slip Response for Specimen 1*-HD-7.5°-2, Amplified Scale .....	129
Figure 5-84 Profile of Specimen 1*-HD-7.5°-2 after Testing .....	129
Figure 5-85 Friction Losses for Specimen 0-SP-90° .....	132
Figure 5-86 Friction Losses for Specimen 1-SP-90° .....	133
Figure 5-87 Friction Losses for Specimen 2-SP-90° .....	134
Figure 5-88 Friction Losses for Specimen 1-SP-30° .....	135
Figure 5-89 Friction Losses for Specimen 2-SP-30° .....	136
Figure 5-90 Friction Losses for Specimen 1-GD-90° .....	137
Figure 5-91 Friction Losses for Specimen 2-GD-90° .....	138
Figure 5-92 Friction Losses for Specimen 1-GD-30° .....	139
Figure 5-93 Friction Losses for Specimen 2-GD-30° .....	140
Figure 5-94 Friction Losses for Specimen 1-HD-90° .....	141
Figure 5-95 Sharp Kink in Strand after Friction Testing .....	142
Figure 5-96 Friction Losses for Specimen 2-HD-90° .....	143
Figure 5-97 Friction Losses for Specimen 1-HD-30° .....	144
Figure 5-98 Friction Losses for Specimen 2-HD-30° .....	145
Figure 5-99 Duct from Specimen 1-GD-90° after Testing .....	146
Figure 5-100 Duct from Specimen 2-GD-90° after Testing .....	147
Figure 5-101 Duct from Specimen 1-GD-30° after Testing .....	147
Figure 5-102 Duct from Specimen 2-GD-30° after Testing .....	148
Figure 5-103 Duct from Specimen 1-HD-90° after Testing .....	148
Figure 5-104 Duct from Specimen 2-HD-90° after Testing .....	149
Figure 5-105 Duct from Specimen 1-HD-30° after Testing .....	149
Figure 5-106 Duct from Specimen 2-HD-30° after Testing .....	150
Figure 6-1 Live End Load-Displacement Behavior, Unoiled Tendons .....	155
Figure 6-2 Live End Load-Displacement Behavior, Tendons Oiled with NC205 .....	155

Figure 6-3 Live End Load-Displacement Behavior, Tendons Oiled with 703D.	156
Figure 6-4 Live End Load-Displacement Behavior, Galvanized Duct.....	159
Figure 6-5 Live End Load-Displacement Behavior, HDPE Duct .....	159
Figure 6-6 Dead End Load-Slip Behavior, Galvanized Duct.....	160
Figure 6-7 Dead End Load-Slip Behavior, HDPE Duct .....	161
Figure 6-8 Average Failure Loads, Galvanized Ducts.....	162
Figure 6-9 Average Failure Loads, HDPE Ducts .....	163
Figure 6-10 Live End Load-Displacement Behavior, Galvanized Duct, Tendon Oiled with NC205 .....	166
Figure 6-11 Live End Load-Displacement Behavior, HDPE Duct, Tendon Oiled with NC205.....	167
Figure 6-12 Dead End Load-Slip Behavior, Galvanized Duct, Tendon Oiled with NC205 .....	168
Figure 6-13 Dead End Load-Slip Behavior, HDPE Duct, Tendon Oiled with NC205 .....	169
Figure 6-14 Average Load Loss, Unoiled Tendons.....	172
Figure 6-15 Average Friction Coefficients, Unoiled Tendons.....	172
Figure 6-16 Reduction in Friction Coefficient, Freshly Oiled Tendons (Average Reduction for Both Oils) .....	174
Figure 6-17 Reduction in Friction Coefficient, Freshly Oiled Tendons .....	175
Figure 6-18 Reduction in Friction Coefficient, One Day after Oiling.....	176
Figure 6-19 Reduction in Friction Coefficient, Freshly Oiled Tendons versus One Day after Oiling .....	177
Figure 6-20 Relationship among Total Angle Change, Coefficient of Friction, and Percent Load Loss .....	183
Figure 6-21 Example of Friction Loss Calculations (Collins and Mitchell 1997) .....	184

# CHAPTER 1

## Introduction

### 1.1 BACKGROUND

Engineered structures must be not only safe and serviceable but also durable. Inadequate attention to durability either in the design or construction phases of a project can result in costly repairs, or in some cases, failure. The failures of two post-tensioned concrete bridges, the Bickton Meadows footbridge in England in 1967 and the Ynys-Y-Gwas Bridge in Wales in 1985, led to a ban on the use of post-tensioned concrete bridges in the UK from 1992 to 1996. Although the vast majority of post-tensioned bridges in the US have performed satisfactorily, corrosion problems in a number of bridges in Florida have again raised concerns about durability in these types of structures. An external tendon in the Niles Channel Bridge in the Florida Keys failed in 1999 due to corrosion at an expansion joint. In 2000, one fully failed external tendon and one partially failed external tendon (5 of 19 strands) were discovered in the Mid-Bay Bridge, located near Pensacola in the panhandle. Nine additional tendons in that bridge were found to have corrosion damage and were replaced by the Florida Department of Transportation. Corroded tendons were also discovered in 2000 in the segmental piers of the Sunshine Skyway, which spans Tampa Bay (ASBI 2000).

These problems highlighted the importance of controlling corrosion in post-tensioned concrete, including the use of new materials and construction methods. New materials have come on the market and are being used in various parts of post-tensioning systems, including strand, anchorages, ducts, duct couplers, and grout. New methods include improved grouting procedures,

grouting sooner after stressing, and applying emulsifiable oils to tendons as temporary corrosion protection during the period between stressing and grouting. However, not all of these materials and methods have been adequately evaluated for their effectiveness, and in some cases they have caused additional problems. For example, tendons coated with emulsifiable oils were often flushed with water before grouting to remove the oil. Disposal of the oil-contaminated flushing water posed environmental problems. In addition, compressed air was often used to remove water from the post-tensioning ducts, and it has been assumed that the advancing grout flow would push out any remaining pockets of water. However, inspections of the grouted tendons often revealed significant voids and corrosion damage, presumably due to the water not being completely removed from the duct.

## **1.2 PROJECT SCOPE AND OBJECTIVES**

The University of Texas at Austin Center for Transportation Research Project 0-4562 began in 2002 in response to these concerns about usage of new technologies and materials for improved durability in post-tensioned concrete structures. The project, entitled “Effect of Emulsifiable Oils Used as Temporary Corrosion Protection in Grouted Post-Tensioned Tendons, and Investigation of Alternate Corrosion-Resistant Post-Tensioning Systems,” was funded by the Texas Department of Transportation (TxDOT) and the Federal Highway Administration (FHWA). Research on the project was conducted at Pennsylvania State University and the Phil M. Ferguson Structural Engineering Laboratory at the University of Texas at Austin.

The project was divided into two distinct phases. The first phase was focused on the effects of emulsifiable oils on bond and friction losses. The ongoing second phase, which is not discussed in this report, is focused on

evaluating a variety of new materials that could improve durability in post-tensioned concrete systems.

As described previously, emulsifiable oils are often used as temporary corrosion protection for post-tensioning tendons. This practice originated because of contractors' desire to delay grouting operations until a significant amount of grouting could be performed at once. The oils were proposed as a way to prevent the onset of corrosion during intentional delays between tendon stressing and grouting, and would also provide some margin of safety against corrosion damage during unexpected construction delays. Since flushing the oiled tendons with water prior to grouting has proven problematic, this practice will likely not continue. Thus if oils are left on the tendons, the effects those oils have on the behavior of post-tensioned systems must be determined.

The objectives of this phase of Project 0-4562 were therefore as follows:

1. Identify emulsifiable oils or other suitable products for providing temporary corrosion protection.
2. Assess the performance of the corrosion-inhibiting products.
3. Investigate how the products affect friction loss during post-tensioning.
4. Determine the impact of corrosion-inhibiting products on bond strength and behavior of multi-strand tendons.
5. Develop recommendations for the use of temporary corrosion protection products and any other related findings.

### **1.3 THESIS SCOPE**

This report addresses only the first phase of Project 0-4562. Preliminary corrosion and single-strand bond tests were performed under the supervision of

Dr. Andrea Schokker at Pennsylvania State University by Salcedo (2003). Large-scale bond tests were performed at the University of Texas at Austin by Diephuis (2004) and the author. Friction tests were performed at the University of Texas at Austin by Icaza (2004). In order to provide a complete summary of all work done in relation to this phase of Project 0-4562, this report contains all relevant results and draws heavily on the reports written by Salcedo (2003), Diephuis (2004), and Icaza (2004).

The report is divided into seven chapters. Chapter 2 provides background information and a literature review of previous relevant research on bond and friction losses. Chapter 3 describes the work done by Salcedo (2003) at Pennsylvania State University, which included corrosion tests and single-strand pullout tests. The results of these tests served as the basis for choosing emulsifiable oils for use in large-scale tests at the University of Texas at Austin. Chapter 4 describes the large-scale experimental program, giving details about test specimens, setups and procedures. Chapter 5 contains the results of the large-scale bond and friction tests. Chapter 6 uses those results to make behavior comparisons, comment on the effects of the variables studied, and make design and specification recommendations. Chapter 7 provides final conclusions and recommendations for the use of temporary corrosion protection in post-tensioned systems.



## **CHAPTER 2**

### **Background Information and Literature Review**

#### **2.1 BOND IN POST-TENSIONED CONCRETE**

This section summarizes a majority of the background information on bond provided in Diephuis (2004).

Bond stress between prestressing strand and concrete or grout is achieved through three primary mechanisms: adhesion, friction, and mechanical restraint. Adhesion, or microscopic interlock, exists only until relative slip occurs between the steel and concrete or grout, at which point the physical bonds are broken (Laldji and Young, 1988). Friction is often called the Hoyer effect and is illustrated in Figure 2-1. When prestressing strand is placed in tension, its diameter decreases. After the concrete or grout has cured and the strand is released, the strand attempts to return to its original diameter at the ends of the member. This action causes a clamping force to be exerted on the strand near the ends, which results in frictional resistance to slip (Collins and Mitchell 1997). Mechanical restraint is due to the irregular surface of the strand, which bears against the helical impressions in the concrete or grout as the strand moves. This action is similar to, but less effective than, mechanical restraint provided by lugs on conventional reinforcing bars (Janney, 1954; Hanson and Kaar, 1959).

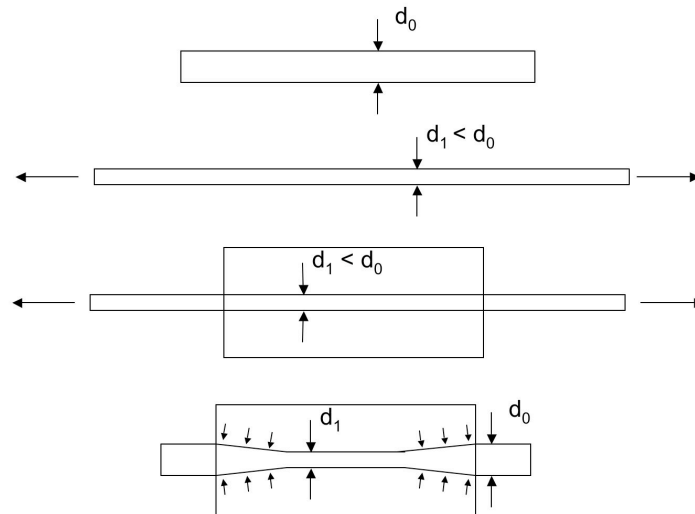


**Figure 2-1 Hoyer Effect (Diephuis 2004)**

Bond stress is required to develop both transfer bond and flexural bond. Transfer bond, which is most applicable to pretensioned members, transfers the prestressing force from the strand or tendon to the concrete upon release. Because slip occurs in the transfer zone due to strain differentials between the steel and concrete (Janney 1954), adhesion does not play a role in developing transfer bond. Friction and mechanical restraint therefore provide transfer bond in prestressed members. Flexural bond is present in any reinforced concrete member subject to bending stresses. Because the steel is loaded in increasing tension, the strand diameter decreases in accordance with Poisson's ratio, destroying adhesion and reducing friction. Flexural bond is therefore due primarily to mechanical restraint at the location of flexural cracks.

### **2.1.1 Previous Single-Strand Bond Research**

Previous research has investigated the effects of the following four variables on bond between a single prestressing strand and concrete or grout:

- strand surface condition
- concrete or grout strength
- confinement
- loading rate

#### ***2.1.1.1 Strand Surface Condition***

Studies by Janney (1954) and Kaar (1959) found that bond performance of rusted strand is up to 30% better than that of clean strand. Barnes et al. (2003) reached similar findings but could not recommend using reduced transfer lengths for rusted strand due to high variability in the data.

Studies using oiled strand by Anderson and Anderson (1976) and Kittleman (1992) reported conflicting results. Anderson and Anderson's study found no reduction in bond for strands coated with oil, while Kittleman found bond performance reduced up to 90% for oiled strand. The latter study also found that flushing the oil from the strand prior to grouting improved bond performance, but that bond for flushed strand was still reduced relative to unoiled strand.

#### ***2.1.1.2 Concrete or Grout Strength***

In spite of three studies which concluded that concrete strength has minimal effect on bond, most research has found a correlation between concrete compressive strength and bond strength. Work by Kaar et al. (1963), later confirmed by Janney (1954) and Salmons and McCrate (1977), included tests of prestress transfer lengths for strands with a nominal diameter of up to 1/2 in. and concrete compressive strengths from 1600 psi to 5000 psi. These researchers all found that concrete strength had no significant effect on bond. However, studies by Stocker and Sozen (1970) found a 10% increase in bond strength for every 1000 psi increase in concrete compressive strength from 2400 psi to 5000 psi. Similarly, Barnes et al. (2003) found that transfer length is proportional to the

ratio of strand stress to the square root of concrete compressive strength at transfer.

### ***2.1.1.3 Confinement***

Researchers generally acknowledge that confinement of concrete or grout affects bond strength, but little quantitative data are available on the effects of confinement.

### ***2.1.1.4 Loading Rate***

Various studies have reached conflicting conclusions about the effect of loading rate on transfer bond. Kaar et al. (1963) compared bond strength for strand released by flame cutting and slow release. This study found 20% and 30% reductions in bond strength for flame-cut 1/2 in. and 0.6 in. strands, respectively. Similar results were reported by Russell and Burns (1997). In contrast, Vos and Reinhardt (1982) found no correlation between loading rate and pullout behavior. Barnes et al. (2003) also found no correlation between prestress release method and bond strength for clean strand and concrete compressive strengths over 7000 psi.

## **2.1.2 Previous Multi-Strand Bond Research**

Previous research on the bond performance of multi-strand post-tensioning tendons falls into five categories:

- transfer length
- effect of tendon size and position in duct
- effect of tendon to duct cross-sectional area ratio
- effect of angle change in steel pipe deviators
- effectiveness of corrugated HDPE ducts

Because bond stresses for multi-strand tendons can be calculated in multiple ways, all test results reported in this section have been converted using the following procedure, shown in Equations 2.1-2.4. An equivalent tendon circumference,  $C_e$ , is calculated based on the tendon area and then multiplied by the bonded length to yield a bonded area. Bond stress is then simply total force divided by bonded area.

$$r_e = \sqrt{\frac{A_{ps}}{\pi}} \quad \text{Equation 2.1}$$

$$C_e = 2 \cdot \pi \cdot r_e \quad \text{Equation 2.2}$$

$$A_b = C_e \cdot L \quad \text{Equation 2.3}$$

$$u = \frac{P}{A_b} \quad \text{Equation 2.4}$$

where:

$r_e$  = equivalent tendon radius

$A_{ps}$  = nominal tendon cross-sectional steel area

$C_e$  = equivalent tendon circumference

$A_b$  = equivalent bonded area

$L$  = bonded length

$u$  = bond stress

$P$  = axial load applied to tendon

For calculations involving bond stress at the grout-duct or duct-concrete interface, the equivalent tendon circumference is replaced by the inner or outer duct diameter, respectively.

### **2.1.2.1 Transfer Length**

Schupack and Johnston (1974) tested a 54-strand tendon with 1/2-in. strands to determine its bond transfer length. The tendon was stressed and grouted

in a curved beam with a smooth-walled, flexible duct 5.5 in. in diameter. Grout strength was approximately 3500 psi. By measuring concrete strains before and after release, the approximate transfer length of the tendon was determined to be 10 ft. This length corresponds to a bond stress of approximately 1500 psi.

#### ***2.1.2.2 Effect of Tendon Size and Position in Duct***

Trost et al. (1978, 1980) performed monotonic pullout tests with four tendon/duct configurations to investigate the effect of tendon size and position in the duct on bond performance. These results were summarized by Radloff (1990). For each configuration, tendons consisted of 0.6-in. strands and were grouted in straight, corrugated steel ducts.

The first two configurations both had four strands and an inner duct diameter of 1.77 in. Four tests were performed with the tendon in the center of the duct, and another four tests were performed with the tendon against the wall of the duct. Average grout strength for each configuration was in the range of 8000-8500 psi. For the first configuration, with the tendon in the center of the duct, average bond stress at 0.1 mm dead end slip was 1200 psi. For the second configuration, with the tendon against the wall of the duct, average bond stress at 0.1 mm dead end slip was 800 psi, or 34% lower than the value for the first series.

The third configuration had three strands and an inner duct diameter of 1.57 in. Only one test was performed, with the tendon in the center of the duct. Grout strength was approximately 7400 psi. The bond stress at 0.1 mm dead end slip was 1300 psi, 5% higher than the value for the first configuration with four strands in the center of the duct.

The final configuration had 19 strands and an inner duct diameter of 3.54 in. Three tests were performed, all with the tendon in the center of the duct. Average grout strength was approximately 5200 psi. The average bond stress at

0.1 mm dead end slip was 1000 psi, 15% lower than the value for the first configuration with four strands in the center of the duct. For these tests, bursting cracks caused sudden failure of the specimen at low levels of dead end slip, and stable pullout was not achieved.

### ***2.1.2.3 Effect of Tendon to Duct Cross-Sectional Area Ratio***

Pullout tests by Braverman (1985) used 1-, 3-, and 5-strand tendons with 3/8-in. diameter strands to determine the effect of tendon to duct cross-sectional area ratio on bond performance. The three tendon sizes corresponded to area ratios of 5%, 14%, and 24%, respectively. In all tests, tendons were grouted in the center of straight, smooth-walled steel ducts and had a bonded length of 12 in. The specimens with 3-strand tendons and an area ratio of 14% failed at the highest bond stress of 1100 psi. Failure of specimens with 5-strand tendons and an area ratio of 24% occurred at the grout-duct interface at significantly lower loads. The average bond stress at this interface was 550 psi.

Similar tests were performed by Osborne (1986), who used 1-, 3-, 5-, 7-, and 11-strand tendons with 3/8-in. diameter strands corresponding to area ratios from 3% to 30%. In all tests, tendons were grouted in the center of straight, smooth-walled steel ducts and had a bonded length of 24 in. The specimens with 5-strand tendons and an area ratio of 14% failed at the highest bond stress of 1600 psi. Failure of specimens with 7- and 11-strand tendons, corresponding to area ratios of 19% and 30% respectively, occurred at the grout-duct or duct-concrete interfaces at significantly lower loads. Disregarding one outlier data point for a 7-strand test, the average bond stress at the duct-grout interface for these tests was 240 psi.

#### ***2.1.2.4 Effect of Angle Change in Steel Pipe Deviators***

Radloff (1990) conducted tests intended to mimic the behavior of external post-tensioning tendons in steel pipe deviators. Tests were performed with 7- or 12-strand tendons with 1/2-in. diameter strands grouted against the wall of nominal 3-in. diameter smooth steel pipes. A total of six tests were performed: one for each tendon size in straight pipes, pipes with a 6 degree angle change, and pipes with a 12 degree angle change.

In place of standard pullout tests, Radloff used an alternative procedure. Tendons were stressed to 50% of their guaranteed ultimate tensile strength and grouted. Three days later, dead end slip was monitored as the tendon was slowly released.

Failure occurred in the straight specimens at the grout-duct interface, while failure in the curved specimens occurred at the tendon-grout interface. Average bond stresses at the grout-duct interface for the straight specimens with 7- and 12-strand tendons were 160 psi and 280 psi, respectively. For the specimens with a 6 degree angle change, average bond stresses at the tendon-grout interface for 7- and 12-strand tendons were 640 psi and 570 psi, respectively. For the specimens with a 12 degree angle change, average bond stresses at the tendon-grout interface for 7- and 12-strand tendons were 350 psi and 390 psi, respectively.

In addition to these results, Radloff reported the results of a single test by Losinger (1977) where failure at the grout-duct interface of a smooth steel pipe was also observed. A 52-strand rock anchor with 0.6-in. strands and a bonded length of 32.8 ft was tested in a grouted 10.7-in. diameter pipe. Failure occurred at the grout-duct interface at an average bond stress of 150 psi at that interface.



#### ***2.1.2.5 Effectiveness of Corrugated HDPE Ducts***

A pullout test performed by VSL International determined that corrugated HDPE ducts could successfully transfer forces from a tendon to a concrete member and that bond stress at the duct-grout interface does not control behavior for this type of duct (VSL International). The test was conducted with a 16-strand tendon consisting of 1/2-in. diameter strands grouted inside a polyethylene duct 3.15 in. in diameter. Failure occurred at the tendon-grout interface at an average bond stress of 890 psi at that interface.

#### **2.1.3 Limitations of Previous Bond Research**

Two important limitations of the research summarized here should be noted. First, although tests have been performed with both corrugated steel and HDPE ducts, no direct comparison has been made between the bond behavior of elements with these two types of ducts. Second, while research has shown significant reduction in the bond performance of single strands coated with emulsifiable oils, there are no data available on bond performance of multi-strand tendons coated with these oils.

### **2.2 FRICTION LOSSES IN POST-TENSIONED CONCRETE**

This section contains a majority of the background information on friction provided in Icaza (2004).

Accurate prediction of prestress losses due to friction is critical for successful design. Over-prediction of losses increases the required tendon area, resulting in uneconomical designs. Over-prediction can also lead to excessive camber and cracking upon strand or tendon release. In contrast, under-prediction of prestress losses can result in low stiffness, causing serviceability problems such as excessive deflections and cracking under service loads. In both cases, cracking

can allow for the ingress of water and chlorides, leading to corrosion problems. Cracking can also exacerbate problems related to fatigue (Hagenberger 2004).

Friction losses in post-tensioned concrete members fall into two categories: curvature friction losses and wobble friction losses. Curvature friction losses are due to intentional angle changes of the tendon inside a curved duct. Wobble friction losses, as shown in Figure 2-2, are due to unintentional angle changes. Wobble losses typically depend on the stiffness, diameter, and type of duct; spacing of duct supports; tendon type; and quality of workmanship. Variation in prestress force due to friction losses is typically represented using Equation 2.5, the derivation of which is included in most prestressed concrete texts and in Icaza (2004).

$$P_B = P_A \cdot e^{\mu(\alpha + KL)} \quad \text{Equation 2.5}$$

where:

$P_B$  = tendon force at point B

$P_A$  = tendon force at point A, closer to the live end than point B

$\mu$  = coefficient of friction

$\alpha$  = total angle change between points A and B

$K$  = wobble coefficient

$L$  = length of tendon between points A and B

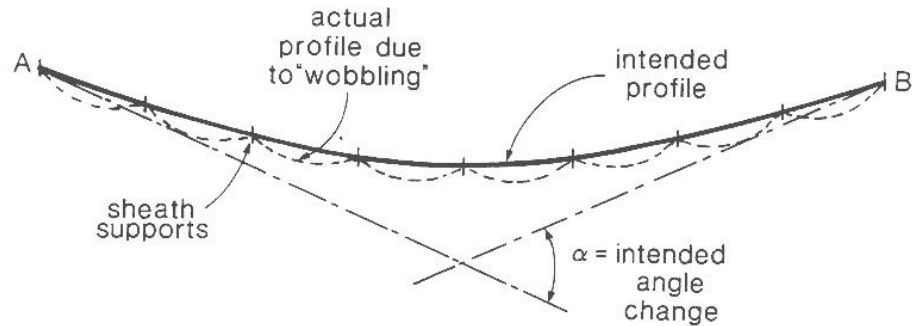


**Figure 2-2 Wobble Friction Losses (Collins and Mitchell 1997)**

Ranges of values for  $\mu$  and K currently recommended for design by ACI, AASHTO, and PTI are given in Table 2-1, Table 2-2, and Table 2-3, respectively.

**Table 2-1 Friction and Wobble Coefficients (ACI 318-02)**

			$\mu$	K (ft <sup>-1</sup> )*
Grouted tendons in metal sheathing		Wire tendons	0.15-0.25	0.0010-0.0015
		High-strength bars	0.08-0.30	0.0001-0.0006
		7-wire strand	0.15-0.25	0.0005-0.0020
Unbonded tendons	Mastic coated	Wire tendons	0.05-0.15	0.0010-0.0020
		7-wire strand	0.05-0.15	0.0010-0.0020
	Pre-greased	Wire tendons	0.05-0.15	0.0003-0.0020
		7-wire strand	0.05-0.15	0.0003-0.0020

\* Ignore wobble friction losses in rigid conduits and for large diameter prestressing steel in semi-rigid conduits.

**Table 2-2 Friction and Wobble Coefficients (AASHTO 1999, 2002)**

Type of Steel	Type of Duct	$\mu$	K (ft <sup>-1</sup> )
Wire or strand	Rigid and semi-rigid galvanized metal sheathing	0.15-0.25 <sup>a</sup>	0.0002
	Polyethylene	0.23	0.0002
	Rigid steel pipe	0.25 <sup>b</sup>	0.0002
High-strength bars	Galvanized metal sheathing	0.15	0.0002

<sup>a</sup> A friction coefficient of 0.25 is appropriate for 12-strand tendons. A lower coefficient may be used for larger tendons and duct sizes.  
<sup>b</sup> Lubrication will probably be required.

**Table 2-3 Friction and Wobble Coefficients (PTI 1990)**

Type of Duct	Range of Values		Recommended for Calculations	
	$\mu$	K (ft <sup>-1</sup> )	$\mu$	K (ft <sup>-1</sup> )
Flexible tubing non-galvanized	0.18-0.26	0.0005-0.0010	0.22	0.00075
Flexible tubing galvanized	0.14-0.22	0.0003-0.0007	0.18	0.00050
Rigid thin-wall tubing non-galvanized	0.20-0.30	0.0001-0.0005	0.25	0.00030
Rigid thin-wall tubing galvanized	0.16-0.24	0-0.0004	0.20	0.00020
Greased and wrapped	0.05-0.15	0.0005-0.0015	0.07	0.00100

## 2.2.1 Previous Friction Research

Previous research has investigated the effects of both duct material and emulsifiable oils on friction losses in post-tensioned concrete. This section first discusses research on duct material carried out as part of a project by the National Cooperative Highway Research Program (NCHRP). Two studies on the effects of strand surface condition, including the effects of emulsifiable oils, are then presented.

### 2.2.1.1 Effect of Duct Material

NCHRP Project 4-15 evaluated then-current practices in corrosion protection of prestressed bridges as well as new materials and systems available at the time (Perenchio et al. 1989). As part of this study, friction tests were conducted using both galvanized steel and HDPE ducts and uncoiled tendons with four strands each. The strands were either bare or epoxy-coated. The average friction coefficients for bare strands were 0.23 and 0.18 for galvanized steel and

HDPE ducts, respectively. The average friction coefficients for epoxy-coated strands were 0.40 and 0.21 for galvanized steel and HDPE ducts, respectively.

#### ***2.2.1.2 Effect of Strand Surface Condition***

Two studies are reviewed here. The first is a small-scale study done by Owens and Moore (CIRIA 1978); the second is a large-scale study done by Tran (1992) and Davis (1993).

Owens and Moore conducted friction tests on single-strand tendons of four different types and three different surface conditions. The strand types were 7-mm wire, 12.7-mm drawn strand, 15.2-mm round wire strand, and 18-mm drawn strand. The three surface conditions were clean, rusty, and oiled. Strands were loaded to 80% of their ultimate capacity in ten to fifteen increments. Results showed an increase in the friction coefficient for rusted strand relative to clean strand but showed no significant difference in the friction coefficients for clean and oiled strands. Friction coefficients for rusted strands ranged from 0.22-0.46. Friction coefficients for clean and oiled strands ranged from 0.09-0.19. Average coefficients for the larger diameter strands tended to be larger than those for smaller strands.

Tests performed by Tran and Davis were part of TxDOT Project 1264, which identified 10 emulsifiable oils as candidates for corrosion protection and lubrication. Small-scale corrosion, friction, and adhesion tests were performed by Hamilton and Davis as a preliminary step to identify oils for large-scale testing (Davis 1993, Kittleman et al. 1993). In small-scale static friction testing, two of the 10 oils provided either no reduction or an increase in the friction coefficient. The other eight oils reduced the friction coefficient from 12% to 27%. Based on these results and the results of corrosion and adhesions tests, the following four

oils were recommended for large-testing: Texaco Soluble D, Wright 502, Dromus B, and Hocut 4284.

Tran (1992) and Davis (1993) performed friction tests using 78-ft concrete beams, each with eight galvanized steel ducts 2-1/8 in. in diameter. Two ducts were straight and six were curved, with the curved ducts each having same total curvature. The beam used by Tran was built monolithically, while Davis’s beam was built segmentally. Tendons consisted of seven 1/2-in. Grade 270 strands and were stressed to 80% of their ultimate tensile strength. The two straight ducts were used to determine the wobble coefficient, while the curved ducts were used to determine curvature friction coefficients.

Tests by Tran were conducted using unoiled tendons as well as all four oils chosen from the preliminary testing. Tests by Davis were conducted using unoiled tendons and Wright 502 only. Reductions in the friction coefficient ranged from 8% to 25% and are shown in Table 2-4.

***Table 2-4 Reductions in Friction Coefficient, Tran and Davis (Davis et al. 1993)***

<b>Lubricant</b>	<b>Reduction in Friction Coefficient</b>	
	<b>Monolithic Beam</b>	<b>Segmental Beam</b>
Texaco Soluble D	19%	-
Wright 502	25%	15%
Dromus B	8%	-
Hocut 4284	17%	-

## **2.2.2 Limitations of Previous Friction Research**

Three important limitations of the research summarized here should be noted. First is the lack of research on friction losses in HDPE ducts, with the exception of NCHRP Project 4-15. Second is the lack of research on the effects of emulsifiable oils on friction losses in HDPE ducts. Finally, previous research on the effect of emulsifiable oils used oils that are no longer commercially available.

## **CHAPTER 3**

### **Preliminary Corrosion and Pullout Tests**

#### **3.1 INTRODUCTION**

Preliminary research for this project was conducted at Pennsylvania State University (PSU) under the supervision of Dr. Andrea Schokker with the following objectives (Salcedo 2003):

- Identify commercially available emulsifiable oils that can provide good or excellent temporary corrosion protection for strands in post-tensioning tendons
- Determine the extent of bond reduction caused by these oils
- Select candidate products to be used for large-scale testing.

Nineteen oils were selected for testing. This chapter describes the selection of the oils, the corrosion tests and results, and finally the pullout tests and results. All the information in this chapter is a summary of Salcedo (2003), which provides a more detailed account of the work done at PSU.

#### **3.2 SELECTION OF OILS**

Oils were selected for the study based on feedback from a survey of material manufacturers, post-tensioning contractors and subcontractors, and practicing engineers. Respondents were asked questions about brands of emulsifiable oils as well as field practices for applying the oils. The original questionnaire, which was made available on-line over a period of five months, can be found in Salcedo (2003). A total of 19 oils comprised the final list, given in Table 3-1.

**Table 3-1 Oil List and Product Description (Descriptions Provided by Manufacturers)**

<b>Oil Number</b>	<b>Producer</b>	<b>Product Name</b>	<b>Product Description</b>
O1	Fuchs Lubricants	Anticorit AQ31	Corrosion inhibitor which yields several levels of protection depending on the concentration levels. Provides effective protection of clean ferrous metal surfaces in high humidity conditions during extended indoor storage. Upon drying, deposition of a thin greasy film that is not resoluble in water, thus providing resistance to condensation. Excellent lubricity.
O2	Citgo	Citcool Concentrate 33	Heavy duty synthetic coolant concentrates containing lubricity agents, anti-corrosion additives. Contains no-oil with improved cleanse ness, solution stability, stable with hard water, and sludge buildup. Biodegradable product with a fungicide to protect against fungal growth. Monitoring against microbial activity over extended periods is advisable. Contain no phenols, nitrites, or heavy metals.
O3	Citgo	Trukut NC205 Cutting Oil	Emulsifiable oil that will readily mix with water to produce a stable emulsion. No chlorinated compounds are present in emulsion. Heavy duty EO with EP additives. Provides efficient and economical cooling and lubrication; in addition to excellent rust protection to both machine and parts.
O4	Shell/Texaco	Dromus ABD 201	General purpose soluble oil with very stable emulsions even with hard waters and at high dilution ratios. Recommended for light machining operations and grinding. Provides good rust protection for both machine and parts.
O5	Shore Chemical Co.	Emulsifiable Cutting Oil	General purpose coolant use in all types of grinding and machining operations. Compatible with ferrous metals, contains anti-foaming agents. Contains corrosive inhibitors to protect steel, copper, and brass.



**Table 3-1 (Cont.) Oil List and Product Description**

<b>Oil Number</b>	<b>Producer</b>	<b>Product Name</b>	<b>Product Description</b>
O6	Five Star	Five Star Protective Coating	NA
O7	Daubert Chemical Co.	Tectyl 603	Polymeric, water emulsifiable corrosion preventive. It contains a special additive system which provides a durable, self-healing, corrosion resistant film. The concentrated coating is an amber liquid.
O8	EF Houghton & Co.	Hocut 795	Heavy duty machining and grinding fluid for use with all metals. Provides greater resistance to microbial degradation of the fluid, reduces the sump side additions of microbial agents. Compatible with hard water, biostable, and provides good lubrication and corrosion protection.
O9	Fuchs Lubricants	Lubrol 215B	Quality soluble oil used for grinding, cutting, drawing and stamping. Contains additives for non-silicone foam control, biostatic microbial control, and exceptional rust control.
O10	Daubert Chemical Co.	NoxRust 703D	Rust preventive oil concentrate that can be diluted with water or petroleum solvent. The product is intended for use in retarding corrosion during shipment and storage of machined parts, tools, phosphate treated steel, finished assemblies, etc.
O11	Daubert Chemical Co.	NoxRust 707	Water soluble corrosion inhibitor that provides high level of temporary protection. Synthetic water base fluid without any oil or oil-based material. Designed as cleaning agent for coiled steel and coated steel products.
O12	Master Builders	Rheocrete 222+	State-of-the-art corrosion-inhibiting admixture formulated to inhibit the corrosion of steel reinforced concrete. Provides two levels of corrosion protection, making it the most effective corrosion-inhibiting admixture available.
O13	Esso/Exxon/Mobile	Rust-Ban 310	NA

**Table 3-1 (Cont.) Oil List and Product Description**

<b>Oil Number</b>	<b>Producer</b>	<b>Product Name</b>	<b>Product Description</b>
O14	Ondeo Nalco	Rustphree 4746A	NA
O15	EF Houghton & Co.	Rust-veto 342	Solvent based for outdoor and severe condition protection.
O16	EF Houghton & Co.	Rust-veto FB20	NA
O17	Daubert Chemical Co.	Tectyl 810	Water emulsifiable, oil concentrate corrosion preventive compound with excellent lubricity for variety of industrial metalworking.
O18	Cortec Corp.	VpCI 377	NA
O19	Cortec Corp.	VpCI 389	Provides excellent protection in outside applications as well as offering excellent salt spray resistance. Environmentally friendly product.

### **3.3 LONG-TERM CORROSION TESTS**

The objective of the corrosion tests was to determine the oils' ability to prevent or slow the progress of corrosion in various conditions. Corrosion tests were performed over a period of six months, with specimens inspected every four weeks. Specimens were exposed to three different environments:

- Environment 1: outdoor exposure to Pennsylvania's natural elements (including winter weather)
- Environment 2: controlled temperature and relative humidity (RH): 73F (23C) and >95% RH
- Environment 3: semi-controlled temperature, variable RH, and partial submersion in a 5% NaCl distilled water solution

Results are in the form of a corrosion rating based on visual examination of the specimens. The following sections describe the specimens, the test setup and procedure, and the corrosion test results.

#### **3.3.1 Description of Specimens**

The final assembly of the specimens is shown in Figure 3-1. Specimens were constructed from 18-in. long sections of prestressing steel (oiled or unoiled), PVC tubing, PVC slip caps, and plastic spacers.

- The prestressing steel was nominal 0.5-in. diameter, low-relaxation seven-wire prestressing strand conforming to ASTM A416 Grade 270 standards. All specimens were cut from the same reel of strand and cleaned with acetone to ensure a uniform surface. The oils were applied with a cup sprayer and were not diluted with water.
- The inner diameter and wall thickness of the PVC tubing was 1-5/32 in. and 1/16 in., respectively. The PVC tubes used for specimens placed outdoors (environment 1) and in a controlled

temperature/humidity chamber (environment 2) had four holes along their length, approximately 3.5 in. apart. A drainage hole on the opposite side was 2.5 in. from the tube end. PVC tubes used for specimens placed in the NaCl solution (environment 3) had four holes, two each on opposite sides, all on the upper half of the tube.

- The PVC slip caps had a diameter of 1-1/4 in.

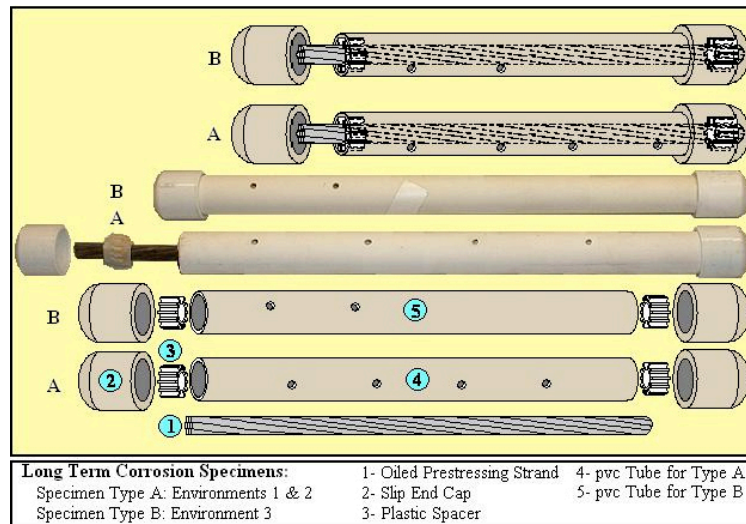


**Figure 3-1 Corrosion Test Specimens**

A total of 177 specimens were tested, as shown in Table 3-2. Three specimens per oil were placed in each of the three environments. Three unoiled specimens each were also placed in the controlled temperature/humidity chamber and the NaCl solution (environments 2 and 3, respectively).

*Table 3-2 Summary of Corrosion Specimens*

<b>Exposure Environment</b>	<b>Total Number of Specimens</b>	<b>Number of Specimens per Oil</b>	<b>Number of Specimens without Oil</b>
Environment 1 (outdoors)	57	3	0
Environment 2 (controlled temp/RH)	60	3	3
Environment 3 (5% NaCl solution)	60	3	3
<b>Total</b>	177	9	6

### **3.3.2 Test Setup and Procedure**

Specimens were held vertically in wooden racks and placed in their respective environments. In the case of the NaCl solution, evaporated solution was refilled every 14 days. Specimens were left untouched between inspections, which took place every month for six months. Detailed information was recorded for each specimen during inspections, and specimens were rated according to the system shown in Table 3-3. Inspections were always performed by the same individual to ensure that corrosion ratings were as consistent as possible. At the end of the six-month period, specimens were removed from the environment. The strands were then removed from the PVC pipes, inspected, and photographed.

**Table 3-3 Rating System for Corrosion Tests**

<b>Rating</b>	<b>Description</b>
1	As received from manufacturer and completely clean from any corrosion products.
2	No signs of corrosion at any level or small spots of rust.
3	Small blisters, superficial but widely spread corrosion, pitting is unusual.
4	Small blisters, uniform corrosion or initial signs of wide pitting in centralized areas.
5	Large blisters, trail of blisters does not exceed 2 in., deep and wide pitting is visible, corrosion products and pitting do not affect more than 50% of the steel area.
6	Large blisters, trail of blisters along the strand exceeds 2 in., deep and wide pitting cover most of the strand surface, corrosion products and pitting affect over 50% of the steel surface, and several forms of corrosion are present simultaneously.
7	High levels of corrosion with visible large areas of steel lost.

**Note:** Rating system is precise to  $\pm 0.5$  (i.e. borderline specimens can receive a rating of 2.5, 3.5, etc.)

### 3.3.3 Test Results

Final results for the corrosion tests are presented in Figure 3-2. A corrosion rating of 4 was selected by the researchers as the standard for “adequate” corrosion protection. As shown, seven of the 19 oils tested met this standard in all three environments at the end of the six-month testing period: O3, O4, O5, O10, O13, O16, and O17. More detailed final results, as well as intermediate corrosion ratings for each specimen, can be found in Salcedo (2003).

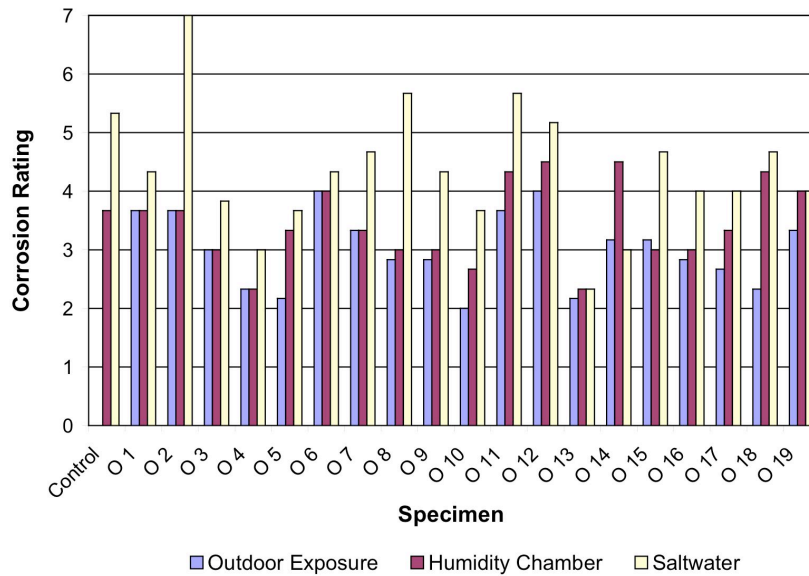


**Figure 3-2 Final Corrosion Test Results**

### 3.4 SINGLE-STRAND PULLOUT TESTS

The objective of the pullout tests was to gain preliminary insight into the oils’ effect on bond strength. Because these tests used only a single strand, results are not representative of how a multi-strand post-tensioned tendon behaves and therefore are only intended for comparative purposes among the oils.

The tests were based on ASTM specification A981-97, “Standard Test Method for Evaluating Bond Strength for 15.2 mm (0.6 in.) Diameter Prestressing Steel Strand, Grade 270, Uncoated, Used in Prestressed Ground Anchors.” The tests were conducted using 0.5 in. diameter strand but otherwise met the A981-97 specifications. The following sections describe the specimens, the test setup and procedure, and the pullout test results.

### 3.4.1 Description of Specimens

A total of 58 specimens were tested, as shown in Table 3-4 below. Six control specimens were tested without any mechanical restraint against twisting, while the six others were restrained as described below in Section 3.4.2.

*Table 3-4 Summary of Pullout Specimens*

<b>Specimen</b>	<b>Number of Tests</b>	<b>Total</b>
Control (Unoiled)	6 restrained, 6 unrestrained	12
Oils 1, 2, 6-12, 14-19	2 each	30
Oils 3-5, 13	4 each	16
<b>Total</b>		<b>58</b>

The final assembly of the specimens is shown in Figure 3-3. Specimens were constructed from 46-in. lengths of prestressing steel (oiled or unoiled), cementitious grout, steel cylinders, and steel base plates.

- The prestressing steel was nominal 0.5 in. diameter, low-relaxation seven-wire prestressing strand conforming to ASTM A416 Grade 270. All specimens were cut from the same reel of strand and were not cleaned prior to assembly, because such cleaning is impractical in the field. The oils were applied with a cup sprayer between 24 and 36 hours prior to grouting. The oils were not diluted with water. A 2-in. debonded section of strand as shown in Figure 3-3 was created by wrapping the strand with electrical or teflon tape.
- Cementitious grout was freshly mixed with Type I portland cement and had a w/c ratio of 0.45. The grout was moist cured in accordance with ASTM specification C511 until at least three test cubes reached a compressive strength of 4000 psi, which typically took 14 days.



- The steel cylinders were 18 in. long, with an outer diameter of 6 in. and a wall thickness of 0.125 in.
- The steel base plates were 6 in. x 7 in. x 3/8 in. and had a 1-1/16 in. diameter hole in the center through which the strand could pass.

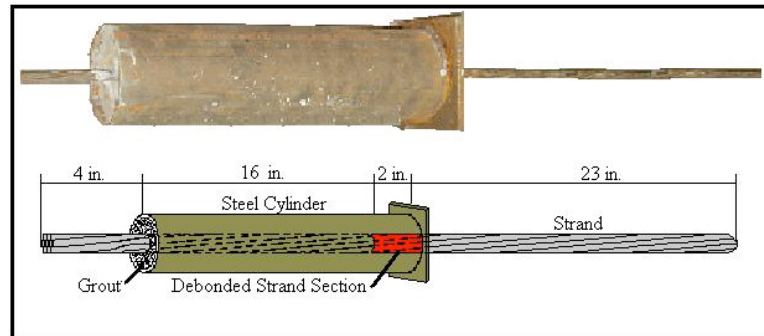
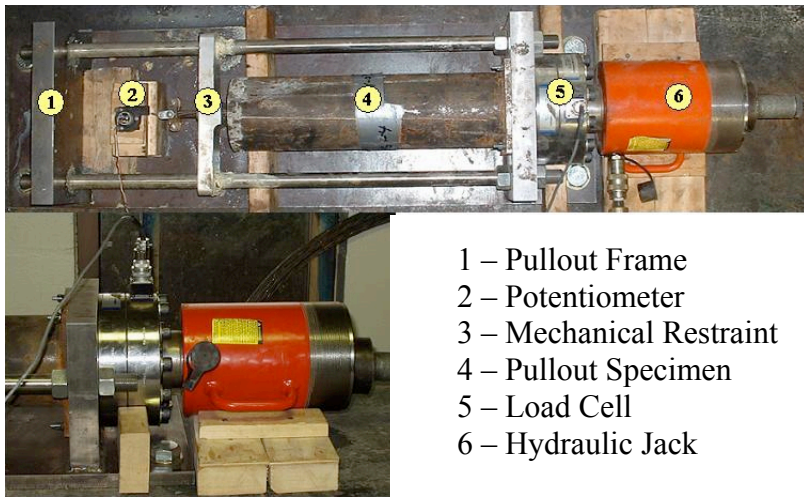


**Figure 3-3 Pullout Test Specimens (Salcedo 2003)**

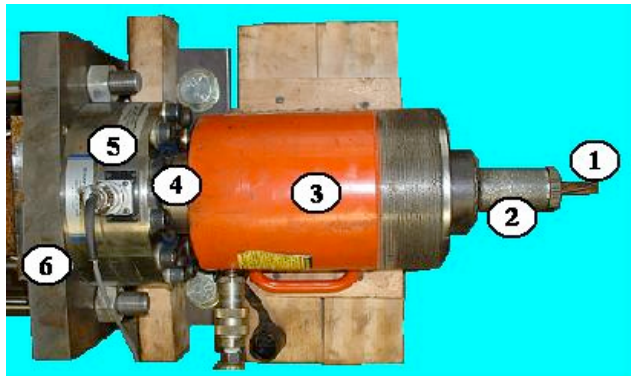
### 3.4.2 Test Setup and Procedure

The test frame is shown below in Figure 3-4 and Figure 3-5. The strand was gripped by a chuck and pulled using a 60-ton hydraulic ram. A load cell and linear potentiometer were used to measure force and displacement at the free end, respectively. Figure 3-6 shows a close-up of the mechanical device used to restrict the strand from twisting as the strand pulled out. This device was used on all tests with the exception of six control (uncoiled) specimens. The data were recorded using a MEGADAC data acquisition system and DasyLab software.



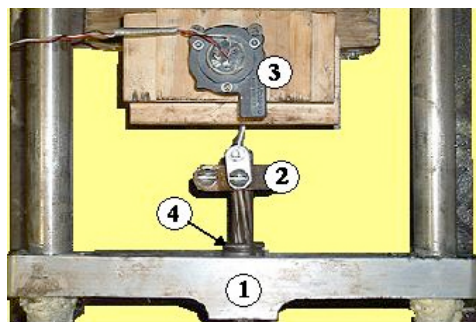
- 1 – Pullout Frame
- 2 – Potentiometer
- 3 – Mechanical Restraint
- 4 – Pullout Specimen
- 5 – Load Cell
- 6 – Hydraulic Jack

*Figure 3-4 Pullout Test Frame (Salcedo 2003)*



- 1 – Prestressing Strand
- 2 – Three Piece Chuck
- 3 – Hydraulic Jack
- 4 – Steel Shim
- 5 – Load Cell
- 6 – Pullout Steel Frame

*Figure 3-5 Pullout Test Frame Close-Up (Salcedo 2003)*



- 1 – Mechanical Restraint
- 2 – Potentiometer Clamp Attachment
- 3 – Potentiometer
- 4 – Two-Piece Chuck

*Figure 3-6 Mechanical Restraint Device Close-Up (Salcedo 2003)*

The pullout tests were performed in two stages. First, a force sufficient to cause anchorage setting was applied to the specimen for a minimum of 3 minutes. Then the specimen was loaded at a rate of 0.1 in./min with a tolerance of  $\pm 25\%$  in accordance with ASTM standard A981-97. The test was stopped once the displacement reached 0.5 in.

### **3.4.3 Test Results**

Final results for all pullout tests are presented in Figure 3-7. Results for only those oils which received a rating of 4 or better in all three environments in the corrosion tests are presented in Figure 3-8 along with control values. A slip value of 0.1 in. was selected by the researchers as the standard for bond failure. This value was determined primarily through phone conversations with members of the North American Strand Producers Association. As shown, average failure loads for oiled specimens were approximately 30% to 95% lower than the average failure load for the restrained control specimens. Average failure loads for the selected oils with favorable corrosion protection ratings shown in Figure 3-8 were approximately 40% to 80% lower than the restrained control. More detailed final results and variability information can be found in Salcedo (2003).

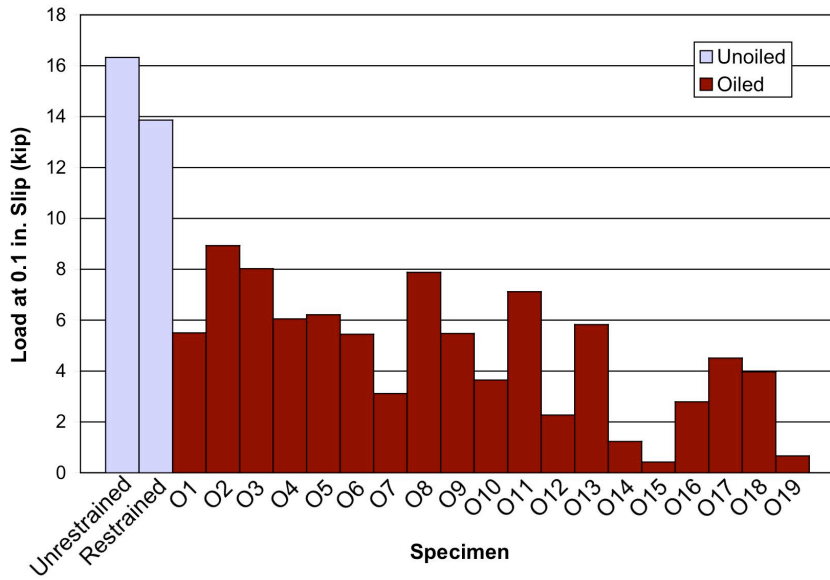


**Figure 3-7 Pullout Test Results, All Oils**

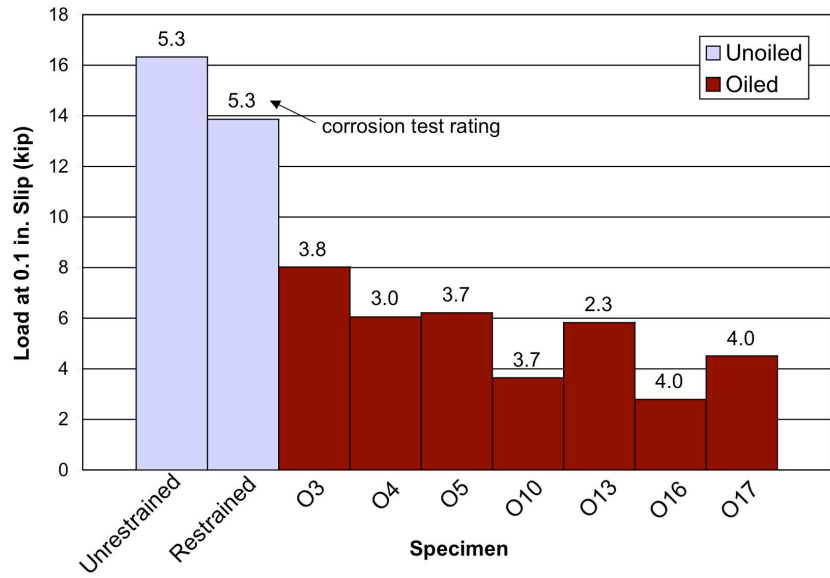


**Figure 3-8 Pullout Test Results, Selected Oils with Corrosion Ratings □4**

### **3.5 SELECTION OF OILS FOR LARGE-SCALE TESTS**

Two candidate oils of the original 19 were selected for large-scale testing based on the results of the corrosion and pullout tests performed at PSU. In order to be considered, the oils must have received a rating of 4.0 or lower in the corrosion tests, which limited the field to seven oils. Of these seven, O3 (Citgo Trukut NC205) and O10 (Daubert VCI NoxRust 703D) were chosen because they were at or near the extremes of the pullout test results: O3 (Trukut NC205) was the best performer, while O10 (NoxRust 703D) was a relatively poor performer. The researchers assumed that using these two oils in large-scale testing would give results which represent both “best case” and “worst case” effects on bond in multi-strand post-tensioned elements for oils that provide good corrosion protection.

## **CHAPTER 4**

### **Large-Scale Experimental Program**

#### **4.1 INTRODUCTION**

After completion of the preliminary corrosion and bond tests at Pennsylvania State University, large-scale tests were performed at the University of Texas at Austin to determine the effects of emulsifiable oils on bond performance and friction losses in post-tensioned concrete members. Twelve-strand tendons with nominal 1/2-in. diameter seven-wire strands were chosen for all tests because they are the smallest tendon that would typically be used in segmental construction. This tendon size maximized the ease and economy of constructing test specimens which were still representative of actual post-tensioned structures.

#### **4.2 COMMON VARIABLES**

Two variables were common to both the bond and friction tests: strand surface condition and duct types. These variables are briefly described below. Additional variables unique to either the bond or friction tests are described in their respective sections.

Tests were performed using strand that was either unoiled or oiled with one of two brands. The two oils chosen for testing were Trukut<sup>®</sup> NC205 and Nox-Rust<sup>®</sup> 703D. As described in Chapter 3, both of these oils provided adequate corrosion protection during accelerated corrosion tests. In single-strand pullout tests, strand coated with NC205 exhibited good bond performance in comparison with other oils. In contrast, strand coated with 703D exhibited poor bond performance. No preliminary friction tests were performed using these oils.

Semi-rigid galvanized steel ducts, high-density polyethylene (HDPE) ducts, and galvanized rigid steel pipes, all shown in Figure 4-1, were used in both the friction and bond tests. The semi-rigid galvanized steel and HDPE ducts are industry standards for post-tensioned construction and are widely available. Steel pipes are commonly used in deviator blocks, where a large tendon angle change is required over a short distance. All three ducts had a 3-in. nominal diameter, the standard size for a 12-strand tendon with 1/2-in. diameter strand.



*Figure 4-1 Ducts (Icaza 2004)*

#### 4.3 MATERIALS

The following materials were used in constructing all bond and friction test specimens.

### **4.3.1 Oils**

The two emulsifiable oils used for bond and friction testing were Trukut<sup>®</sup> NC205, produced by Citgo, and Nox-Rust<sup>®</sup> 703D, produced by Daubert VCI, Inc. These oils were not mixed with water before being applied to the tendons, in order to be consistent with the preliminary bond tests done at Pennsylvania State University.

### **4.3.2 Prestressing Strand**

All tendons consisted of nominal 1/2-in. diameter, low-relaxation seven-wire prestressing strand conforming to ASTM A416 Grade 270 standards. A single reel of strand was used for all friction tests and for bond tests with tendons that were unoiled or freshly oiled with NC205. Because the original reel did not contain enough strand for the remaining bond tests, a second reel from the same manufacturer was used for bond specimens tested using 703D oil and NC205 oil allowed to dry for 10 days. The strand from both reels was free of any visible rust.

### **4.3.3 Ducts**

Nominal 3-in. diameter ducts, shown in Figure 4-1, were used in all specimens. The galvanized steel duct was industry standard, with an inner diameter of 2.92 in. and an outer diameter of 3.20 in. The HDPE duct, also industry standard, had an inner diameter of 2.92 in. and an outer diameter of 3.18 in. The outer diameter of the ribs was 3.55 in. The galvanized rigid pipe was Schedule 40 steel pipe bent to either a 10-ft or 30-ft centerline radius and hot-dipped. The inner and outer diameters were 3.06 in. and 3.53 in., respectively.



#### 4.3.4 Mild Steel

Mild steel bars used in the reinforcement cages were all Grade 60 and conformed to ASTM A615 standards. All rebar was ordered from a local supplier, and cages were tied in the lab.

#### 4.3.5 Post-Tensioning Hardware

Post-tensioning anchor heads and wedges were ordered from VSL International and are pictured in Figure 4-2. The anchor heads were part of the VSL EC 12-05 anchors. The accompanying trumpets and spiral reinforcement were not used. Anchor heads were used multiple times, but new wedges were used for each bond and friction test.

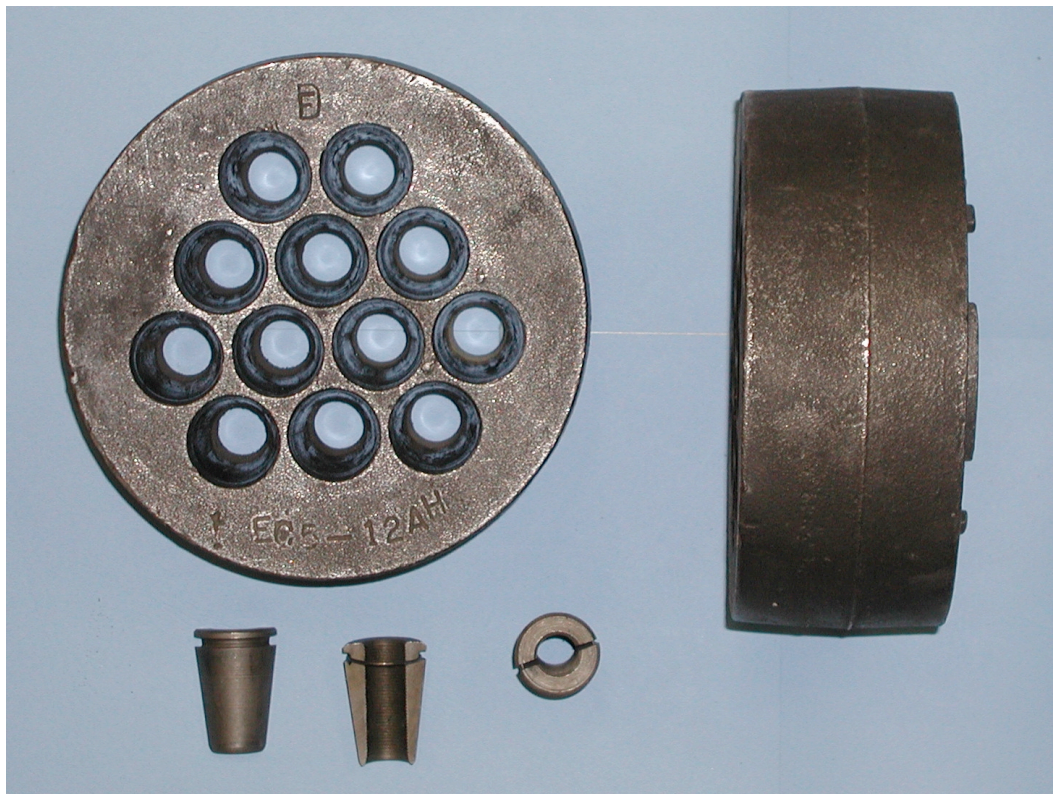


*Figure 4-2 Post-Tensioning Hardware (Diephuis 2004)*

#### **4.3.6 Concrete**

Concrete was supplied by a local ready-mix plant and designed for a 28-day compressive strength of 5000 psi. Actual concrete strength on the day of testing was determined by performing standard compression tests of 6 x 12 in. cylinders prepared during the cast. Detailed concrete strengths are reported in Chapter 5 but ranged from approximately 3800 psi to 8400 psi.

#### **4.3.7 Grout (Bond Tests Only)**

Pre-packaged SikaGrout<sup>®</sup> 300PT was used in all bond specimens. This brand of grout conforms to the PTI Guide Specifications for Grouting of Post-Tensioned Structures (2000) and is designed for a 28-day compressive strength of 8000 psi. Actual grout strength on the day of tendon release and the day of testing was determined by performing standard compression tests of 4 x 8 in. cylinders prepared when the grout was mixed. Detailed grout strengths are reported in Chapter 5 but ranged from approximately 7600 psi to 9800 psi.

#### **4.3.8 Concrete Debonder (Friction Tests Only)**

As described in Section 4.5, a debonder was used between the permanent and replaceable parts of the friction test specimens. This debonder, which is sometimes used for match casting in segmental construction, is a mixture of Murphy<sup>®</sup> Oil Soap and talc. Approximately 14 lb of talc was used for each gallon of soap.

### **4.4 BOND TESTS**

The primary objective of the bond tests was to determine the effect of emulsifiable oils on bond performance in grouted post-tensioned concrete members. The secondary objectives were to determine how bond performance is affected by the duct material and by the amount of time between oiling and

grouting. These effects were determined using multi-strand monotonic pullout tests, similar to the smaller-scale single-strand tests performed at Pennsylvania State University. The selection of duct materials and oil brands, which were common to both the bond and friction tests, is discussed in Section 4.2. Following is a discussion of the additional variables unique to the bond tests as well as descriptions of the test specimens and testing procedure.

#### **4.4.1 Additional Variables**

In addition to varying the strand surface condition and duct type, the main variables considered during bond testing were bonded length and amount of time between oiling and grouting for oiled specimens.

The bonded length of a tendon in a curved duct depends on the centerline length of the duct (and thus the overall length of the member) and the tendon angle change from one end of the member to the other. Several lengths were tested before finding a length which did not fully develop the tendon but still allowed the peak load during testing to approach the ultimate strength of the tendon. A large number of specimens were either too long, and thus pullout was not achieved, or too short, and thus the peak load was too low. The results of these unsuccessful tests are not reported here but can be found in Diephuis (2004). Once a suitable bonded length was determined, all tests were performed using specimens of this length.

The amount of time between oiling and grouting was varied in response to observations that oils dry rapidly over time (Salcedo 2003). In order to determine whether emulsifiable oils have less effect on bond if given time to dry, four tests were performed using the NC205 oil and grouting ten days after oiling. Typical oiled specimens, which used both NC205 and 703D, were grouted only two days after oiling.

#### 4.4.2 Description of Specimens

The bond specimens were simply-supported, grouted post-tensioned beams. The tendons were left extending from the ends so they could be anchored to a ram and pulled out. Descriptions of overall specimen geometry, reinforcement layout, and construction sequence follow.

##### 4.4.2.1 Specimen Geometry

Overall dimensions for the bond specimens discussed in this report are shown in Figure 4-3. Specimens were 2 ft square in cross-section with a centerline duct length of 44 in. Because straight tendons are rarely used in post-tensioned members, curved ducts were installed. Members with galvanized and HDPE ducts typically have curvature radii of 30 ft or more, while rigid pipes in deviator blocks typically have curvature radii of 30 ft or less. In order to be representative of actual members with all three duct types, a 30-ft radius of curvature was chosen for all bond specimens. This radius of curvature required a total tendon angle change of 7.5 degrees over the length of the member. The tendon profile was asymmetrical, with only one end inclined. The ends of the specimens were constructed perpendicular to the tangent of the duct.

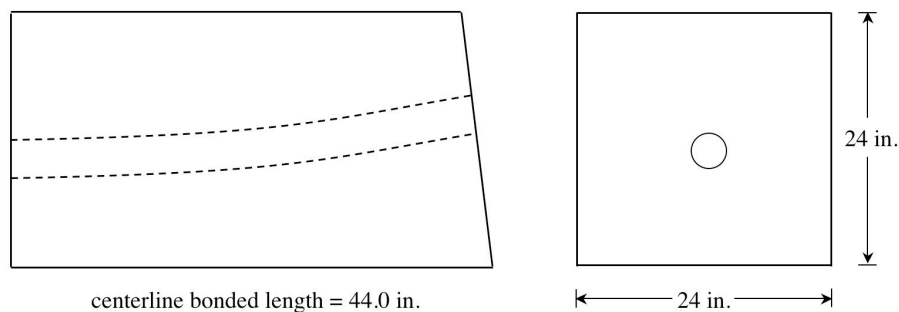


**Figure 4-3 Bond Specimen Elevation and Cross-Section**

Prior to grouting, a prestress force was applied to the tendon to bring it into contact with the top of the duct, to ensure the tendon position was similar to that found in actual post-tensioned members.

#### 4.4.2.2 Reinforcement Layout

The layout of reinforcement used in the bond specimens is shown in Figure 4-4. Four straight #7 bars were used on both the top and bottom of the cage. Transverse reinforcement consisted of closed #4 hoops and #4 cross-ties spaced at 5 in on center.

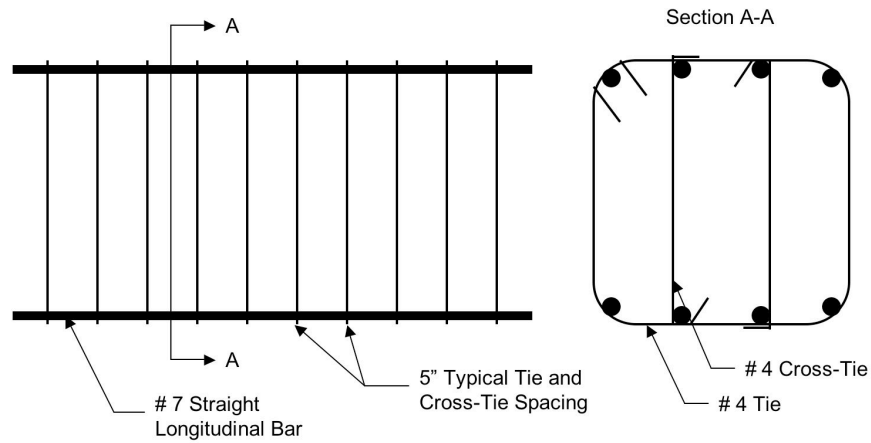


**Figure 4-4 Bond Specimen Reinforcement Layout**

#### 4.4.2.3 Construction Sequence

A brief overview of the construction sequence for one bond specimen is provided here. Specimens were generally prepared and tested in duplicate pairs. Detailed information on the preparation of bond specimens can be found in Diephuis (2004).

Prior to casting concrete, the reinforcement cage and duct were placed in the formwork as shown in Figure 4-5. This figure shows one of the original

specimens built by Diephuis and is not representative of the actual specimen geometry and reinforcement layout used for the bond tests discussed in this report. However, the general process of assembling the cages, ducts, and formwork did not change. The duct was tied to the cage with wire to create the desired profile and to ensure the duct did not move during placement of the concrete.

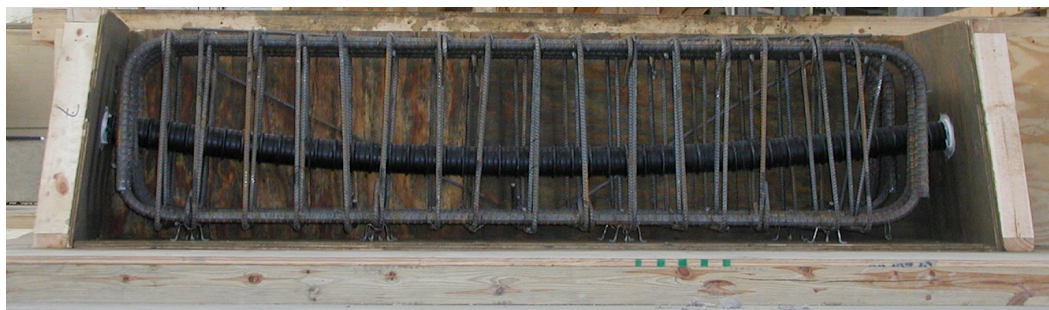


***Figure 4-5 Assembled Specimen Cage, Duct, and Formwork***

After initial set of the concrete, forms were removed and the ends of the duct ground even with the faces of the beam. As shown in Figure 4-6, a bearing plate, hydraulic rams, and a reaction beam were placed at each end of the specimen. The tendon was then fed through the specimen as shown in Figure 4-7, being oiled with a garden sprayer as it was inserted on specimens where oil was to be applied. The tendon was anchored to the reaction beams at both ends using the anchor heads and wedges shown in Figure 4-2, and vents for grouting were inserted at both ends of the duct. The rams were then extended to stress the tendon to a load of approximately 6.3 kip, bringing it in contact with the top of the duct. After stressing, a “seal” was created at each end of the beam using simple wooden forms and expanding insulation foam as shown in Figure 4-8. The complete prestressing setup is shown in Figure 4-9. The specimen was grouted with a hand pump either two or ten days after initial stressing. The tendon was released five days after grouting, and the specimen was tested one day after release.

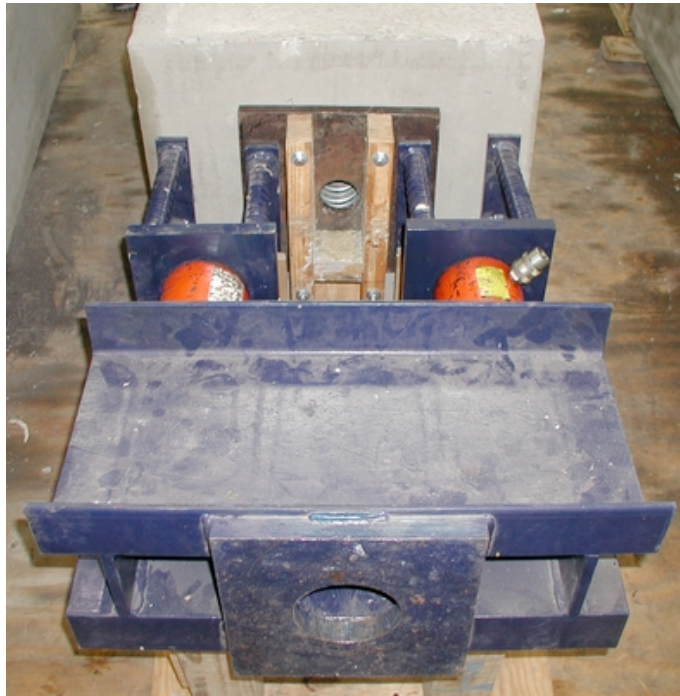


*Figure 4-6 Specimen Ready for Installation of Tendon*



*Figure 4-7 Oil Application*

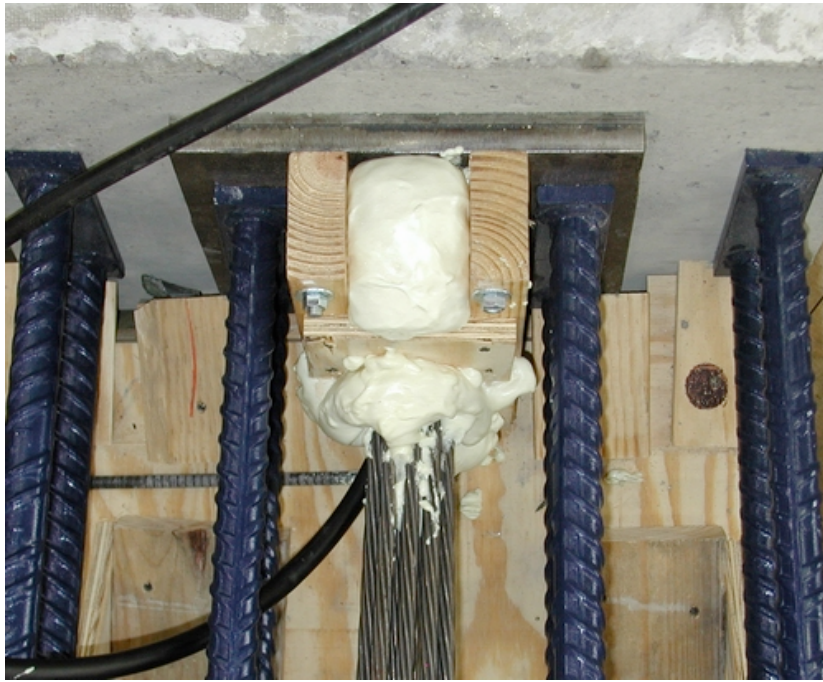


*Figure 4-8 Sealing of Duct Ends*

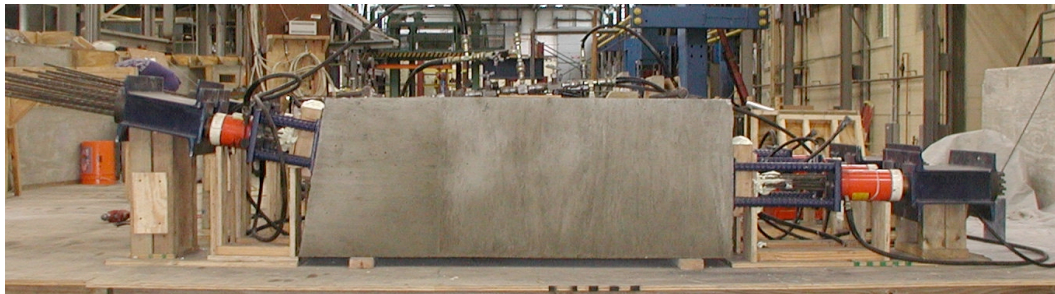


*Figure 4-9 Complete Prestressing Setup*

#### **4.4.3 Description of Tests**

Figure 4-10 shows a bond specimen ready for testing. The strands extending out of the beam were left long enough on the live end to be anchored to a bearing plate on the end of the ram; on the dead end they were cut approximately 1-2 in. from the face of the beam. No bearing plates or other



hardware were used for the bond tests; the ram was placed directly against the face of the beam.



*Figure 4-10 Bond Specimen Ready for Testing*

#### ***4.4.3.1 Instrumentation and Data Acquisition***

Test data consisted of load measurements at the live end and displacement measurements at both the live and dead ends of the specimens. Load measurements were taken using a 2000-psi electronic pressure transducer. Displacement measurements were taken using linear potentiometers. On the live end, a 5-in. potentiometer was clamped to the bearing plate on the ram cylinder and extended to the body of the ram as shown in Figure 4-11. On the dead end, a 2-in. potentiometer was placed on the cross-sectional surface of a single strand on the inside of the tendon as shown in Figure 4-12. In all tests, the tendon was observed to move as a unit. Any differential movement among the strands was thus negligible. All instruments were calibrated to ensure accuracy before the first tests were performed.

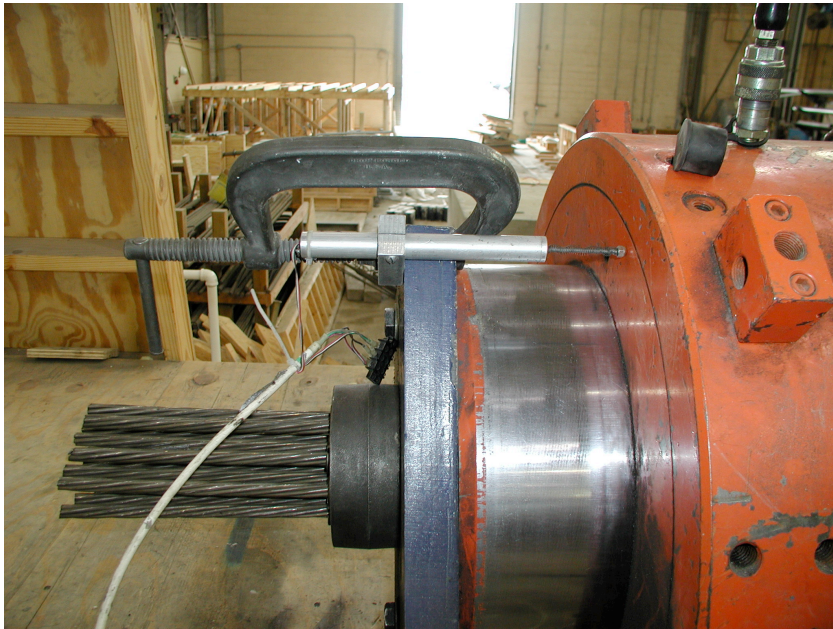


***Figure 4-11 Live End Linear Potentiometer Placement***



***Figure 4-12 Dead End Linear Potentiometer Placement***

The data were read by a Hewlett-Packard HP7500 scanner connected to a desktop personal computer and recorded with National Instruments LabVIEW software, which also provided real-time monitoring.

#### ***4.4.3.2 Testing Sequence***

The following describes the sequence followed during testing:

1. The tendon was placed through the cylinder of the 2,000-kip hydraulic ram. The ram was then placed flush with the live end of the specimen.
2. The cylinder of the ram was extended approximately 12 in. to ensure there would be enough room to cut the anchor head off with a grinder after the test was complete.
3. The anchor head was placed on the tendon, against the bearing plate at the end of the ram cylinder, and the wedges were seated by hand.
4. The pressure transducer and linear potentiometers were put into place.
5. The ram was extended and the tendon loaded slowly, with data being logged at approximately 5-10 kip intervals, until the tendon began to pull out. Once pullout began, the load often stabilized or dropped, so data were logged at approximately 0.1-in. strand movement intervals at the live end.
6. Early tests were typically stopped once the load reached 80-90% of the guaranteed ultimate tensile strength of the tendon, or approximately 400 kips. In later tests, the specimen was typically loaded until either wires began breaking or the live end displacement approached 4 in.

7. The ram cylinder was retracted and the anchor head cut off so the ram could be removed.

## **4.5 FRICTION TESTS**

The primary objective of the friction tests was to determine the effect of emulsifiable oils on friction losses in post-tensioned concrete members. The secondary objectives were to determine how friction losses are affected by the duct material, radius of curvature, and time between oiling and post-tensioning. These losses were determined by constructing curved beams and measuring the total force at the live and dead ends during post-tensioning. The difference between the two forces corresponds to the friction losses along the length of the duct. The selection of duct materials and oil brands, which were common to both the bond and friction tests, is discussed in Section 4.2. Following is a discussion of the additional variables unique to the friction tests as well as descriptions of the test specimens and testing procedure.

### **4.5.1 Additional Variables**

In addition to varying the strand surface condition and duct type, the main variables considered during friction testing were tendon radius of curvature and amount of time between oiling and stressing for oiled specimens.

Two different radii of curvature were chosen for friction testing: 30 ft and 10 ft. The Standard Specification for Highway Bridges (AASHTO 2002) and the Guide Specifications for Design and Construction of Segmental Concrete Bridges (AASHTO 1999) require a 30-ft minimum radius of curvature for HDPE ducts and a 10-ft minimum radius of curvature for all other materials. Because friction losses are inversely proportional to radius of curvature, these two lower bounds for the radius were chosen for the friction tests. Although a 10-ft radius of curvature is not currently allowed for HDPE ducts, friction tests on HDPE ducts

with a 10-ft radius were performed for comparison purposes and to evaluate the performance of this material at this curvature.

Similarly to the bond tests, the amount of time between oiling and friction testing was varied in response to observations (Salcedo 2003) that oils dry rapidly over time. In order to determine whether emulsifiable oils have less effect on friction losses if given time to dry, friction tests were performed immediately after oiling and were repeated with the same tendons one day later.

#### **4.5.2 Description of Specimens**

The friction specimens consisted of a duct embedded in a removable concrete arc (shaded lightly in Figure 4-13) cast inside the cavity of a permanent concrete reaction beam (shaded darkly in Figure 4-13). The permanent beam, which was heavily reinforced, was designed to resist the full compression load caused by the post-tensioning of the tendon. The removable infill, prevented from bonding to the permanent beam through use of a concrete debonder, allowed for easy replacement of the duct. Descriptions of overall specimen geometry, reinforcement layout, and construction sequence follow.

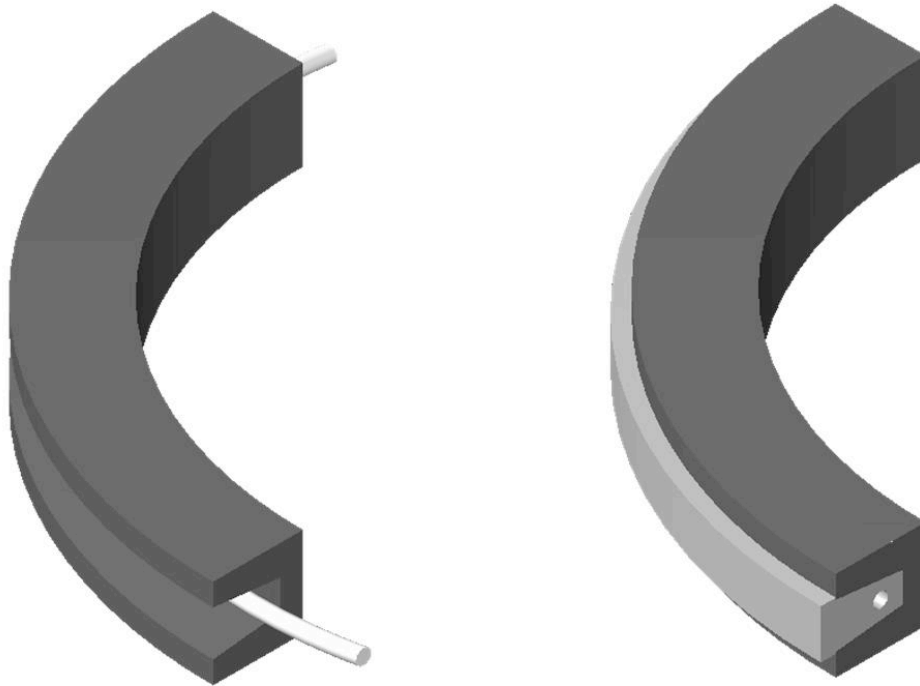


*Figure 4-13 Placement of Duct and Casting of Removable Part (Icaza 2004)*

#### ***4.5.2.1 Specimen Geometry and Reinforcement Layout***

Two permanent beams were built, one with a 30-ft radius of curvature and one with a 10-ft radius of curvature. The permanent part of each beam had a 24-in. square C-shaped cross-section, as shown in Figure 4-14, and centerline length of 188.5 in, as shown in Figure 4-15. Heavy reinforcement, shown with overall dimensions in Figure 4-14, was provided so that this part of the specimen could carry all forces generated during post-tensioning. Diagonal ties resisted radial forces, and additional reinforcement ensured the beam could resist any moment due to incidental eccentricities during post-tensioning. The beam also contained enough reinforcement to support its own weight when being lifted.

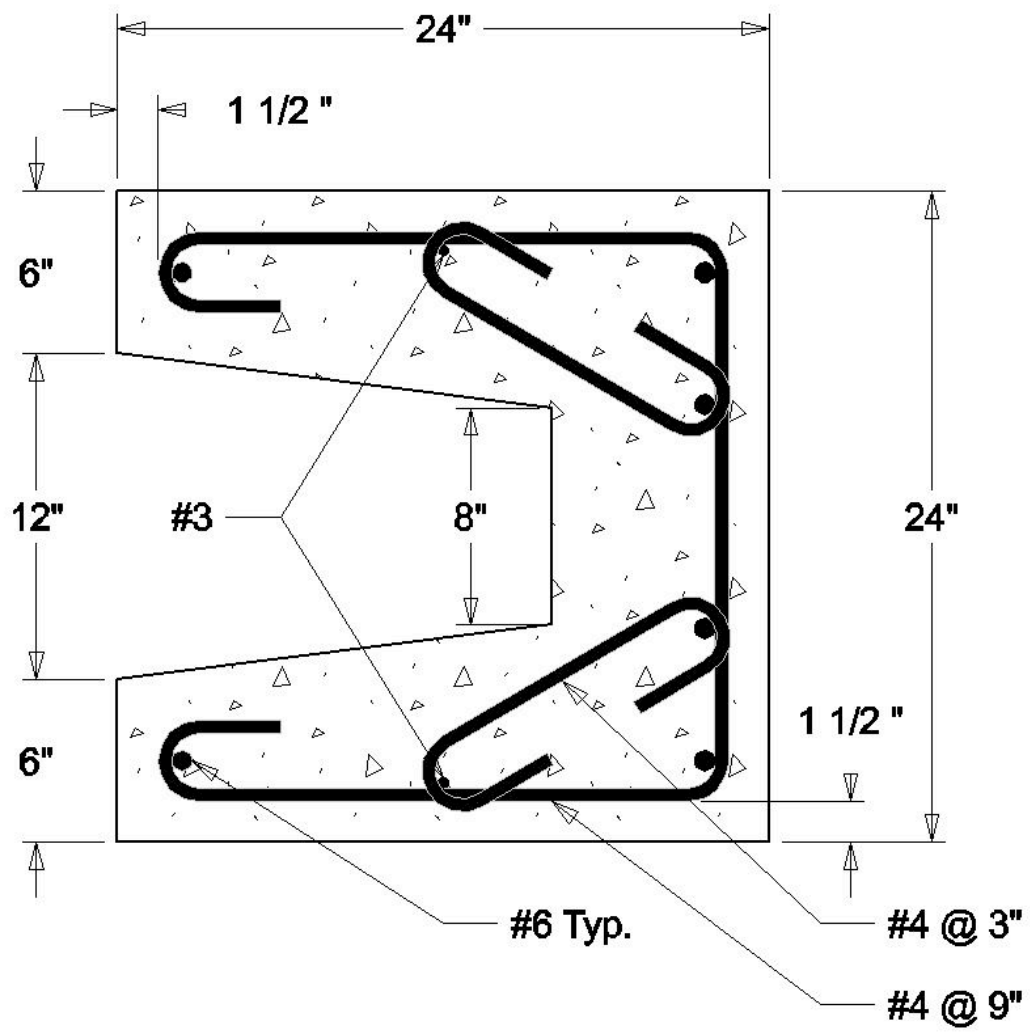


*Figure 4-14 Permanent Reaction Beam Cross-Section (Icaza 2004)*

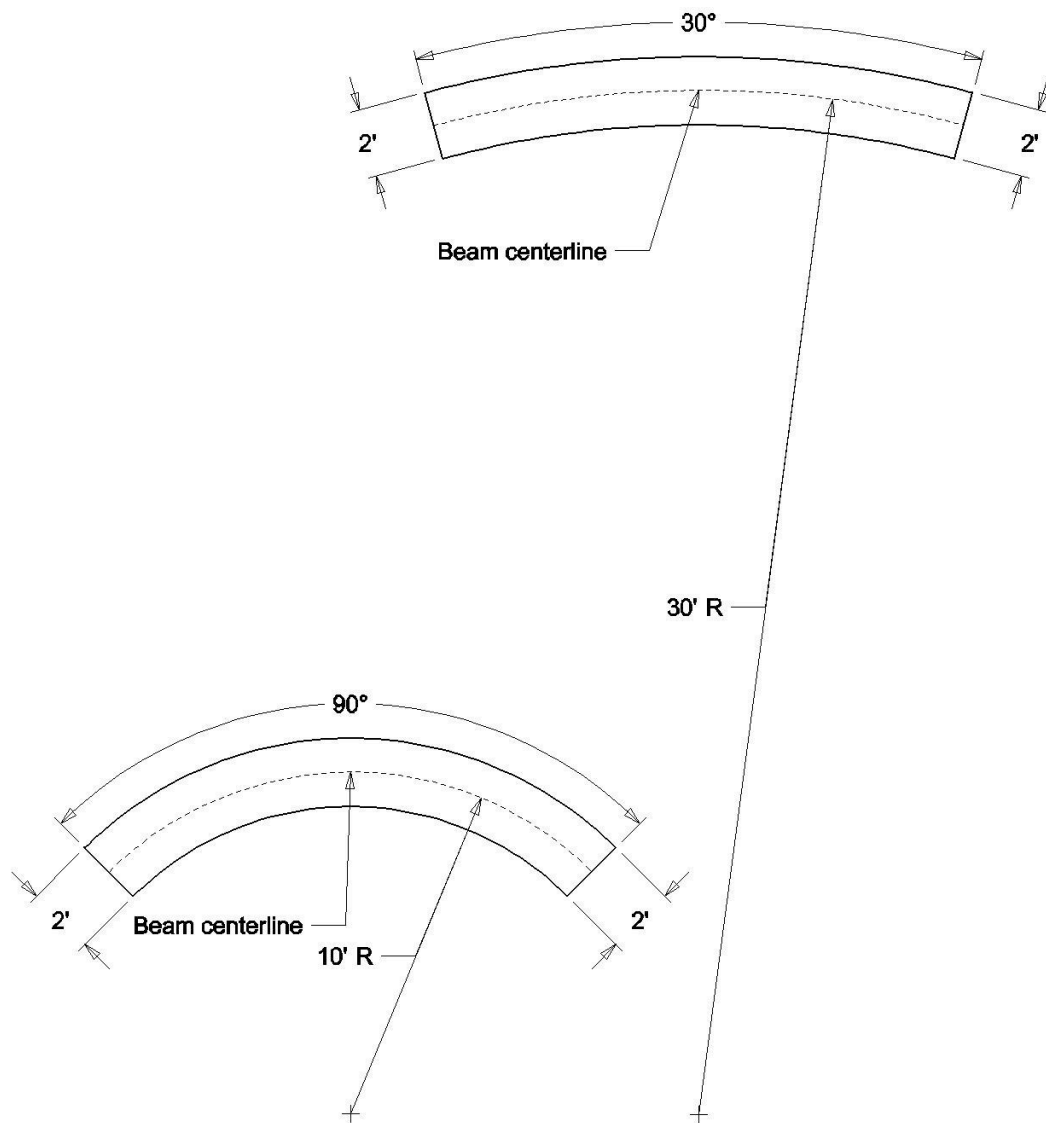


**Figure 4-15 Plan View of Beams (Icaza 2004)**

The replaceable part of each beam had a tapered cross-section, as indicated in the completed cross-section shown in Figure 4-16. Because the permanent reaction beam was designed to carry all loads due to post-tensioning, the initial three sets of specimens (all containing rigid steel pipe) did not contain any mild steel reinforcement. However, after one inner arc cracked during



removal, the remaining specimens were lightly reinforced with two #3 transverse ties spaced at approximately 24 in. and four #3 bars as longitudinal reinforcement, shown in Figure 4-16. This reinforcement prevented cracking and ensured the inner arcs could be removed safely.

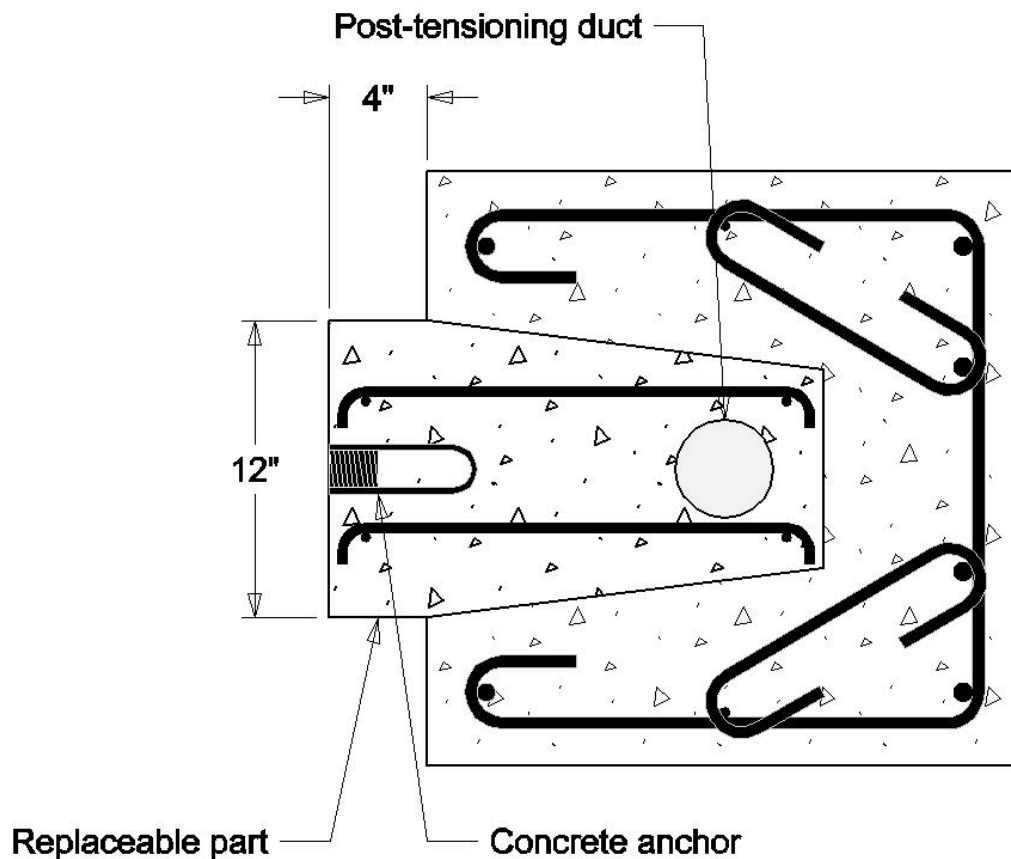


*Figure 4-16 Complete Beam Cross-Section Schematic (Icaza 2004)*

#### **4.5.2.2 Construction Sequence**

A brief overview of the construction sequence for one friction specimen is provided here. Information on the construction of the permanent reaction beams

and more details concerning the construction of the inner arcs can be found in Icaza (2004).

Before casting the inner arc, a debonder was applied to the inner surfaces of the permanent reaction beam. The duct was placed inside the reaction beam cavity, held in place by either wooden blocks (in the case of the rigid steel pipe) or pieces of styrofoam cut to fit the inner portion of the cavity (in the case of the HDPE and galvanized ducts). For most specimens, light reinforcement was also placed inside the cavity. After casting, forms were removed, and the ends of the ducts cut flush with the ends of the beam. A photo of the actual completed cross-section is shown in Figure 4-17.



*Figure 4-17 Complete Beam Cross-Section*

### 4.5.3 Description of Tests

A schematic drawing of the test setup is shown in Figure 4-18. Steel bearing plates were placed on each end of the specimen before placing the ram on the live end and the steel chair with load cells on the dead end. Prior to the main friction tests, a set of tests was performed to determine what friction losses occurred due to the contact between the tendon and the machined holes in the bearing plates and chair. These “hardware” losses could then be subtracted from the total losses measured during friction testing to ensure the results represented only the friction losses occurring inside the duct. A more detailed description of these hardware friction loss tests can be found in Icaza (2004).

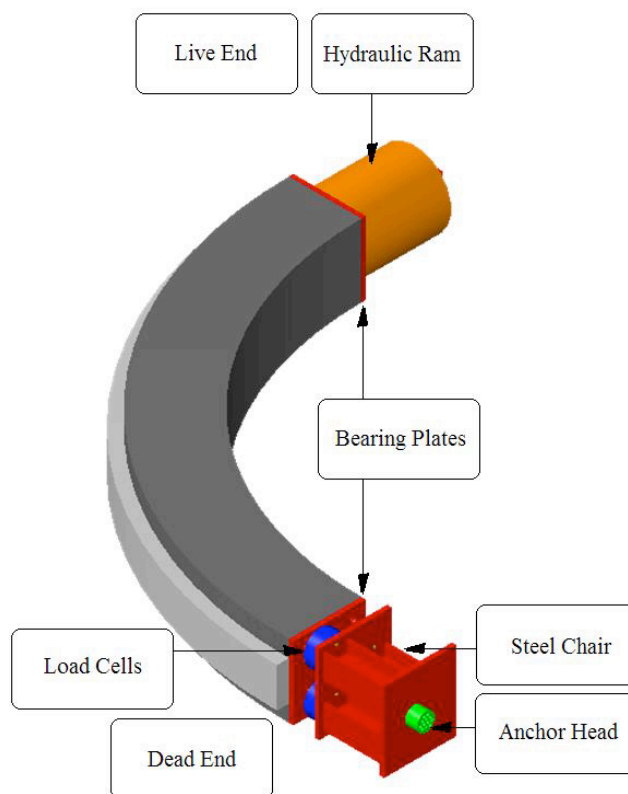


*Figure 4-18 Friction Test Setup (Icaza 2004)*

#### ***4.5.3.1 Instrumentation and Data Acquisition***

Test data consisted of load measurements at both the live and dead ends and displacement measurements at the live end of the specimens. Load measurements were taken at the live end using a 2000-psi electronic pressure transducer. Load measurements were taken at the dead end using three 200-kip load cells. Displacement measurements were taken using linear potentiometers. On the live end, a 5-in. potentiometer was clamped to the bearing plate on the ram cylinder and extended to the body of the ram. Details of the live and dead ends are shown in Figure 4-19 and Figure 4-20, respectively. All instruments were calibrated to ensure accuracy before the first tests were performed.

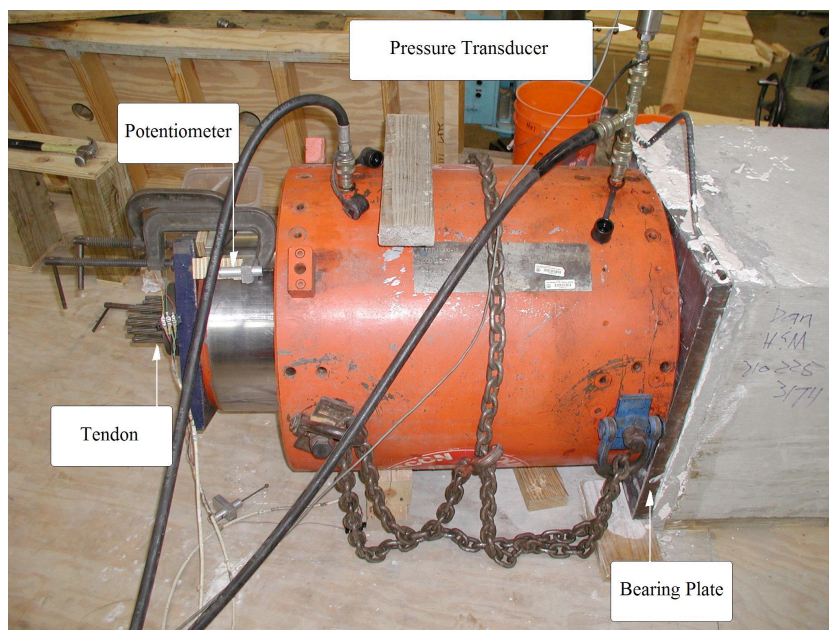


***Figure 4-19 Friction Test Live End Detail***

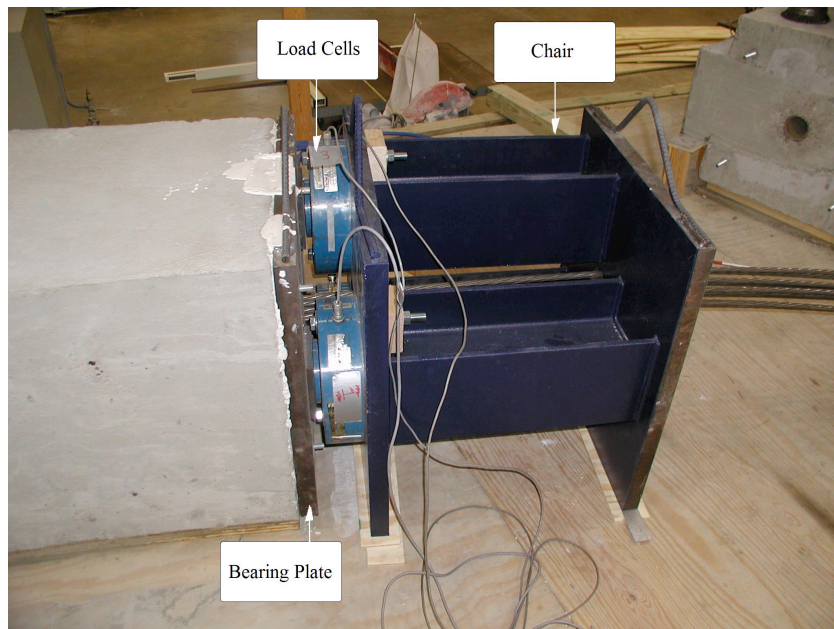


***Figure 4-20 Friction Test Dead End Detail***

The data were read by a Hewlett-Packard HP7500 scanner connected to a desktop personal computer and recorded with National Instruments LabVIEW software, which also provided real-time monitoring.

#### ***4.5.3.2 Testing Sequence***

The following describes the sequence followed during each round of tests, which were done for one radius of curvature (10 ft or 30 ft), one oil (NC205 or 703D), and one duct type (rigid steel pipe, galvanized steel duct, or HDPE duct). In order to test all combinations of variables, there were 12 rounds of tests.

1. One uncoiled tendon was inserted into the beam and anchored to the ram cylinder on the live end and to the steel chair holding the load cells at the dead end. This tendon was stressed to 80% of its guaranteed ultimate tensile strength three separate times, with data being collected at approximately 10-kip load intervals. Steel split

rings were used at the dead end to separate the anchor head from the steel chair. At the completion of each loading cycle, one set of rings was removed and the ram extended at the live end to close the gap. This procedure shifted the tendon along the length of the duct so the tendon would not be in the exact same position during every loading.

2. After the unoiled tests, the anchor head was cut off the live end with a grinder, the tendon was removed, and a new oiled tendon was inserted into the beam. This freshly oiled tendon was stressed twice in the exact same manner as the unoiled tendon.
3. After two tests of the freshly oiled tendon, the same tendon was again tested twice the following day, after the oil had been given time to dry.
4. After removing the tendon, ram, and testing hardware (steel chair with load cells, bearing plates), the inner arc of concrete was removed to allow for the construction of a new specimen.

## **CHAPTER 5**

### **Large-Scale Test Results**

#### **5.1 INTRODUCTION**

This chapter presents test results for large-scale bond and friction tests performed at the University of Texas at Austin. Bond tests were performed by the author and by Diephuis (2004), in many cases in conjunction. Because the results of all bond tests are used to draw conclusions and make recommendations in Chapter 6, tests performed by both parties are presented. The person primarily responsible for testing each specimen is indicated as part of the appropriate subsection heading. Friction tests were performed by Icaza (2004). Although the author did not perform these tests, results are included here because they are used to draw conclusions and make recommendations in Chapter 6.

#### **5.2 BOND TESTS**

This section presents the results from all tests of bond specimens with a 44-in. centerline bonded length. Any exceptions are noted in the appropriate subsection. Table 5-1 presents a summary of the specimens, including duct type, strand surface condition, tester (Diephuis or Lüthi), grout cylinder strength at tendon release, and grout and concrete cylinder strengths at testing. Results for all bond specimens not discussed in this report can be found in Diephuis (2004).

For each specimen, two figures are given. The first shows two plots: one plot shows live end displacement versus load while a second plot shows dead end slip versus load over the entire range of displacements. The second figure has a single plot that shows dead end slip versus load on an amplified scale. A dashed

vertical line is included on the latter plot at 0.02 in., because this value of dead end slip is used for comparison purposes in Chapter 6. The data on all plots were modified as described in Diephuis (2004) to eliminate displacements registered in the initial stages of loading as the hydraulic ram came into full contact with the specimen.

A naming scheme was used to distinguish among the various specimens. The scheme denotes strand surface condition, duct type, tendon angle change, and specimen number as described below:

- A number denotes strand surface condition. The number “0” indicates the tendon was unoiled, “1” indicates the tendon was oiled with Trukut NC205, and “2” indicates the tendon was oiled with NoxRust 703D. If the oil was allowed to dry for ten days before grouting, the initial number is followed by an asterisk (\*).
- A two-letter combination indicates duct type. “SP” denotes a rigid steel pipe, “GD” denotes a galvanized duct, and “HD” denotes an HDPE duct.
- Total tendon angle change from one end of the duct to the other is given in degrees. All the specimens discussed in this section had an angle change of 7.5 degrees, which corresponds to a centerline bonded length of 44 in. Some specimens tested by Diephuis (2004) had different angle changes.
- The specimen number is given to distinguish among otherwise identical specimens. The number indicates the order in which the specimens were tested.

For example, specimen 2-HD-7.5°-2 contained a tendon oiled with NoxRust 703D inside an HDPE duct; the total tendon angle change was 7.5 degrees, and the specimen was the second of this type to be tested.



**Table 5-1 Bond Specimen Summary**

Specimen Name	Duct Type	Surface Condition	Tester	Grout Strength Release (psi)	Grout Strength Test (psi)	Concrete Strength Test (psi)
0-SP-7.5°-1	rigid pipe	unoiled	Diephuis	8680	9110	7160
0-SP-7.5°-2	rigid pipe	unoiled	Diephuis	8680	9110	7160
0-SP-7.5°-3	rigid pipe	unoiled	Lüthi	7730	7610	4720
0-SP-7.5°-4	rigid pipe	unoiled	Lüthi	7730	7610	4720
1-SP-7.5°-1	rigid pipe	NC205	Diephuis	8360	8290	8080
1-SP-7.5°-2	rigid pipe	NC205	Diephuis	8360	8290	8080
2-SP-7.5°-1	rigid pipe	703D	Lüthi	7990	8100	3780
2-SP-7.5°-2	rigid pipe	703D	Lüthi	7990	8100	3780
0-GD-7.5°-1	galvanized	unoiled	Diephuis	8210	8530	5650
0-GD-7.5°-2	galvanized	unoiled	Diephuis	8380	8655	5980
0-GD-7.5°-3	galvanized	unoiled	Diephuis	8380	8655	5980
1-GD-7.5°-1	galvanized	NC205	Diephuis	8620	7600	7450
1-GD-7.5°-2	galvanized	NC205	Diephuis	8620	7600	7450
2-GD-7.5°-1	galvanized	703D	Lüthi	8880	8650	8440
2-GD-7.5°-2	galvanized	703D	Lüthi	8880	8650	8440
2-GD-7.5°-3	galvanized	703D	Lüthi	8180	8550	5900
2-GD-7.5°-4	galvanized	703D	Lüthi	8180	8550	5900
1*-GD-7.5°-1	galvanized	NC205, 10 days drying time	Lüthi	8770	8810	6800
1*-GD-7.5°-2	galvanized	NC205, 10 days drying time	Lüthi	not available	not available	7290

**Table 5-1 (Cont.) Bond Specimen Summary**

Specimen Name	Duct Type	Surface Condition	Tester	Grout Strength Release (psi)	Grout Strength Test (psi)	Concrete Strength Test (psi)
0-HD-7.5 <sup>o</sup> -1	HDPE	unoiled	Diephuis	7660	7980	7140
0-HD-7.5 <sup>o</sup> -2	HDPE	unoiled	Diephuis	8520	8370	6600
0-HD-7.5 <sup>o</sup> -3	HDPE	unoiled	Diephuis	8520	8370	6600
1-HD-7.5 <sup>o</sup> -1	HDPE	NC205	Diephuis	8560	9780	8080
1-HD-7.5 <sup>o</sup> -2	HDPE	NC205	Diephuis	8560	9780	8080
2-HD-7.5 <sup>o</sup> -1	HDPE	703D	Lüthi	8340	8710	8380
2-HD-7.5 <sup>o</sup> -2	HDPE	703D	Lüthi	7920	8140	6700
2-HD-7.5 <sup>o</sup> -3	HDPE	703D	Lüthi	7920	8140	6700
1*-HD-7.5 <sup>o</sup> -1	HDPE	NC205, 10 days drying time	Lüthi	8770	8810	6800
1*-HD-7.5 <sup>o</sup> -2	HDPE	NC205, 10 days drying time	Lüthi	not available	not available	7290

## **5.2.1 Steel Pipe Specimens**

Two pairs of steel pipe specimens with unoiled tendons were tested. During testing of the first pair, the initial failure occurred at the duct-concrete interface, and the pipe began pulling out of the concrete. In order to prevent this failure mode, an additional pair of specimens was constructed with four shear studs welded to the underside of each pipe and distributed along its length. These studs kept the pipe in place during testing and ensured that pullout failure occurred either at the strand-grout or grout-duct interface. Results are reported here for all four specimens with unoiled tendons.

One pair of steel pipe specimens containing tendons oiled with NC205 were tested, as were one pair of specimens containing tendons oiled with 703D.

### ***5.2.1.1 0-SP-7.5<sup>o</sup>-1 (Diephuis)***

Live end load-displacement and dead end load-slip response for 0-SP-7.5<sup>o</sup>-1 are shown in Figure 5-1. The figure indicates that a peak load of 67.1 kip was achieved, at which point a pronounced reduction in resistance occurred. The dead end load-slip response is shown on an amplified scale in Figure 5-2. The figure indicates that dead end slip did not reach 0.02 in. before failure.

Failure of this specimen occurred at the duct-concrete interface. Figure 5-3 shows the specimen after testing, with the duct and tendon pulled several inches out of the specimen.

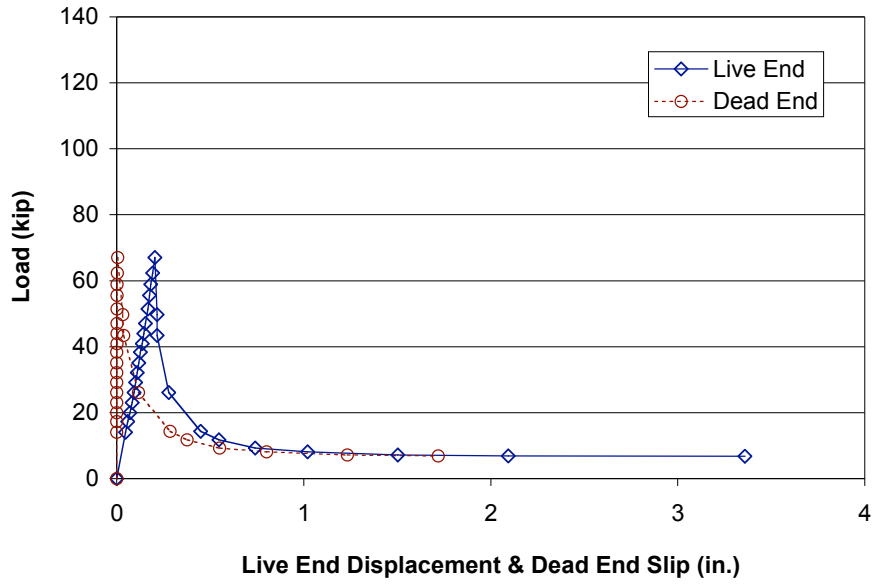


**Figure 5-1 Live End Load-Displacement and Dead End Load-Slip Behavior for Specimen 0-SP-7.5°-1**

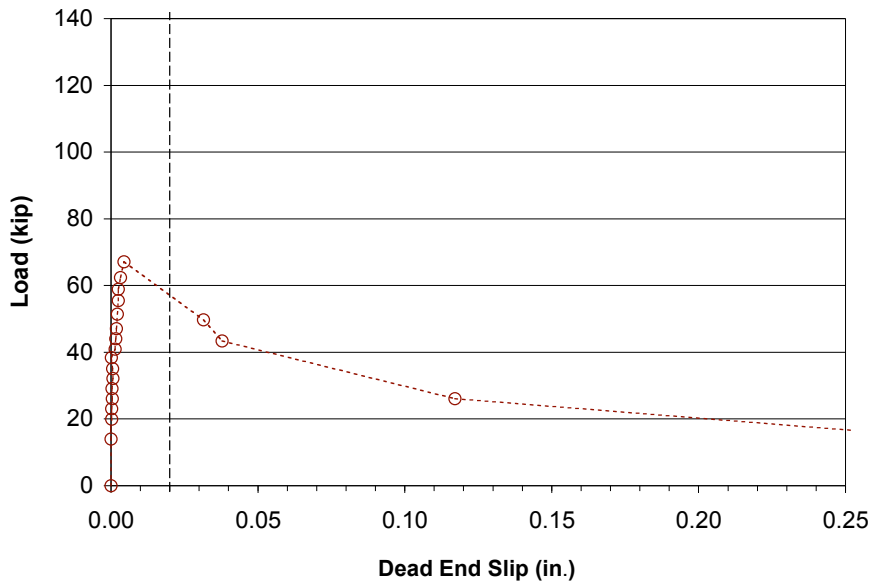


**Figure 5-2 Dead End Load-Slip Response for Specimen 0-SP-7.5°-1, Amplified Scale**



*Figure 5-3 Live End of Specimen 0-SP-7.5°-1 after Testing*

#### **5.2.1.2 0-SP-7.5°-2 (Diephuis)**

Live end load-displacement and dead end load-slip response for 0-SP-7.5°-2 are shown in Figure 5-4. The figure indicates that a peak load of 89.1 kip was achieved, at which point a pronounced reduction in resistance occurred. The dead end load-slip response is shown on an amplified scale in Figure 5-5. The figure indicates that dead end slip did not reach 0.02 in. before failure.

Failure of this specimen occurred at the duct-concrete interface. Figure 5-6 shows the specimen after testing, with the duct and tendon pulled several inches out of the specimen.

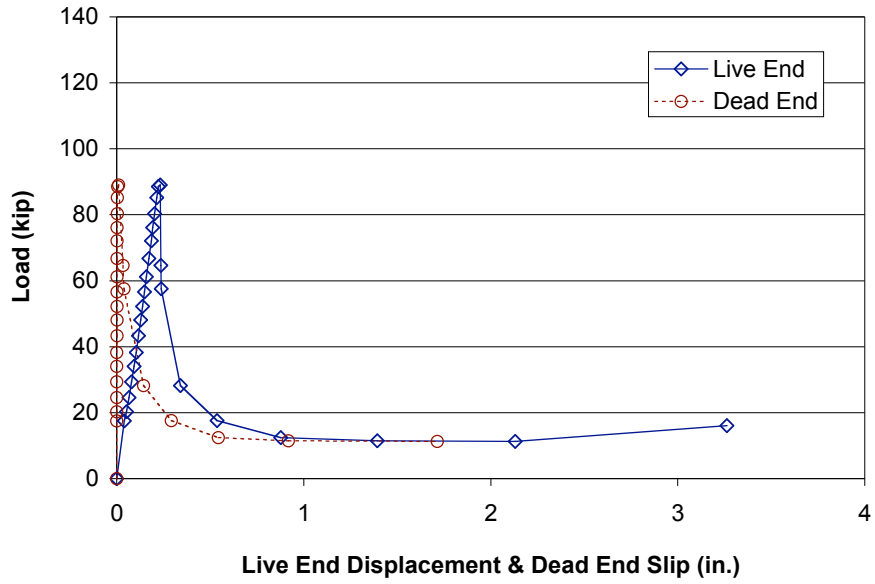


**Figure 5-4 Live End Load-Displacement and Dead End Load-Slip Behavior for Specimen 0-SP-7.5°-2**

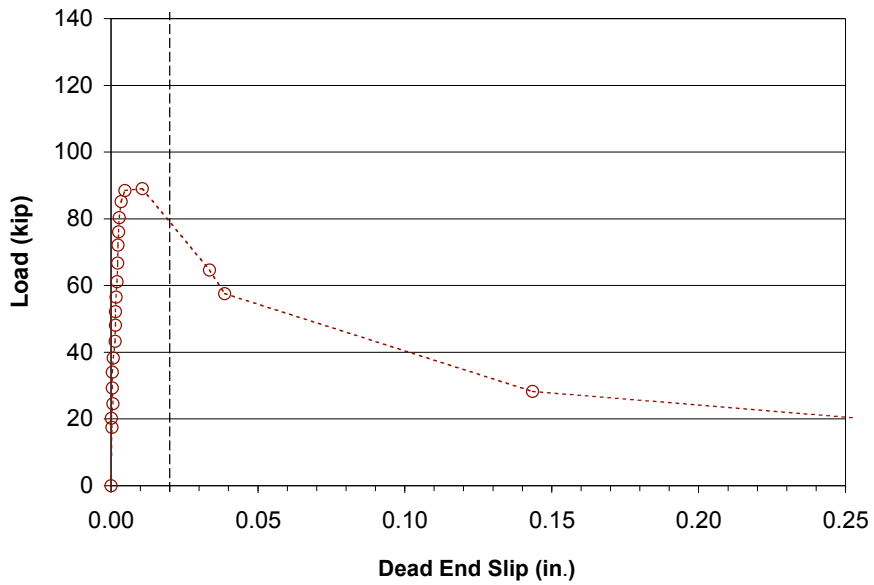


**Figure 5-5 Dead End Load Slip Response for Specimen 0-SP-7.5°-2, Amplified Scale**



*Figure 5-6 Live End of Specimen 0-SP-7.5°-2 after Testing*

#### **5.2.1.3 0-SP-7.5°-3 (Lüthi)**

Live end load-displacement and dead end load-slip response for 0-SP-7.5°-3 are shown in Figure 5-7. The figure indicates that an initial peak load of 64.1 kip was achieved, at which point a reduction in resistance occurred. The dead end load-slip response is shown on an amplified scale in Figure 5-8. The figure indicates that dead end slip reached 0.02 in. at a load of 58.9 kip, and very little dead end slip occurred prior to a load of approximately 40 kip.

Failure of this specimen occurred at the grout-duct interface. After the initial peak load was reached, the resistance dropped by more than a third and then began increasing again. This trend was presumably due to the misalignment of the ram and the grout plug as the plug was pulled from the specimen. The ram

pulled the grout plug normal to the face of the specimen while the plug rotated out of the specimen as a rigid body through the curved duct. Misalignment caused mechanical interlock, which allowed the load to exceed the initial peak level. Toward the end of testing, the shear studs failed and the pipe began pulling out of the concrete. This secondary failure occurred well after the initial failure. A photograph of this specimen after testing was not available.

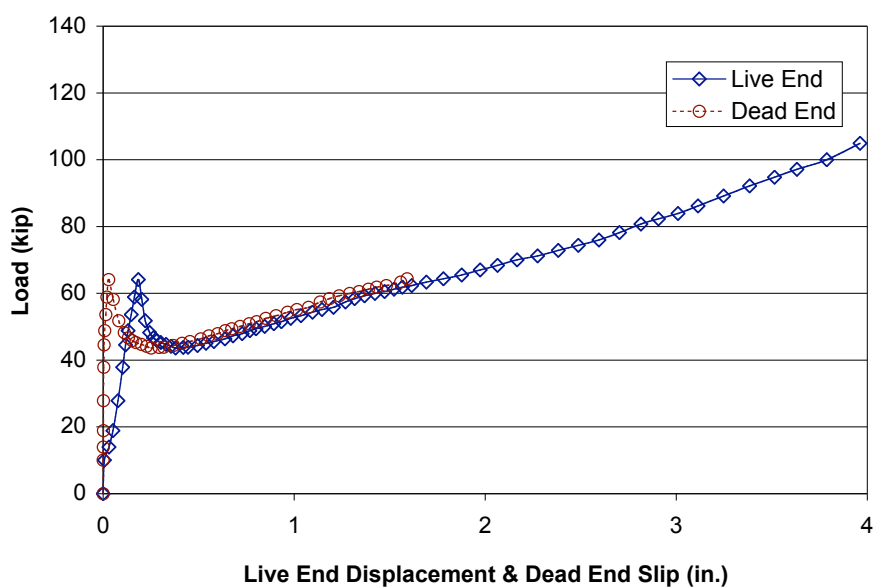


***Figure 5-7 Live End Load-Displacement and Dead End Load-Slip Response for Specimen 0-SP-7.5°-3***



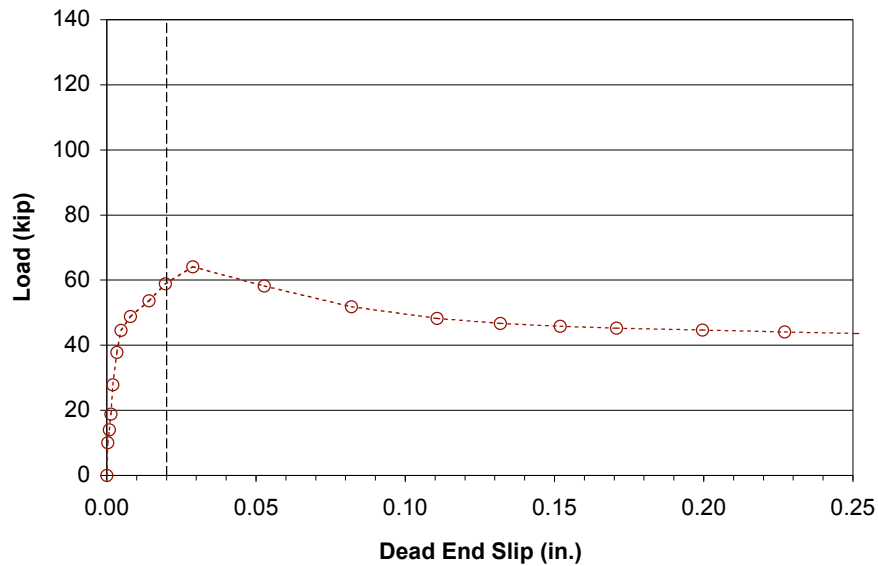


***Figure 5-8 Dead End Load-Slip Response for Specimen 0-SP-7.5°-3, Amplified Scale***

***5.2.1.4 0-SP-7.5°-4 (Lüthi)***

Live end load-displacement and dead end load-slip response for 0-SP-7.5°-4 are shown in Figure 5-9. The figure indicates that an initial peak load of 54.0 kip was achieved, at which point a reduction in resistance occurred. The dead end load-slip response is shown on an amplified scale in Figure 5-10. The figure indicates that dead end slip reached 0.02 in. at the initial peak load, and very little dead end slip occurred prior to a load of approximately 40 kip.

Failure of this specimen occurred at the grout-duct interface. After the initial peak load was reached, the resistance dropped by about one-third and then began increasing again. This trend was presumably due to the interlock of the grout plug and the duct as described in Section 5.2.1.3. A photograph of this specimen after testing was not available.

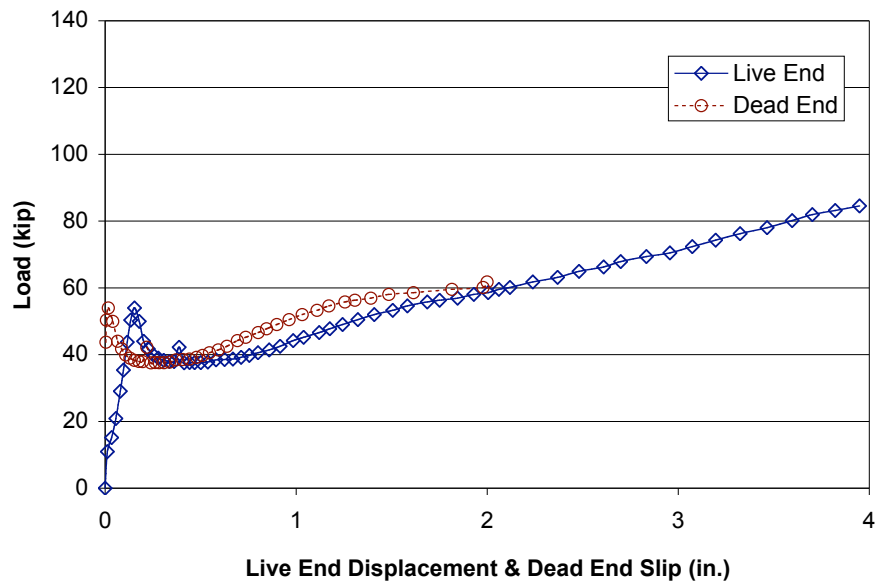


**Figure 5-9 Live End Load-Displacement and Dead End Load-Slip Response for Specimen 0-SP-7.5°-4**

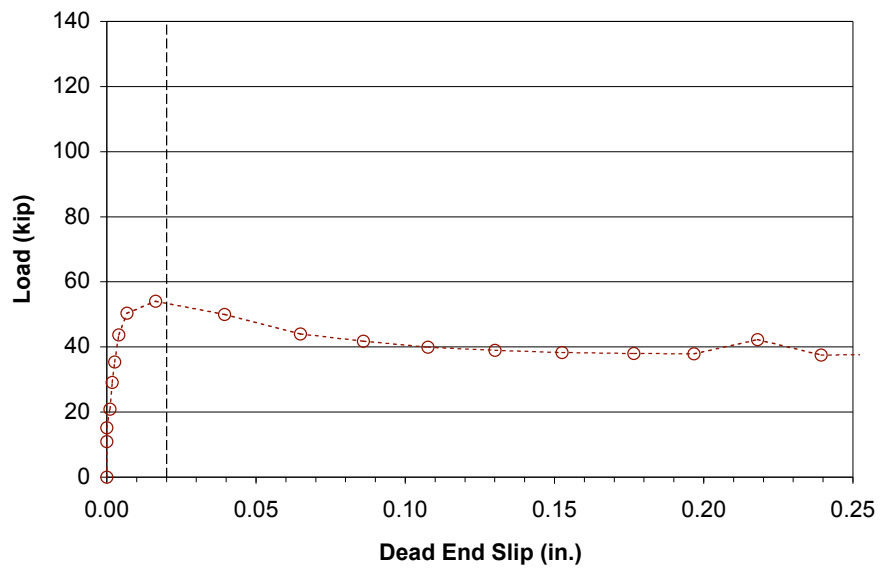


**Figure 5-10 Dead End Load-Slip Response for Specimen 0-SP-7.5°-4, Amplified Scale**

#### **5.2.1.5 1-SP-7.5<sup>o</sup>-1 (Diephuis)**

Live end load-displacement and dead end load-slip response for 1-SP-7.5<sup>o</sup>-1 are shown in Figure 5-11. The figure indicates that an initial peak load of 39.3 kip was achieved, at which point a significant reduction in resistance occurred. The dead end load-slip response is shown on an amplified scale in Figure 5-12. The figure indicates that dead end slip reached 0.02 in. at a load of 4.1 kip, and significant dead end slip began accumulating immediately upon loading.

This specimen failed in multiple modes. Immediately upon loading, the tendon began slipping relative to the grout. After approximately 0.1 in. of slip, the grout began to slip relative to the pipe. Finally, as the peak load was reached, the pipe began to slip relative to the concrete.

Upon removal of the hydraulic ram after testing, a dark residue was observed on the top of the grout plug. The residue was most likely oil which had dripped off the strands and accumulated in the duct before grouting. This residual oil may have contributed to the failure observed at the grout-duct interface. Figure 5-13 shows the specimen after testing.

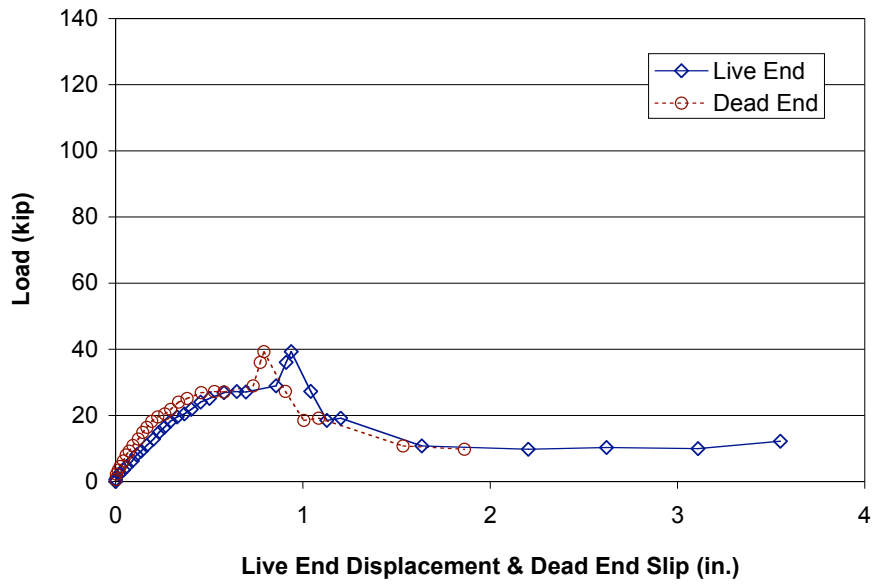


**Figure 5-11 Live End Load-Displacement and Dead End Load-Slip Response for Specimen 1-SP-7.5°-1**

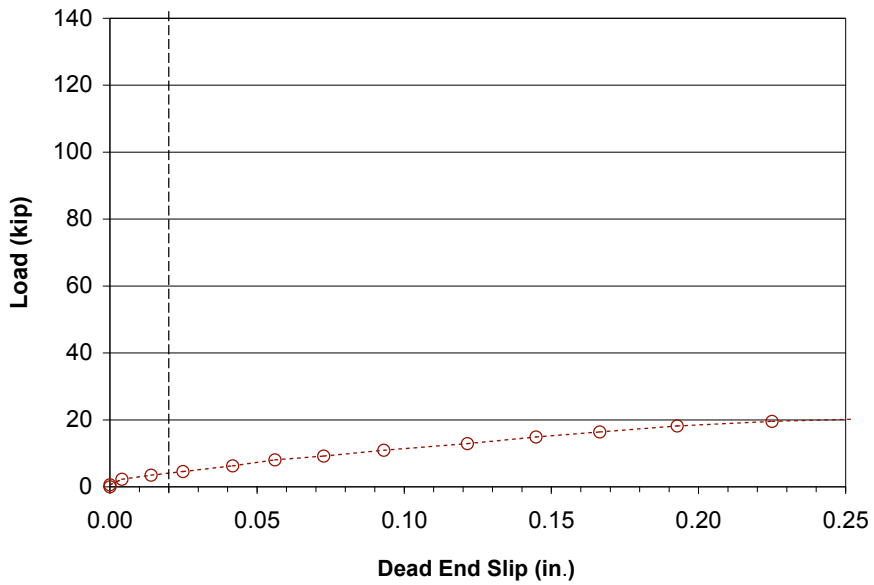


**Figure 5-12 Dead End Load-Slip Response for Specimen 1-SP-7.5°-1, Amplified Scale**



*Figure 5-13 Live End of Specimen 1-SP-7.5°-1 after Testing*

#### **5.2.1.6 1-SP-7.5°-2 (Diephuis)**

Live end load-displacement and dead end load-slip response for 1-SP-7.5°-2 are shown in Figure 5-14. The figure indicates that a load of 32.3 kip was achieved before the load spiked sharply to 76.3 kip. At this point the pipe began pulling out of the beam, and the load dropped rapidly. The dead end load-slip response is shown on an amplified scale in Figure 5-15. The figure indicates that dead end slip reached 0.02 in. at a load of 4.1 kip, and significant dead end slip began accumulating immediately upon loading.

Initial failure of this specimen occurred at the grout-duct interface. At a load of 32.9 kip and a live end displacement of over 3 in., there was a sharp spike in the load, presumably due to the grout plug “kinking” inside the duct as

described in Section 5.2.1.3. At this point, failure occurred at the duct-concrete interface, and the pipe began pulling out of the beam.

Upon removal of the hydraulic ram after testing, a dark residue was observed on the top of the grout plug. The residue was most likely oil which had dripped off the strands and accumulated in the duct before grouting. This residual oil may have contributed to the failure observed at the grout-duct interface. Figure 5-16 shows the specimen after testing.

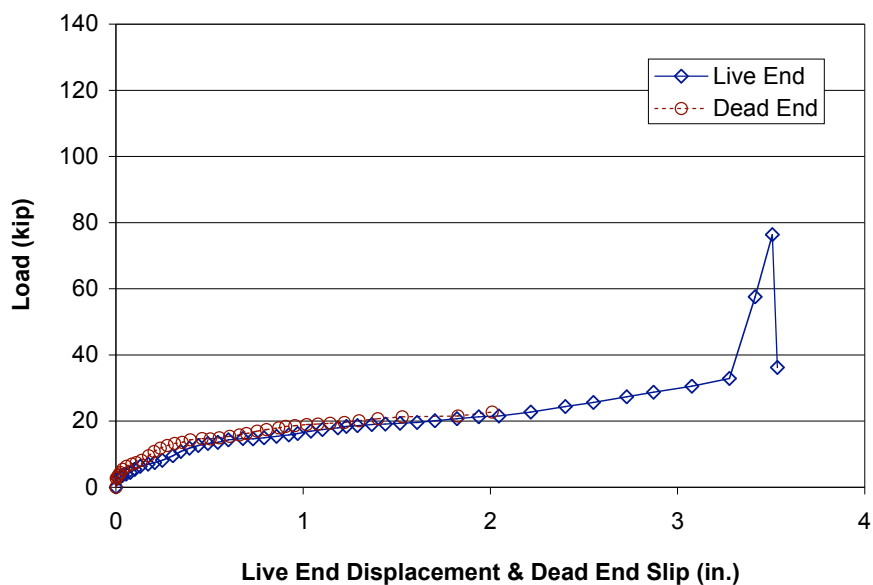


**Figure 5-14 Live End Load-Displacement and Dead End Load-Slip Response for Specimen 1-SP-7.5°-2**

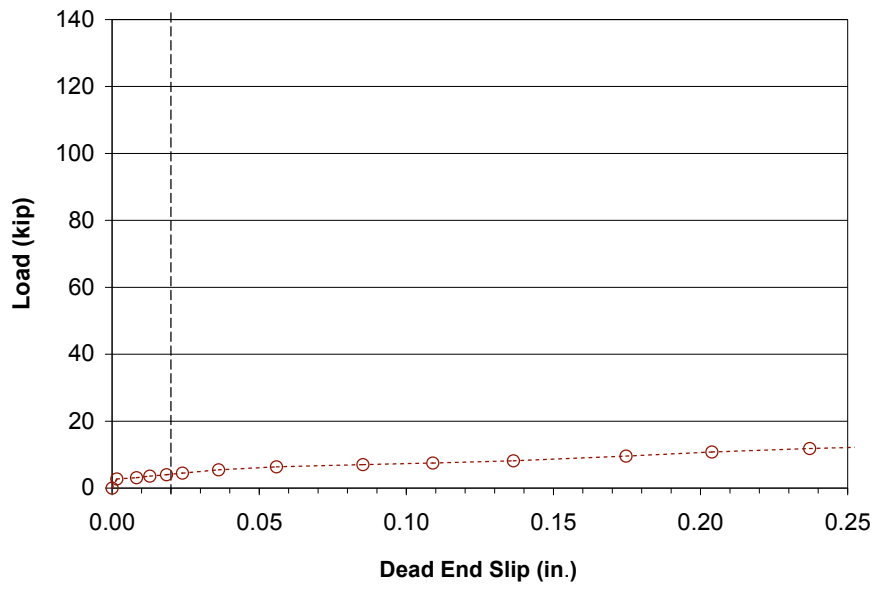


***Figure 5-15 Dead End Load-Slip Response for Specimen 1-SP-7.5°-2, Amplified Scale***



***Figure 5-16 Live End of Specimen 1-SP-7.5°-2 after Testing***

### 5.2.1.7 2-SP-7.5<sup>o</sup>-1 (Lüthi)

Live end load-displacement and dead end load-slip response for 2-SP-7.5<sup>o</sup>-1 are shown in Figure 5-17. The figure indicates that a peak load of 75.5 kip was achieved. The dead end load-slip response is shown on an amplified scale in Figure 5-18. The figure indicates that dead end slip reached 0.02 in. at a load of 18.9 kip, and significant dead end slip began accumulating after the load reached approximately 10 kip.

Failure of this specimen occurred at the grout-duct interface but did not result in a drop in resistance. The load steadily increased over the entire range of displacements. Toward the end of testing, the pipe began pulling out of the concrete. This secondary failure occurred well after the initial failure. Figure 5-19 shows the specimen after testing.

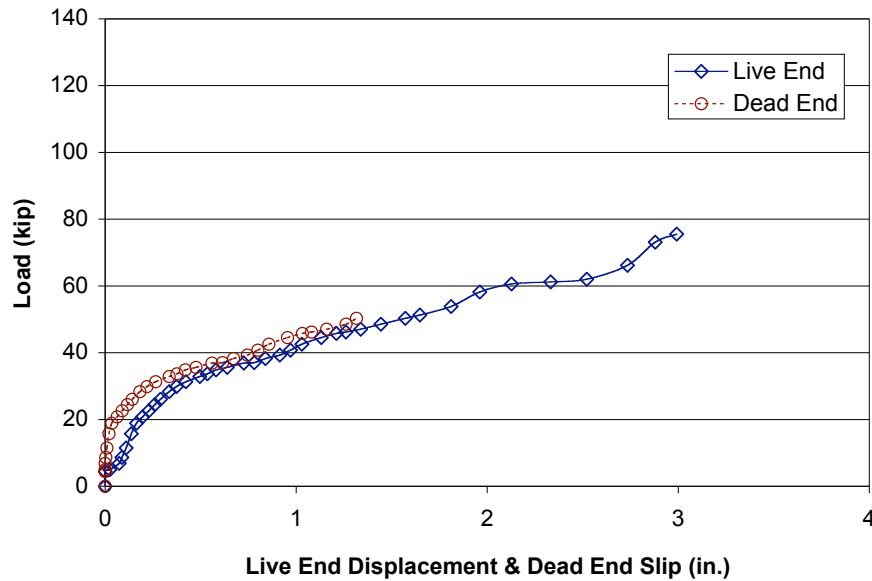


**Figure 5-17 Live End Load-Displacement and Dead End Load-Slip Response for Specimen 2-SP-7.5<sup>o</sup>-1**



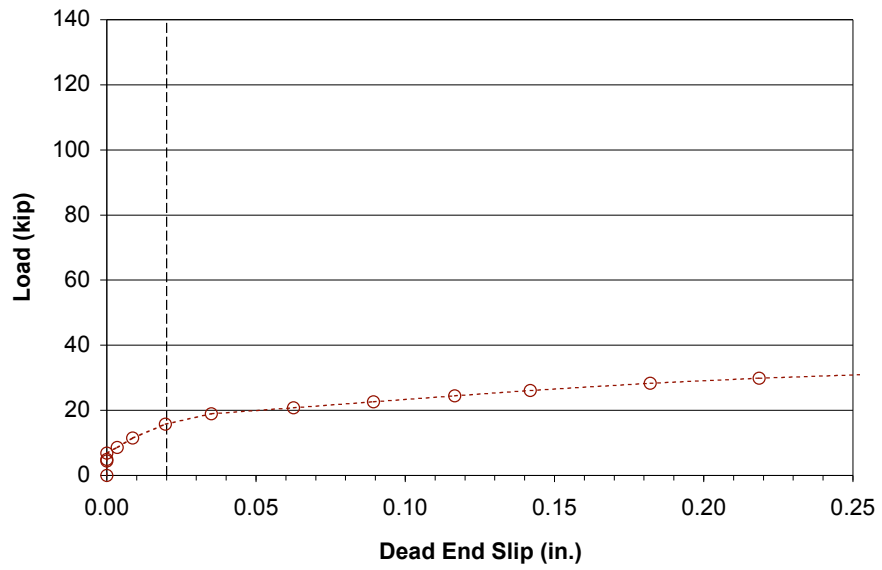


***Figure 5-18 Dead End Load-Slip Response for Specimen 2-SP-7.5<sup>0</sup>-1, Amplified Scale***



***Figure 5-19 Live End of Specimen 2-SP-7.5<sup>0</sup>-1 after Testing***

### 5.2.1.8 2-SP-7.5°-2 (Lüthi)

Live end load-displacement and dead end load-slip response for 2-SP-7.5°-2 are shown in Figure 5-20. The figure indicates that a peak load of 58.5 kip was achieved. The dead end load-slip response is shown on an amplified scale in Figure 5-21. The figure indicates that dead end slip reached 0.02 in. at a load of 14.6 kip, and significant dead end slip began accumulating after the load reached approximately 10 kip.

Failure of this specimen occurred at the grout-duct interface but did not result in a drop in resistance. The load steadily increased over the entire range of displacements. Figure 5-22 shows the specimen after testing.

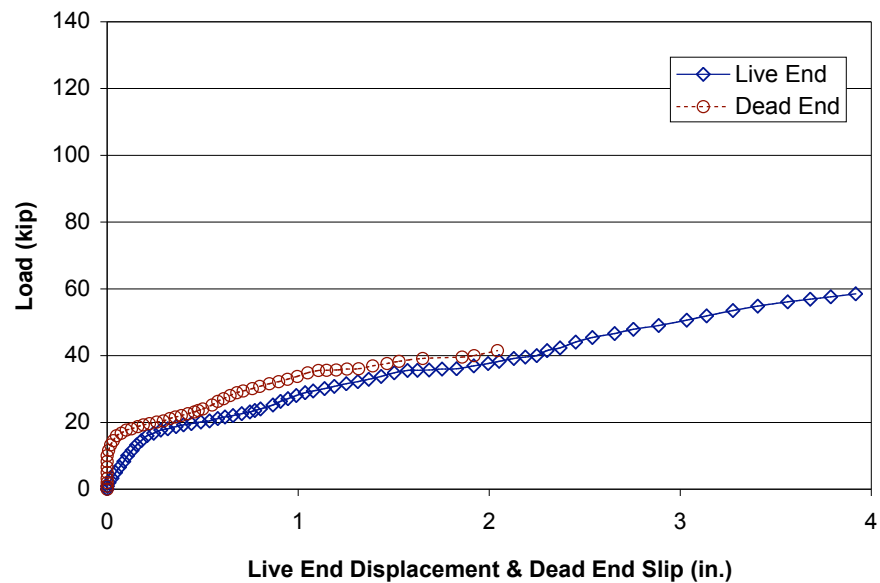


**Figure 5-20 Live End Load-Displacement and Dead End Load-Slip Response for 2-SP-7.5°-2**

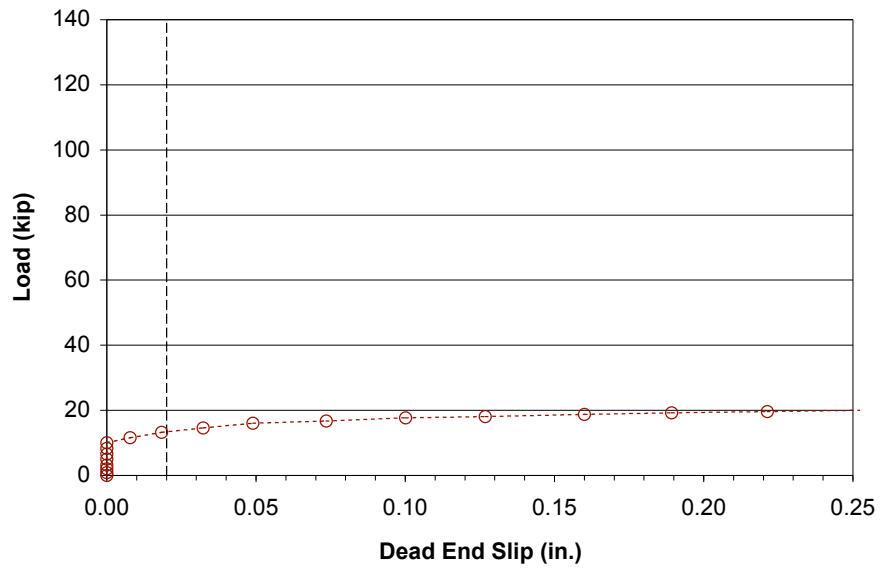


***Figure 5-21 Dead End Load-Slip Response for Specimen 2-SP-7.5<sup>0</sup>-2, Amplified Scale***



***Figure 5-22 Live End of Specimen 2-SP-7.5<sup>0</sup>-2 after Testing***

## 5.2.2 Galvanized Duct Specimens

Three galvanized duct specimens with unoiled tendons were tested. The first specimen was part of a mismatched pair tested in order to determine the appropriate centerline bonded length for all tests. That pair consisted of one specimen with a 5 degree tendon angle change and a centerline bonded length of 31.4 in., and one specimen with a 7.5 degree tendon angle change and a centerline bonded length of 44.0 in. This latter size was determined to be the most appropriate, and subsequent tests were performed in matching pairs. For completeness, this original “test length” specimen (0-GD-7.5°-1) is discussed in addition to the pair of specimens constructed later (0-GD-7.5°-2 and 0-GD-7.5°-3).

One pair of specimens containing tendons oiled with NC205 were tested, as were two pairs containing tendons oiled with 703D. An extra pair of these latter specimens was constructed and tested because of inconsistent results between the first two specimens.

### 5.2.2.1 0-GD-7.5°-1 (*Diephuis*)

Live end load-displacement and dead end load-slip response for 0-GD-7.5°-1 are shown in Figure 5-23. The figure indicates that an initial peak load of 382 kip was achieved, at which point a sharp reduction in resistance occurred. The dead end load-slip response is shown on an amplified scale in Figure 5-24. The figure indicates that dead end slip reached 0.02 in. at a load of 307 kip, and dead end slip began accumulating immediately upon loading.

Failure occurred in this specimen at the tendon-grout interface. After the initial peak load was reached, the resistance dropped and then began increasing again. This trend was presumably due to mechanical interlock between the grout and the irregular surface of the duct as the tendon moved through the specimen.

Significant cracking occurred at the initial peak load. Figure 5-25 shows the pattern of cracking observed in the specimen, with splitting cracks radiating out from the duct. The crack on top of the specimen extended to the live end, and cracks on the sides of the specimen extended approximately three-quarters of the length of the specimen.

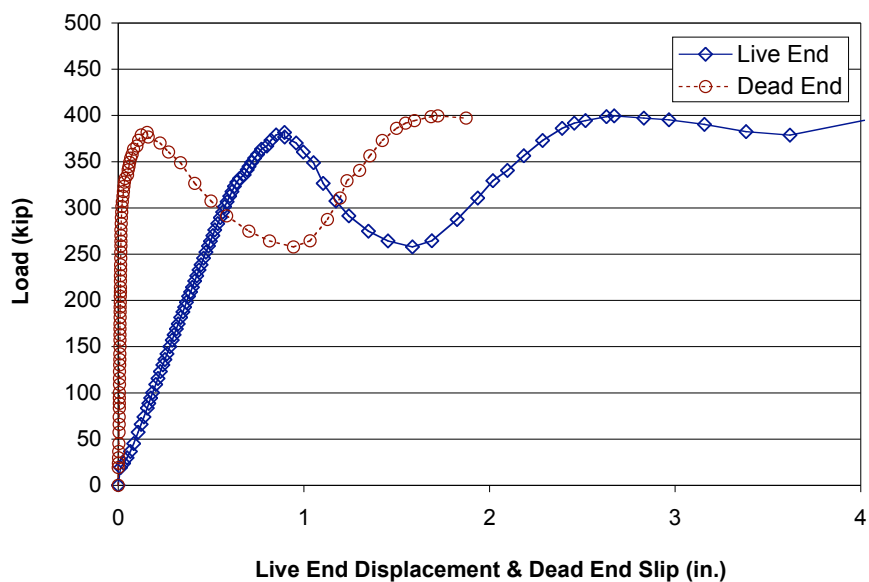


**Figure 5-23 Live End Load-Displacement and Dead End Load-Slip Response for Specimen 0-GD-7.5°-1**

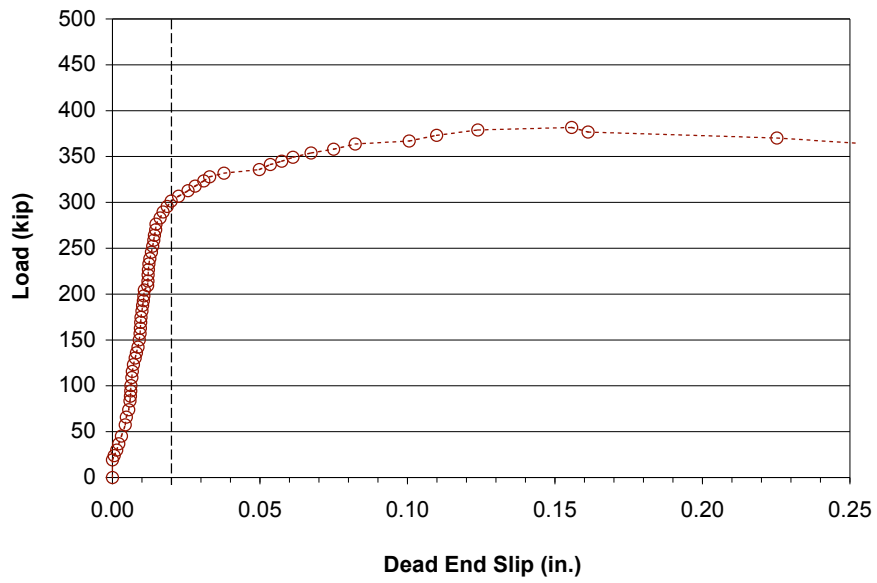


***Figure 5-24 Dead End Load-Slip Response for Specimen 0-GD-7.5°-1, Amplified Scale***



***Figure 5-25 Profile of Specimen 0-GD-7.5°-1 after Testing***

#### **5.2.2.2 0-GD-7.5°-2 (Diephuis)**

Live end load-displacement and dead end load-slip response for 0-GD-7.5°-2 are shown in Figure 5-26. The figure indicates that an initial peak load of 345 kip was achieved, at which point a sharp reduction in resistance occurred. The dead end load-slip response is shown on an amplified scale in Figure 5-27. The figure indicates that dead end slip reached 0.02 in. at a load of 276 kip, and very little dead end slip occurred prior to a load of approximately 250 kip.

Failure occurred in this specimen at the tendon-grout interface. After the initial peak load was reached, the resistance dropped and then began increasing again. This trend was presumably due to mechanical interlock between the grout and the irregular surface of the duct as the tendon moved through the specimen.

Significant cracking occurred at the initial peak load. Figure 5-28 shows the pattern of cracking observed in the specimen, with one large splitting crack running down the entire length of the center of the specimen.

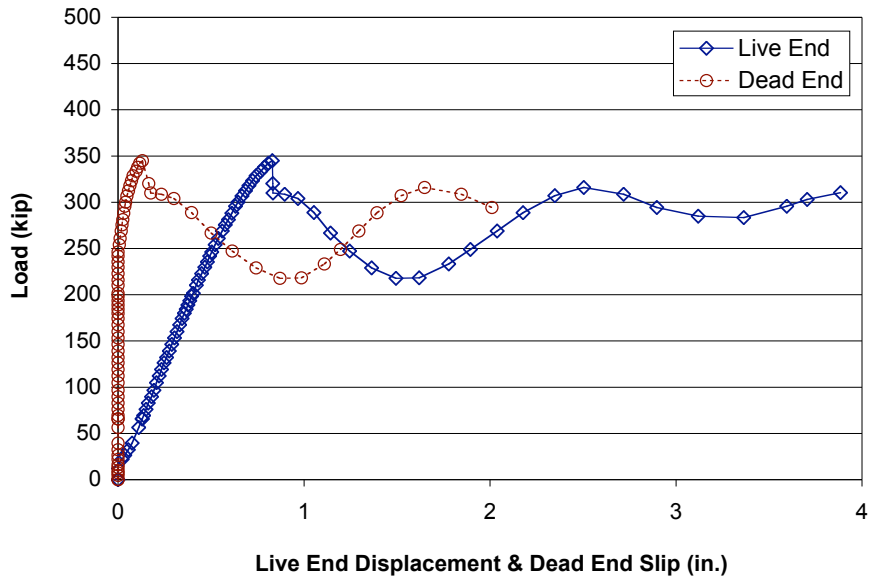


**Figure 5-26 Live End Load-Displacement and Dead End Load-Slip Response for Specimen 0-GD-7.5°-2**

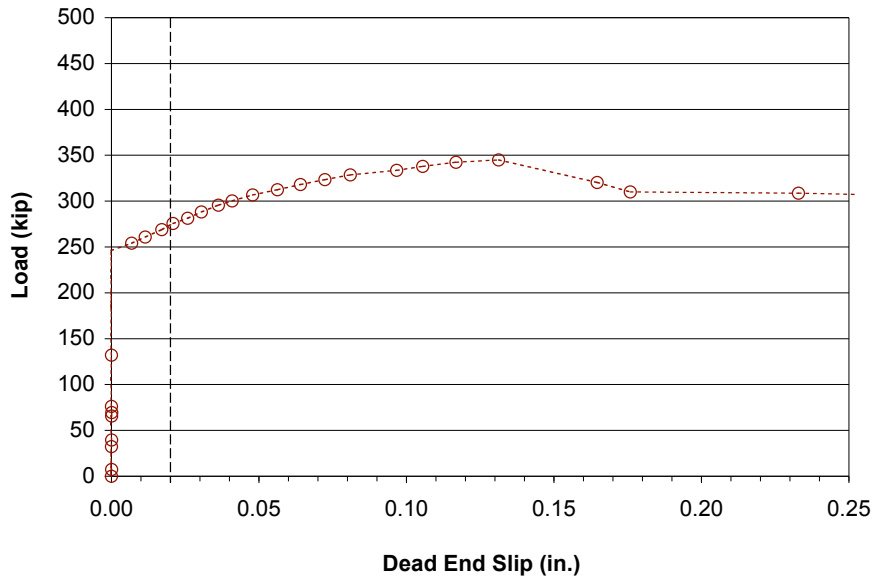


**Figure 5-27 Dead End Load-Slip Response for Specimen 0-GD-7.5°-2, Amplified Scale**



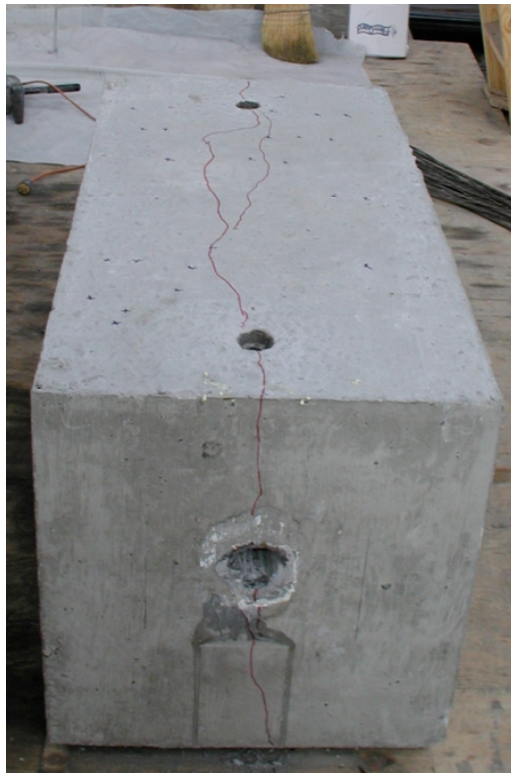


*Figure 5-28 Photo of Specimen 0-GD-7.5°-2 after Testing*

#### **5.2.2.3 0-GD-7.5°-3 (Diephuis)**

Live end load-displacement and dead end load-slip response for 0-GD-7.5°-3 are shown in Figure 5-29. The figure indicates that an initial peak load of 360 kip was achieved, at which point a sharp reduction in resistance occurred. The dead end load-slip response is shown on an amplified scale in Figure 5-30. The figure indicates that dead end slip reached 0.02 in. at a load of 306 kip, and dead end slip began accumulating after the load reached approximately 80 kip.

Failure occurred in this specimen at the tendon-grout interface. After the initial peak load was reached, the resistance dropped and then began increasing again. This trend was presumably due to mechanical interlock between the grout and the irregular surface of the duct as the tendon moved through the specimen.

Significant cracking occurred at the initial peak load. Figure 5-31 shows the pattern of cracking observed in the specimen, with splitting cracks radiating out from the duct. The crack on top of the specimen extended to the live end, and cracks on the sides of the specimen extended approximately three-quarters of the length of the specimen.

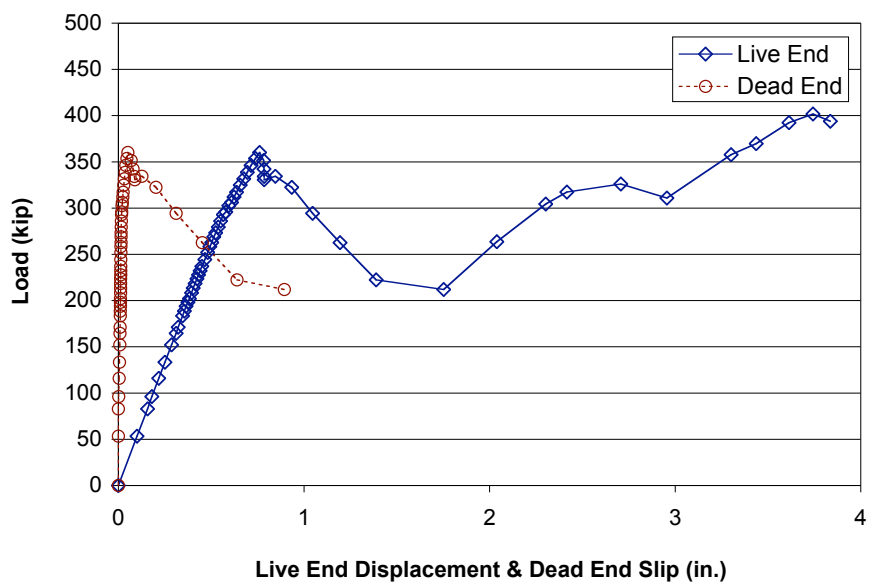


**Figure 5-29 Live End Load-Displacement and Dead End Load-Slip Response for Specimen 0-GD-7.5°-3**

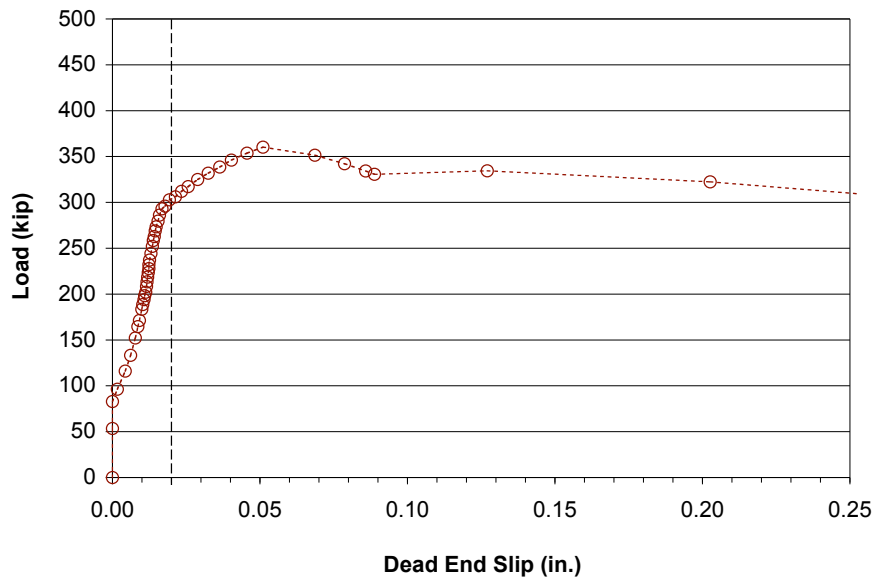


*Figure 5-30 Dead End Load-Slip Response for Specimen 0-GD-7.5°-3, Amplified Scale*



*Figure 5-31 Profile of Specimen 0-GD-7.5°-3 after Testing*

#### **5.2.2.4 1-GD-7.5°-1 (Diephuis)**

Live end load-displacement and dead end load-slip response for 1-GD-7.5°-1 are shown in Figure 5-32. The figure indicates that a peak load of 434 kip was achieved. The dead end load-slip response is shown on an amplified scale in Figure 5-33. The figure indicates that dead end slip reached 0.02 in. at a load of 77.3 kip, and dead end slip began accumulating rapidly once the load reached this level.

A complete pullout failure was not achieved for this specimen. Testing was halted for safety reasons because the peak load had exceeded the guaranteed ultimate tensile strength of the tendon.

Hairline cracks were observed on the specimen only after testing was completed, and therefore the load at cracking is unknown. Figure 5-34 shows the pattern of cracking observed in the specimen, with splitting cracks radiating out from the duct, and longitudinal cracks on the top and sides extending approximately three-quarters of the length of the specimen.

The gap in the dead end data seen in Figure 5-32 occurred because the head of the dead end linear potentiometer caught on a piece of grout after the tendon began pulling inside of the beam. The head of the potentiometer was freed when the problem was recognized, and accurate readings were taken for the remainder of the test.

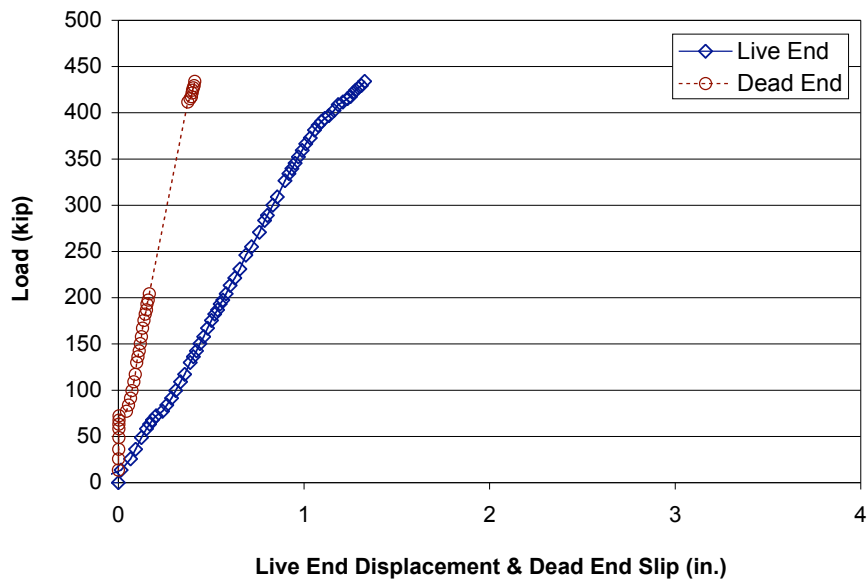


**Figure 5-32 Live End Load-Displacement and Dead End Load-Slip Response for Specimen 1-GD-7.5°-1**

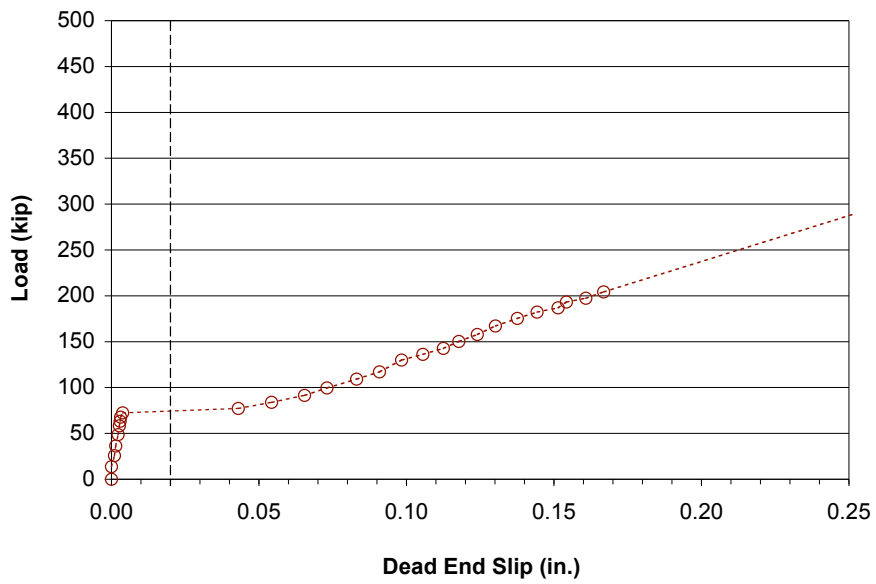


**Figure 5-33 Dead End Load-Slip Response for Specimen 1-GD-7.5°-1, Amplified Scale**



*Figure 5-34 Profile of Specimen 1-GD-7.5°-1 after Testing*

#### **5.2.2.5 1-GD-7.5°-2 (Diephuis)**

Live end load-displacement and dead end load-slip response for 1-GD-7.5°-2 are shown in Figure 5-35. The figure indicates that a peak load of 437 kip was achieved. The dead end load-slip response is shown on an amplified scale in Figure 5-36. The figure indicates that dead end slip reached 0.02 in. at a load of 54.3 kip, and dead end slip began accumulating rapidly once the load reached this level.

A complete pullout failure was not achieved for this specimen. Testing was halted for safety reasons because the peak load had exceeded the guaranteed ultimate tensile strength of the tendon.

Hairline cracks were observed on the specimen only after testing was completed, and therefore the load at cracking is unknown. Figure 5-37 shows the pattern of cracking observed in the specimen, with splitting cracks radiating out from the duct, and two longitudinal cracks extending approximately ninety percent of the length of the specimen.

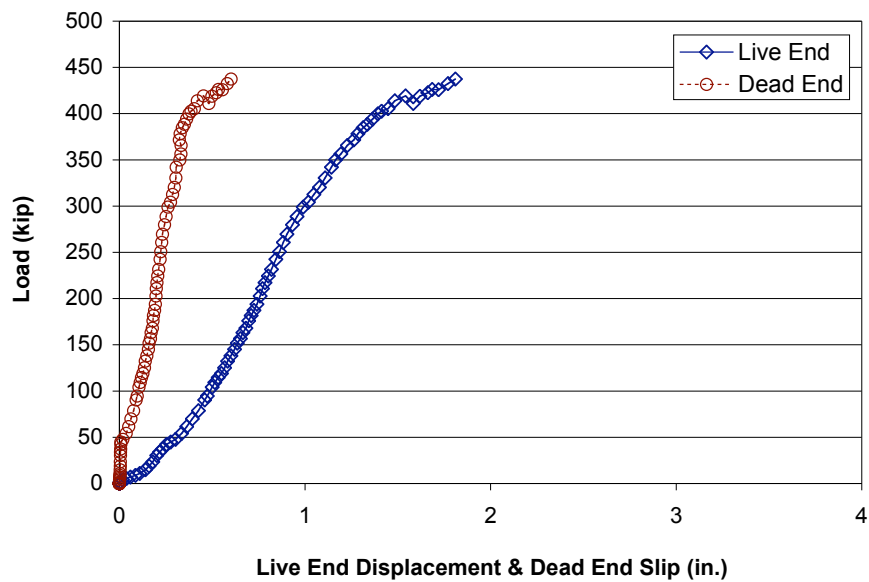


***Figure 5-35 Live End Load-Displacement and Dead End Load-Slip Response for Specimen 1-GD-7.5°-2***

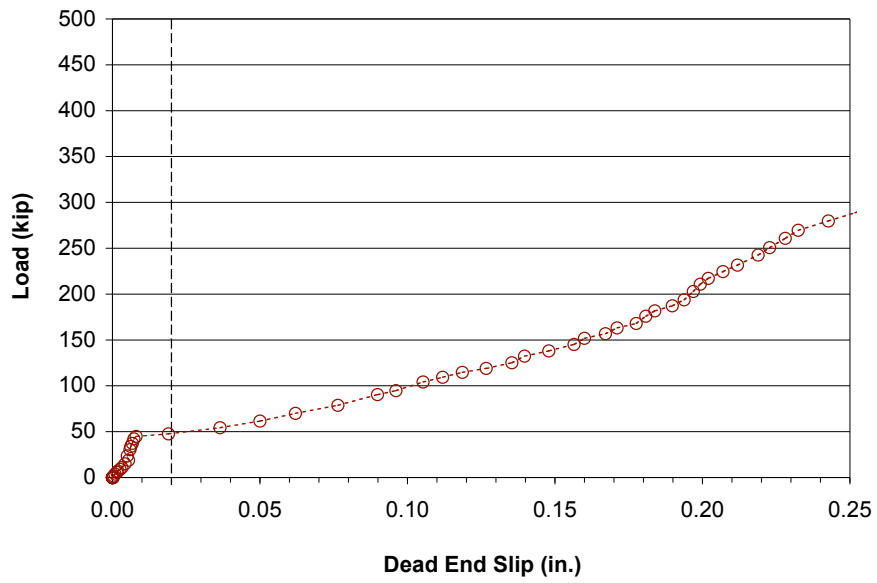


***Figure 5-36 Dead End Load-Slip Response for Specimen 1-GD-7.5°-2, Amplified Scale***



***Figure 5-37 Profile of Specimen 1-GD-7.5°-2 after Testing***



### 5.2.2.6 2-GD-7.5°-1 (Lüthi)

Live end load-displacement and dead end load-slip response for 2-GD-7.5°-1 are shown in Figure 5-38. The figure indicates that a peak load of 436 kip was achieved. The dead end load-slip response is shown on an amplified scale in Figure 5-39. The figure indicates that dead end slip reached 0.02 in. at a load of 100 kip, and dead end slip began accumulating almost immediately upon loading.

A complete pullout failure was not achieved for this specimen. Testing was halted for safety reasons when wires began breaking.

Figure 5-40 and Figure 5-41 show the pattern of cracking observed in the specimen. Splitting cracks radiated out from the duct on the dead end. The top crack extended the entire length of the specimen and down the live end to the duct. One longitudinal crack extended halfway down the side of the specimen.

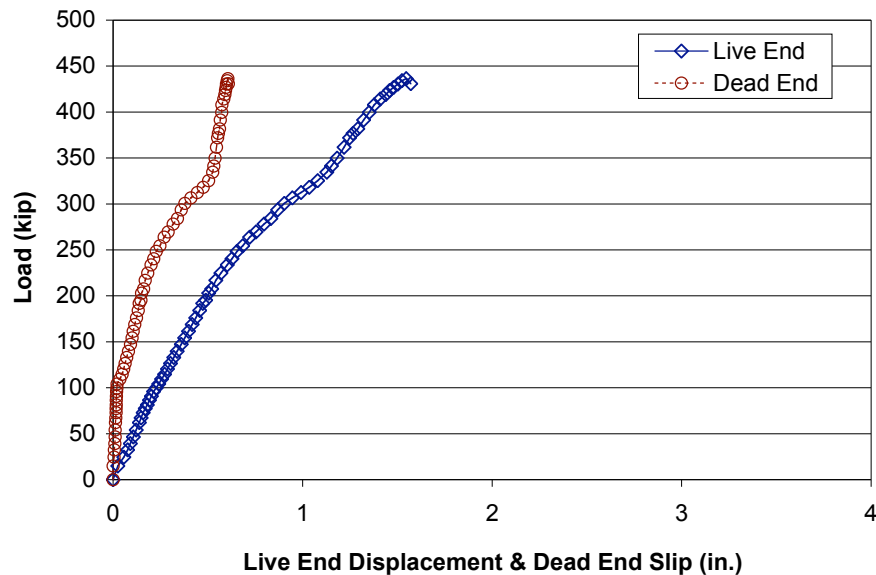


*Figure 5-38 Live End Load-Displacement and Dead End Load-Slip Response for Specimen 2-GD-7.5°-1*

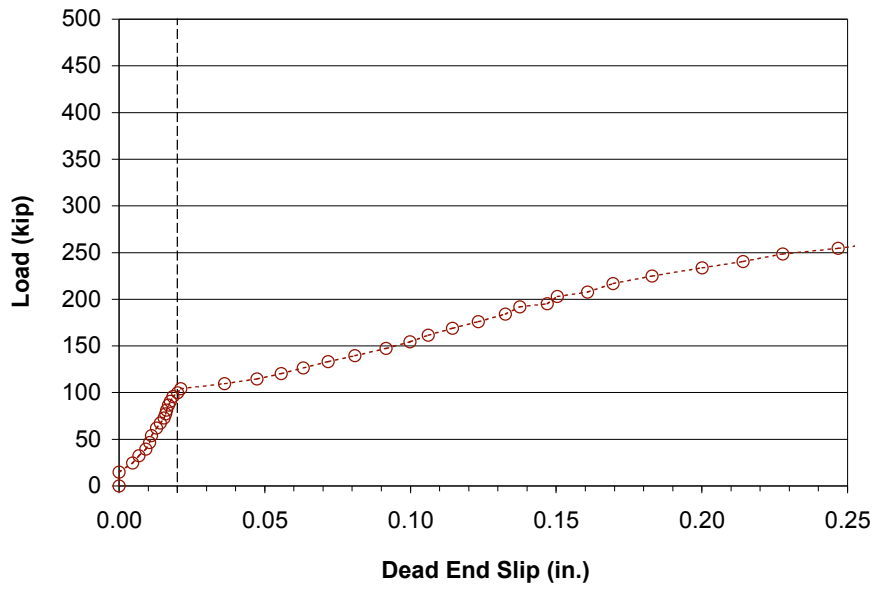


*Figure 5-39 Dead End Load-Slip Response for Specimen 2-GD-7.5°-1, Amplified Scale*

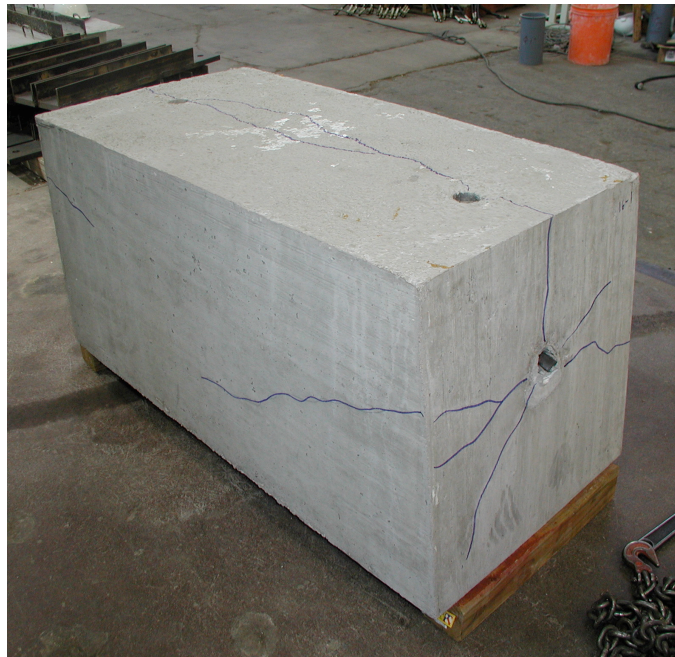


*Figure 5-40 Profile of Specimen 2-GD-7.5°-1 after Testing*



*Figure 5-41 Live End and Top of Specimen 2-GD-7.5°-1 after Testing*

#### **5.2.2.7 2-GD-7.5°-2 (Lüthi)**

Live end load-displacement and dead end load-slip response for 2-GD-7.5°-2 are shown in Figure 5-42. The figure indicates that a peak load of 481 kip was achieved. The dead end load-slip response is shown on an amplified scale in Figure 5-43. The figure indicates that dead end slip reached 0.02 in. at a load of 269 kip, and dead end slip began accumulating almost immediately upon loading.

Failure occurred in this specimen at the tendon-grout interface. After the peak load was reached, the load remained stable through large displacements.

No cracking was observed in this specimen; therefore no photo is included.

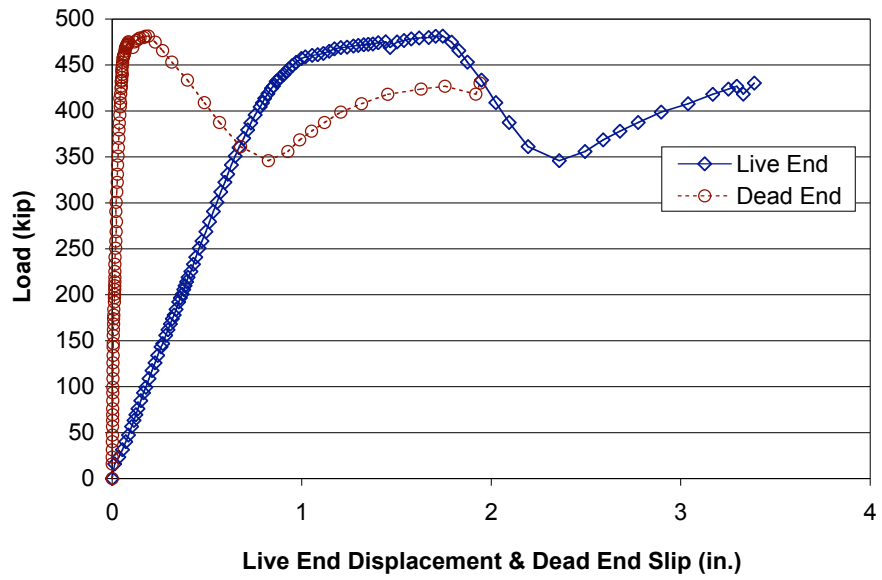


**Figure 5-42 Live End Load-Displacement and Dead End Load-Slip Response for Specimen 2-GD-7.5°-2**

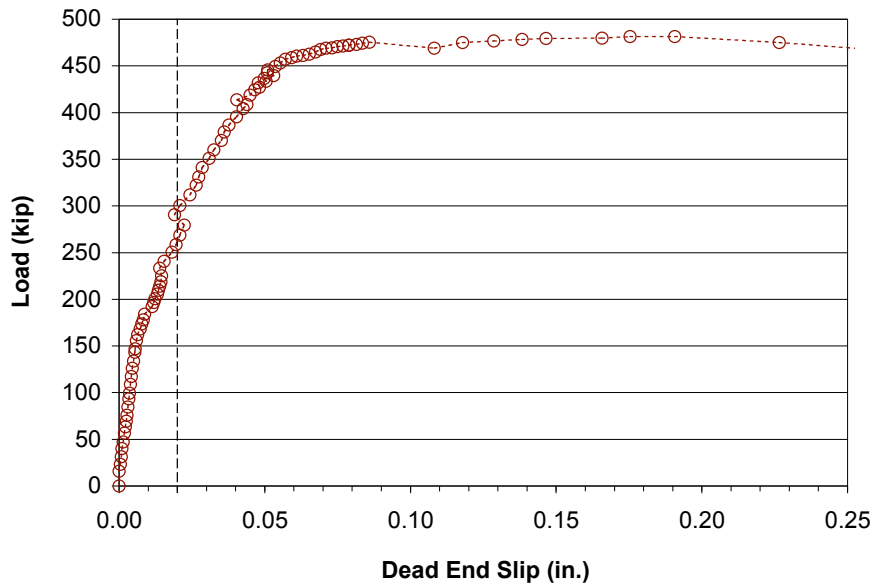


**Figure 5-43 Dead End Load-Slip Response for Specimen 2-GD-7.5°-2, Amplified Scale**

### 5.2.2.8 2-GD-7.5°-3 (Lüthi)

Live end load-displacement and dead end load-slip response for 2-GD-7.5°-3 are shown in Figure 5-44. The figure indicates that a peak load of 455 kip was achieved. The dead end load-slip response is shown on an amplified scale in Figure 5-45. The figure indicates that dead end slip reached 0.02 in. at a load of 150 kip, and dead end slip began accumulating almost immediately upon loading.

Failure occurred in this specimen at the tendon-grout interface. After the peak load was reached, the load remained stable through large displacements.

Significant cracking occurred at the initial peak load. Figure 5-46 shows the pattern of cracking observed in the specimen, with one splitting crack radiating out from the duct and across the top of the specimen to the live end.

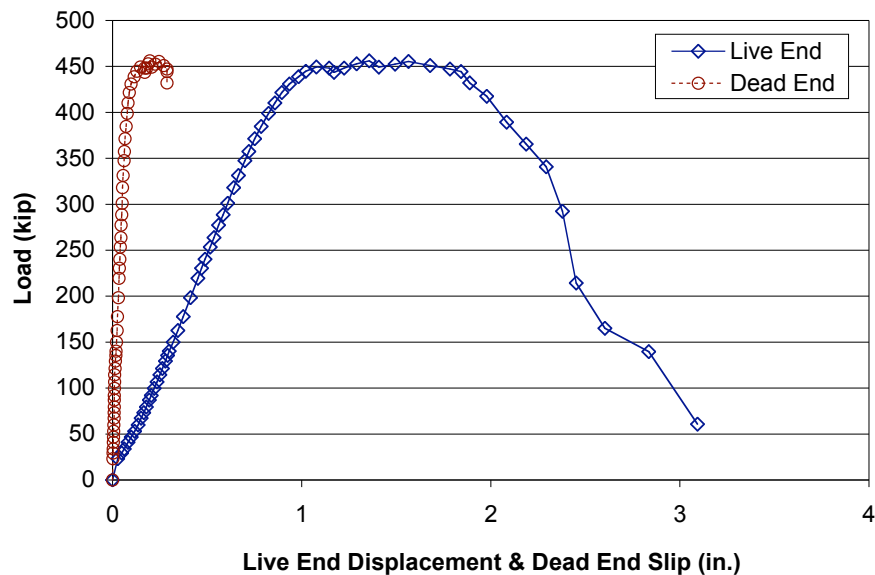


**Figure 5-44 Live End Load-Displacement and Dead End Load-Slip Response for Specimen 2-GD-7.5°-3**

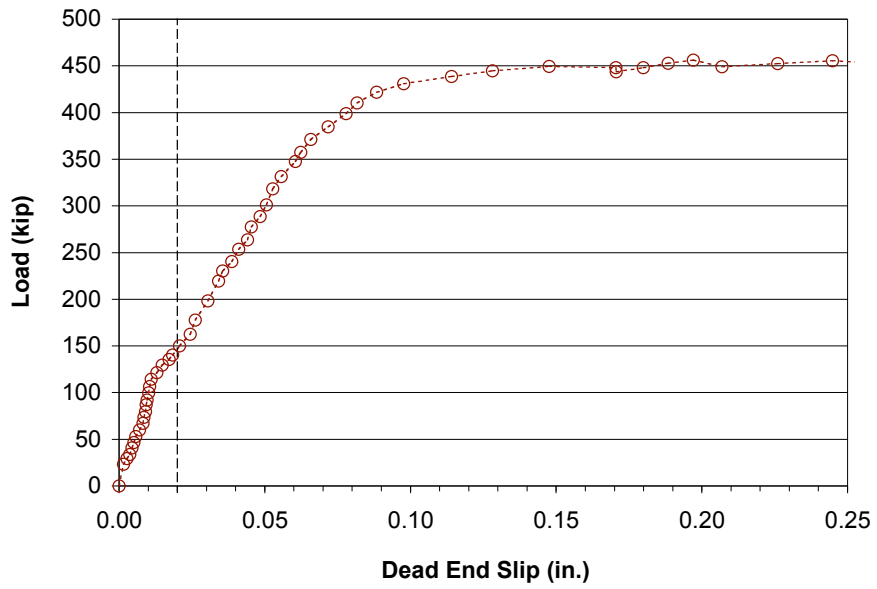


**Figure 5-45 Dead End Load-Slip Response for Specimen 2-GD-7.5°-3, Amplified Scale**



**Figure 5-46 Photo of Specimen 2-GD-7.5°-3 after Testing**

### 5.2.2.9 2-GD-7.5°-4 (Lüthi)

Live end load-displacement and dead end load-slip response for 2-GD-7.5°-4 are shown in Figure 5-47. The figure indicates that a peak load of 460 kip was achieved. The dead end load-slip response is shown on an amplified scale in Figure 5-48. The figure indicates that dead end slip reached 0.02 in. at a load of 368 kip, and dead end slip began accumulating slowly almost immediately upon loading.

Failure occurred in this specimen at the tendon-grout interface. After the peak load was reached, the load remained stable through approximately 0.5 in. of displacement and then dropped sharply.

Significant cracking occurred at the initial peak load. Figure 5-49 shows the pattern of cracking observed in the specimen, with one splitting crack radiating out from the duct and across the top of the specimen to the live end.

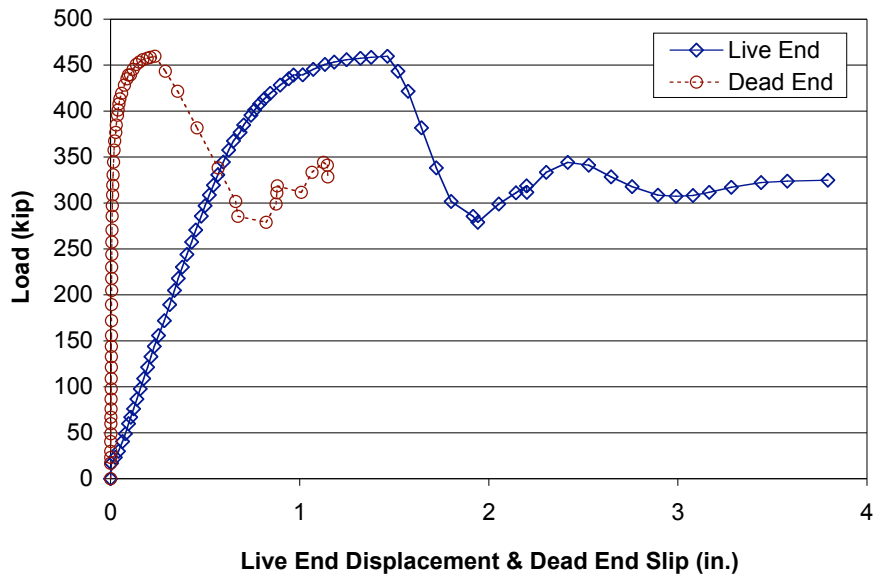


**Figure 5-47 Live End Load-Displacement and Dead End Load-Slip Response for Specimen 2-GD-7.5°-4**

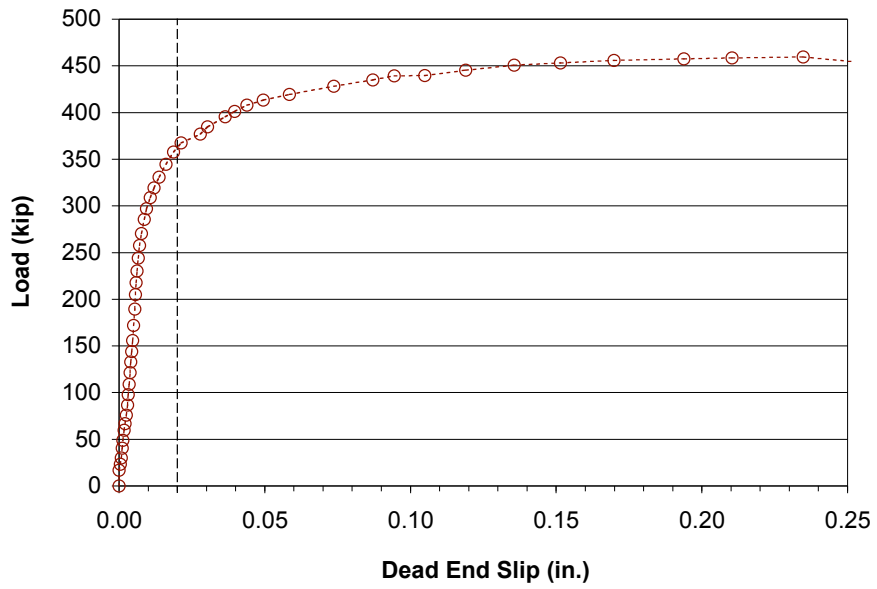


***Figure 5-48 Dead End Load-Slip Response for Specimen 2-GD-7.5°-4, Amplified Scale***



***Figure 5-49 Profile of Specimen 2-GD-7.5°-4 after Testing***



#### **5.2.2.10 1\*-GD-7.5°-1 (Lüthi)**

Live end load-displacement and dead end load-slip response for 1\*-GD-7.5°-1 are shown in Figure 5-50. The figure indicates that a peak load of 473 kip was achieved. The dead end load-slip response is shown on an amplified scale in Figure 5-51. The figure indicates that dead end slip reached 0.02 in. at a load of 79.7 kip, and dead end slip began accumulating rapidly once the load reached this level.

Failure occurred in this specimen at the tendon-grout interface. After the peak load was reached, the load remained stable through approximately 1 in. of displacement and then dropped sharply when wires began breaking.

Significant cracking occurred at the initial peak load. Figure 5-52 shows the pattern of cracking observed in the specimen, with one splitting crack radiating out from the duct and across the top of the specimen to the live end. Splitting cracks also radiated from the duct at the live end (not pictured), presumably due to forces generated as the wires broke.

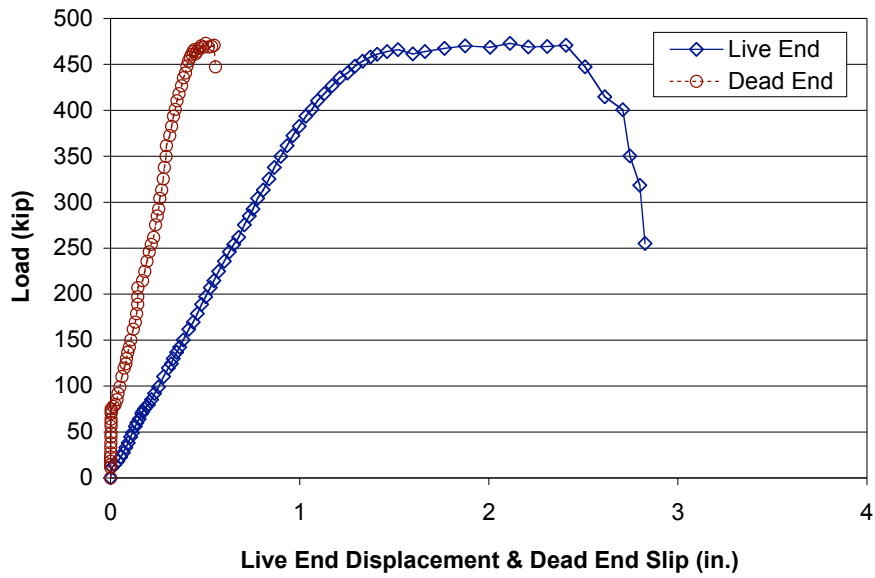


**Figure 5-50 Live End Load-Displacement and Dead End Load-Slip Response for Specimen 1\*-GD-7.5°-1**

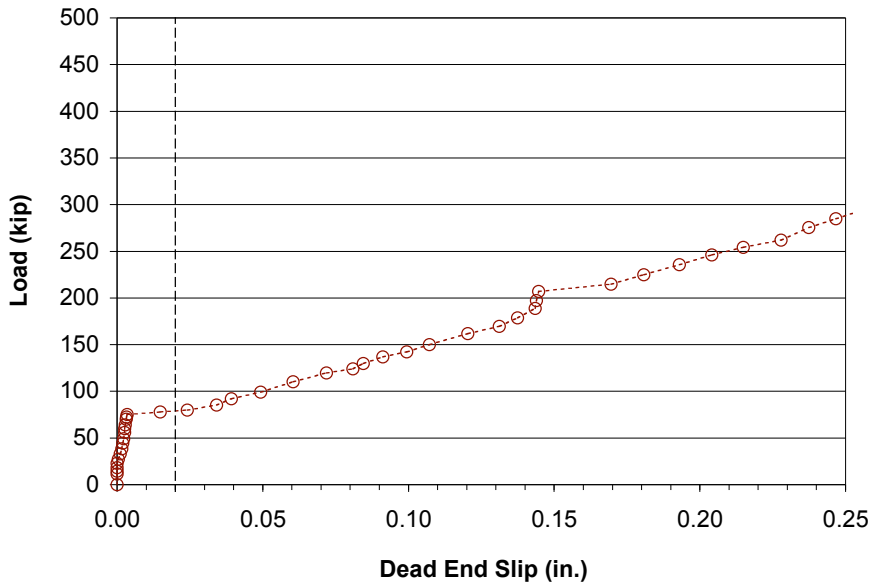


**Figure 5-51 Dead End Load-Slip Response for Specimen 1\*-GD-7.5°-1, Amplified Scale**



*Figure 5-52 Profile of Specimen 1\*-GD-7.5°-1 after Testing*

#### **5.2.2.11 1\*-GD-7.5°-2 (Lüthi)**

Live end load-displacement and dead end load-slip response for 1\*-GD-7.5°-2 are shown in Figure 5-53. The figure indicates that a peak load of 480 kip was achieved. The dead end load-slip response is shown on an amplified scale in Figure 5-54. The figure indicates that dead end slip reached 0.02 in. at a load of 298 kip, and dead end slip began accumulating slowly almost immediately upon loading.

A complete pullout failure was not achieved for this specimen. Testing was halted for safety reasons when wires began breaking.

No cracking was observed in this specimen; therefore no photo is included.

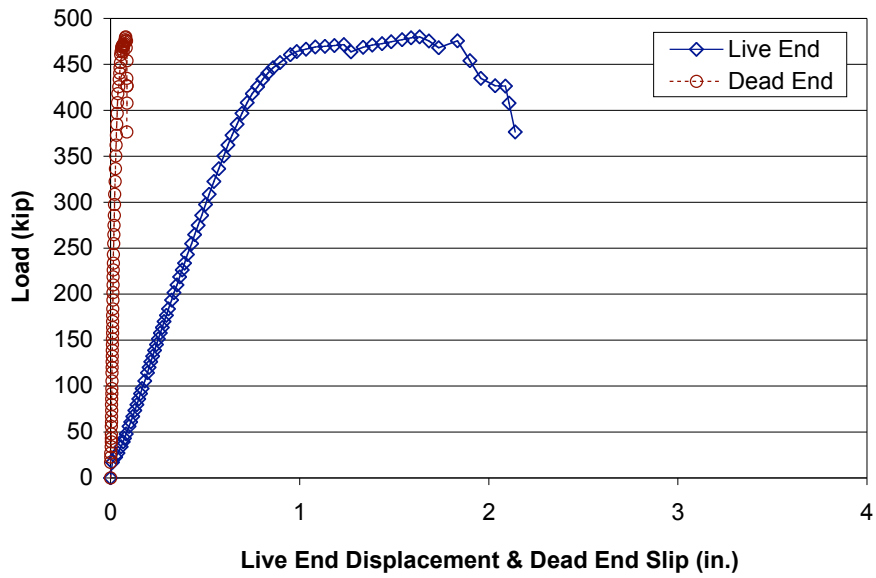


**Figure 5-53 Live End Load-Displacement and Dead End Load-Slip Response for Specimen 1\*-GD-7.5°-2**

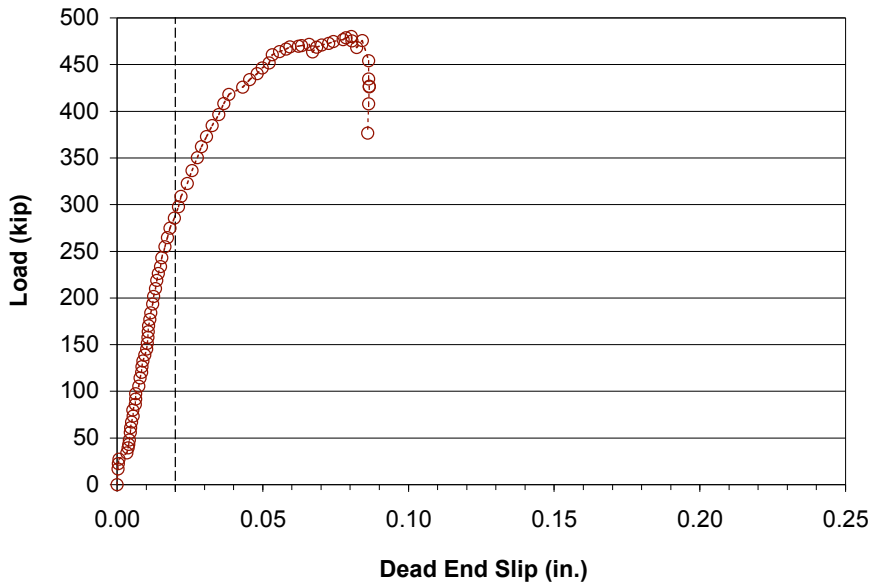


**Figure 5-54 Dead End Load-Slip Response for Specimen 1\*-GD-7.5°-2, Amplified Scale**

### 5.2.3 HDPE Duct Specimens

Three HDPE duct specimens with unoiled tendons were tested. The first specimen was part of a mismatched pair tested in order to determine the appropriate centerline bonded length for all tests. That pair consisted of one specimen with a 5 degree tendon angle change and a centerline bonded length of 31.4 in., and one specimen with a 7.5 degree tendon angle change and a centerline bonded length of 44.0 in. This latter size was determined to be the most appropriate, and subsequent tests were performed in matching pairs. For completeness, this original “test length” specimen (0-HD-7.5°-1) is discussed in addition to the pair of specimens constructed later (0-HD-7.5°-2 and 0-HD-7.5°-3).

One pair of specimens containing tendons oiled with NC205 were tested, as were two pairs containing tendons oiled with 703D. An extra pair of these latter specimens were constructed because of problems with the electronic data acquisition equipment while testing the second specimen from the first pair. Accurate data were therefore only collected for one specimen, 2-HD-7.5°-1. A second pair, 2-HD-7.5°-2 and 2-HD-7.5°-3, were constructed and tested at a later date.

#### 5.2.3.1 0-HD-7.5°-1 (*Diephuis*)

Live end load-displacement and dead end load-slip response for 0-HD-7.5°-1 are shown in Figure 5-55. The figure indicates that a peak load of 228 kip was achieved, at which point a reduction in resistance occurred. The dead end load-slip response is shown on an amplified scale in Figure 5-56. The figure indicates that dead end slip reached 0.02 in. at a load of 196 kip, and dead end slip began accumulating slowly immediately upon loading.

Failure occurred in this specimen at the tendon-grout interface. After the initial peak load was reached, the resistance dropped and then began increasing again. This trend was presumably due to mechanical interlock between the grout and the irregular surface of the duct as the tendon moved through the specimen.

Significant longitudinal splitting cracks were observed once the test was completed. A photograph of this specimen after testing was not available.

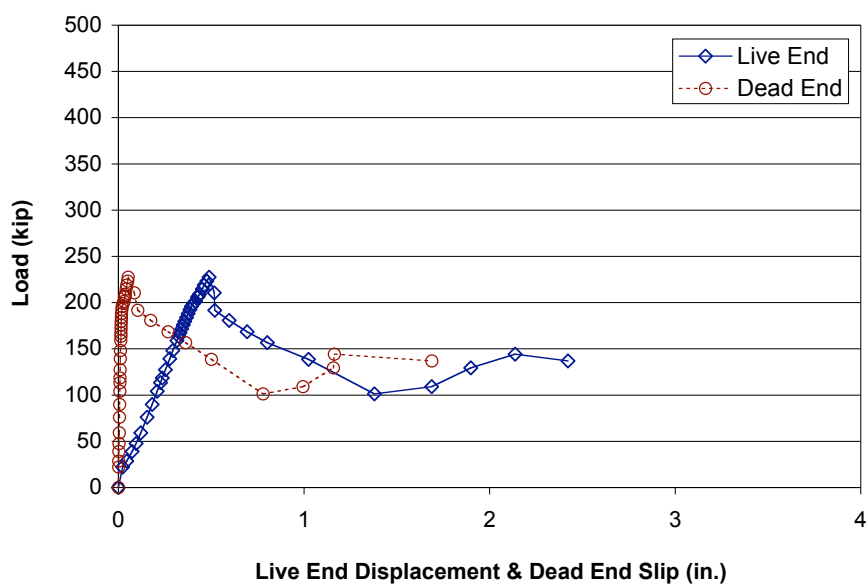


**Figure 5-55 Live End Load-Displacement and Dead End Load-Slip Response for Specimen 0-HD-7.5°-1**

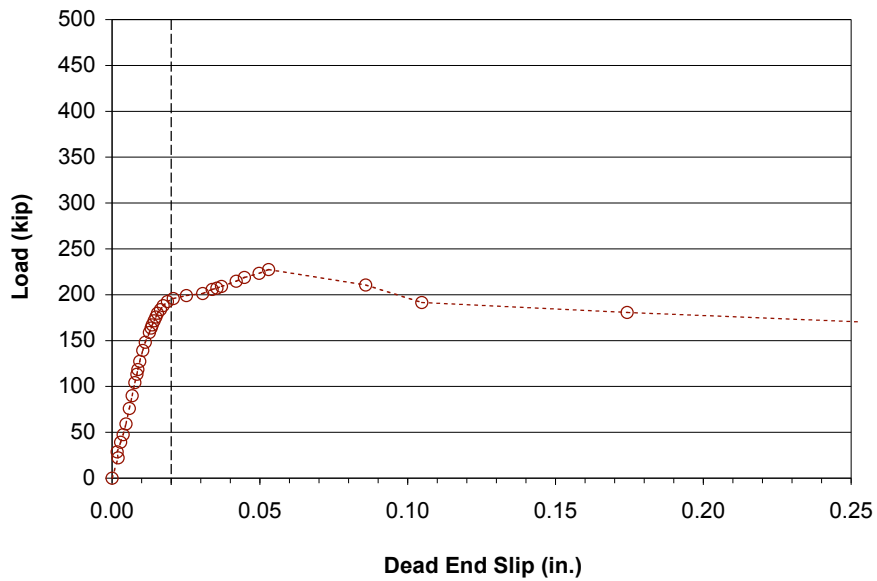


***Figure 5-56 Dead End Load-Slip Response for Specimen 0-HD-7.5°-1, Amplified Scale***

### ***5.2.3.2 0-HD-7.5°-2 (Diephuis)***

Live end load-displacement and dead end load-slip response for 0-HD-7.5°-2 are shown in Figure 5-57. The figure indicates that a peak load of 311 kip was achieved, at which point a reduction in resistance occurred. The dead end load-slip response is shown on an amplified scale in Figure 5-58. The figure indicates that dead end slip reached 0.02 in. at a load of 288 kip, and dead end slip began accumulating slowly immediately upon loading.

Failure occurred in this specimen at the tendon-grout interface. After the initial peak load was reached, the resistance dropped and then began increasing again. This trend was presumably due to mechanical interlock between the grout and the irregular surface of the duct as the tendon moved through the specimen.

Significant cracking occurred at the initial peak load. Figure 5-59 shows the pattern of cracking observed in the specimen, with one splitting crack radiating from the top and bottom of the duct. The crack extended the entire length of the specimen.

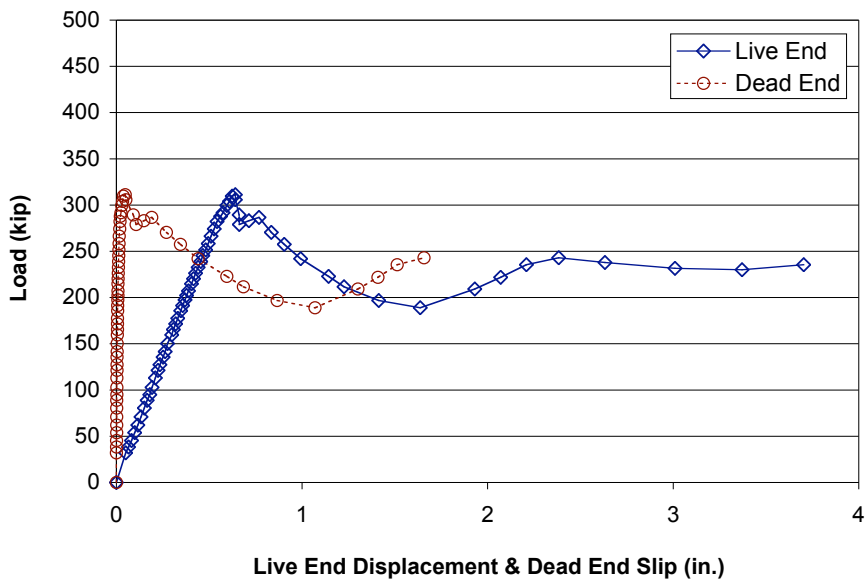


***Figure 5-57 Live End Load-Displacement and Dead End Load-Slip Response for Specimen 0-HD-7.5°-2***



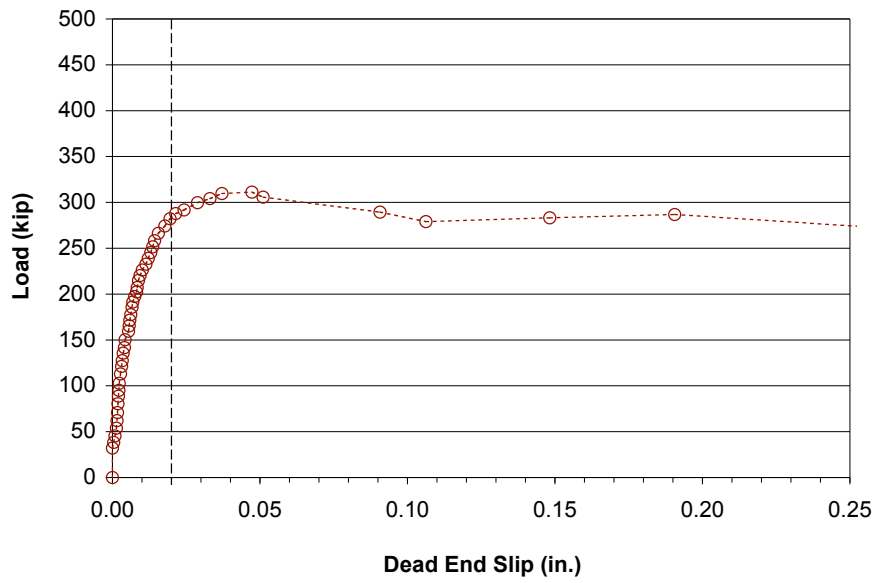


***Figure 5-58 Dead End Load-Slip Response for Specimen 0-HD-7.5°-2, Amplified Scale***



***Figure 5-59 Dead End of Specimen 0-HD-7.5°-2 after Testing***

### 5.2.3.3 0-HD-7.5°-3 (Diephuis)

Live end load-displacement and dead end load-slip response for 0-HD-7.5°-3 are shown in Figure 5-60. The figure indicates that a peak load of 307 kip was achieved, at which point a reduction in resistance occurred. The dead end load-slip response is shown on an amplified scale in Figure 5-61. The figure indicates that dead end slip reached 0.02 in. at a load of 287 kip, and dead end slip began accumulating slowly once the load reached approximately 50 kip.

Failure occurred in this specimen at the tendon-grout interface. After the initial peak load was reached, the resistance dropped and then began increasing again. This trend was presumably due to mechanical interlock between the grout and the irregular surface of the duct as the tendon moved through the specimen.

Significant cracking occurred at the initial peak load. Figure 5-62 and Figure 5-63 show the pattern of cracking observed in the specimen, with splitting cracks spreading out radially from the duct at the dead end. The crack on the top extended the entire length of the specimen, as did a crack on one side. A separate crack on the other side extended almost the entire length of the specimen.

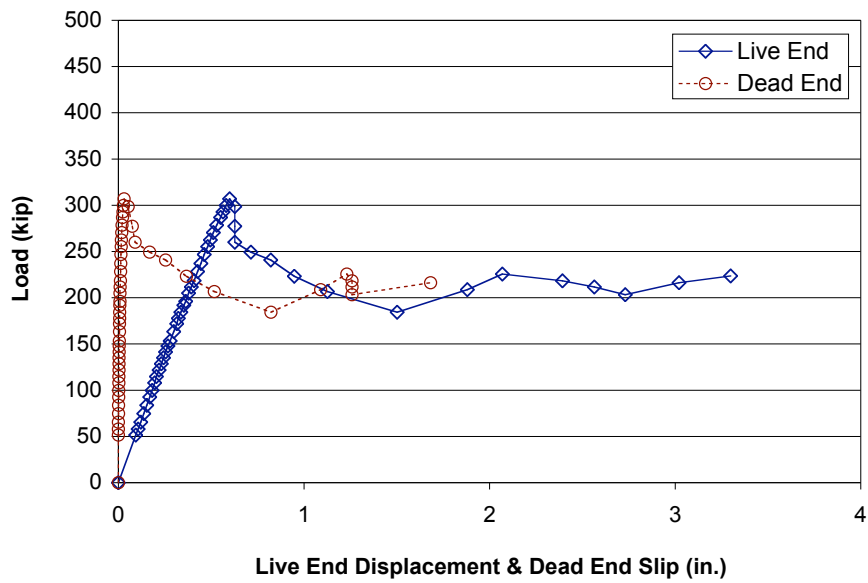


**Figure 5-60 Live End Load-Displacement and Dead End Load-Slip Response for Specimen 0-HD-7.5°-3**

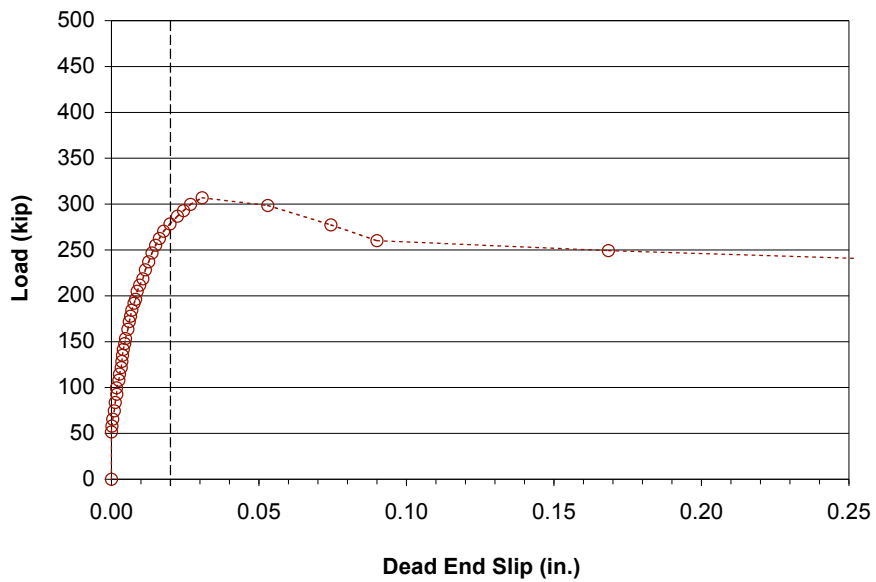


**Figure 5-61 Dead End Load-Slip Response for Specimen 0-HD-7.5°-3, Amplified Scale**

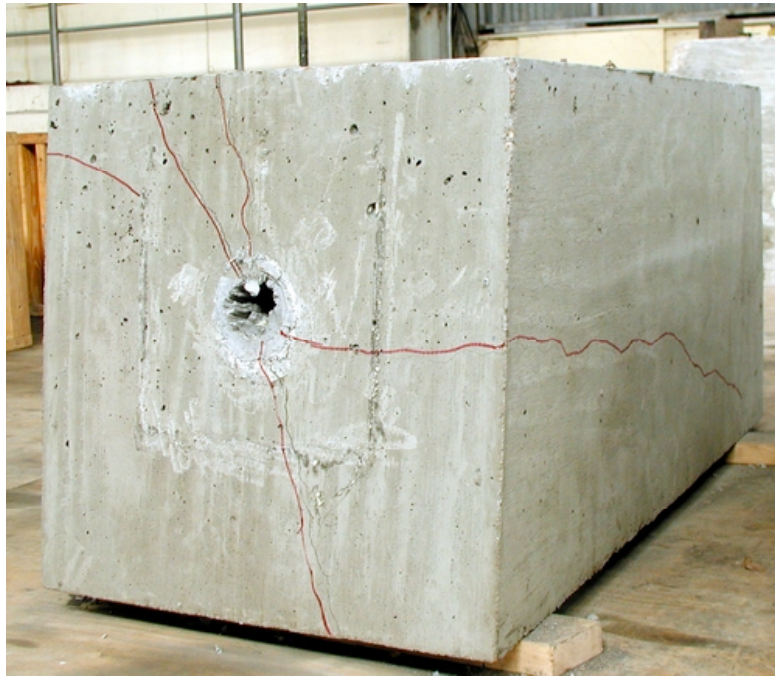


*Figure 5-62 Profile of Specimen 0-HD-7.5°-3 after Testing*

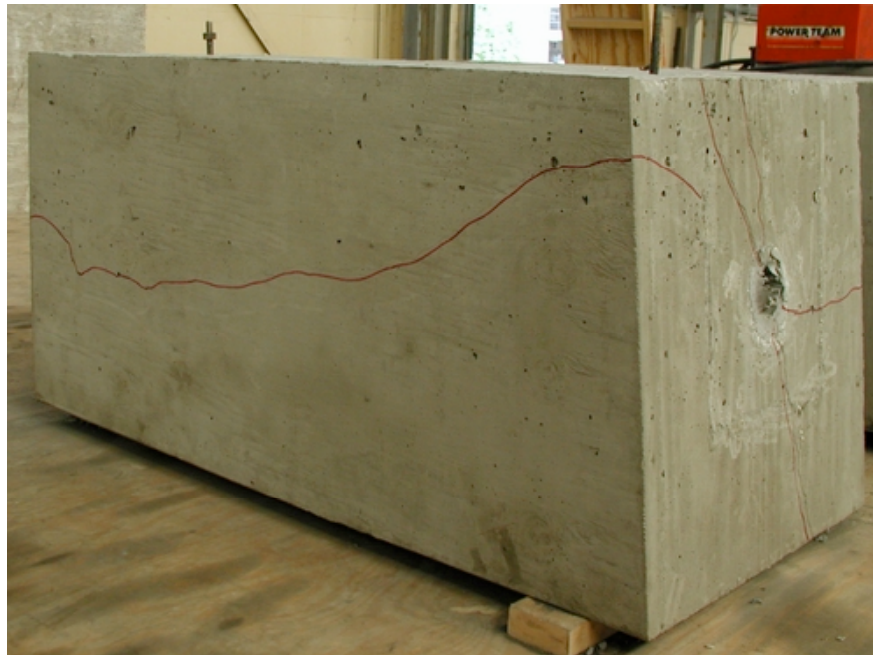


*Figure 5-63 Profile 2 of Specimen 0-HD-7.5°-3 after Testing*

#### **5.2.3.4 1-HD-7.5°-1 (Diephuis)**

Live end load-displacement and dead end load-slip response for 1-HD-7.5°-1 are shown in Figure 5-64. The figure indicates that a peak load of 322 kip was achieved, at which point a reduction in resistance occurred. The dead end load-slip response is shown on an amplified scale in Figure 5-65. The figure indicates that dead end slip reached 0.02 in. at a load of 34.3 kip, and dead end slip began accumulating rapidly immediately upon loading.

This specimen and its companion, 1-HD-7.5°-2, behaved differently from any specimens with steel pipes or galvanized ducts. Before failure eventually occurred at the tendon-grout interface, the slope of the load-displacement and load-slip plots increased, indicating an increased resistance to pullout. The cause of this behavior is not clear. One hypothesis is that the oil destroyed adhesion between the tendon and the grout, causing the tendon to move more freely at low load levels. As the displacement increased, however, mechanical interlock between the grout and the irregular surface of the tendon may have caused increased stiffness.

At the peak load, significant cracking of the specimen occurred. Figure 5-66 shows the pattern of cracking observed in the specimen, with splitting cracks spreading out radially from the duct at the dead end. The crack on the top extended the entire length of the specimen, and cracks along the sides extended approximately three-quarters of the length of the specimen.

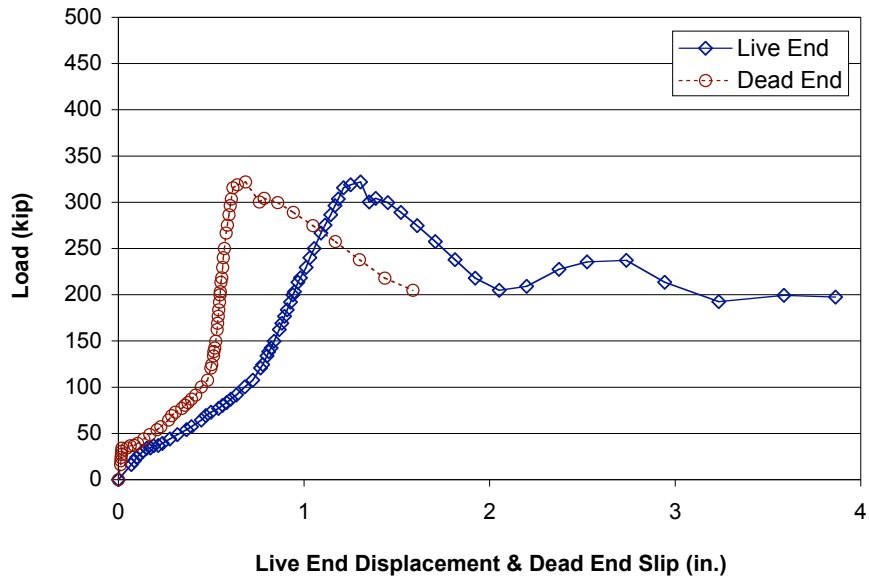


**Figure 5-64 Live End Load-Displacement and Dead End Load-Slip Response for Specimen 1-HD-7.5°-1**

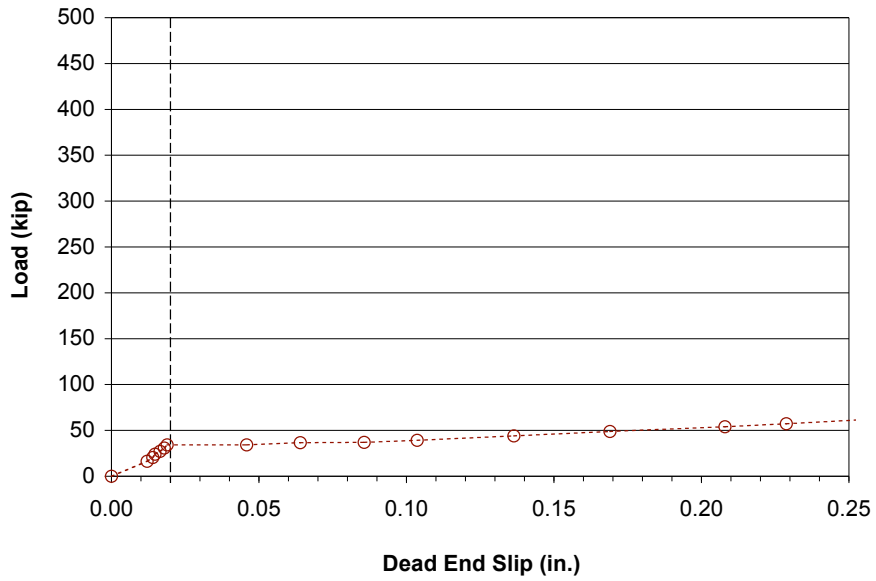


**Figure 5-65 Dead End Load-Slip Response for Specimen 1-HD-7.5°-1, Amplified Scale**



*Figure 5-66 Profile of Specimen 1-HD-7.5°-1 after Testing*

#### **5.2.3.5 1-HD-7.5°-2 (Diephuis)**

Live end load-displacement and dead end load-slip response for 1-HD-7.5°-2 are shown in Figure 5-67. The figure indicates that a peak load of 325 kip was achieved, at which point a reduction in resistance occurred. The dead end load-slip response is shown on an amplified scale in Figure 5-68. The figure indicates that dead end slip reached 0.02 in. at a load of 6.5 kip, and dead end slip began accumulating rapidly immediately upon loading.

This specimen and its companion, 1-HD-7.5°-1, behaved differently from any specimens with steel pipes or galvanized ducts. Before failure eventually occurred at the tendon-grout interface, the slope of the load-displacement and load-slip plots increased, indicating an increased resistance to pullout. The cause

of this behavior is not clear, but the behavior may be due to poor adhesion between the tendon and the grout as described in Section 5.2.3.4.

Significant cracking occurred at the initial peak load. Figure 5-69 shows the pattern of cracking observed in the specimen, with one splitting crack radiating out from the duct and across the top of the specimen to the live end.

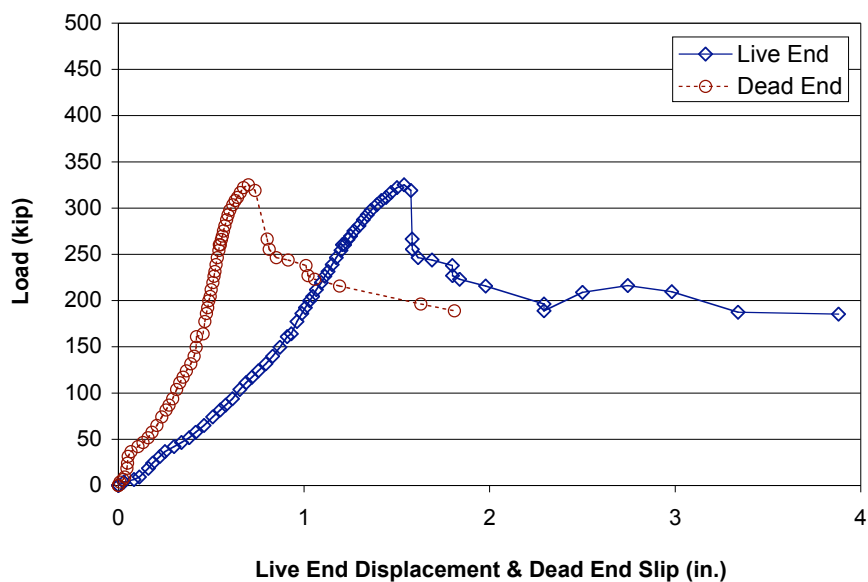


**Figure 5-67 Live End Load-Displacement and Dead End Load-Slip Response for Specimen 1-HD-7.5°-2**



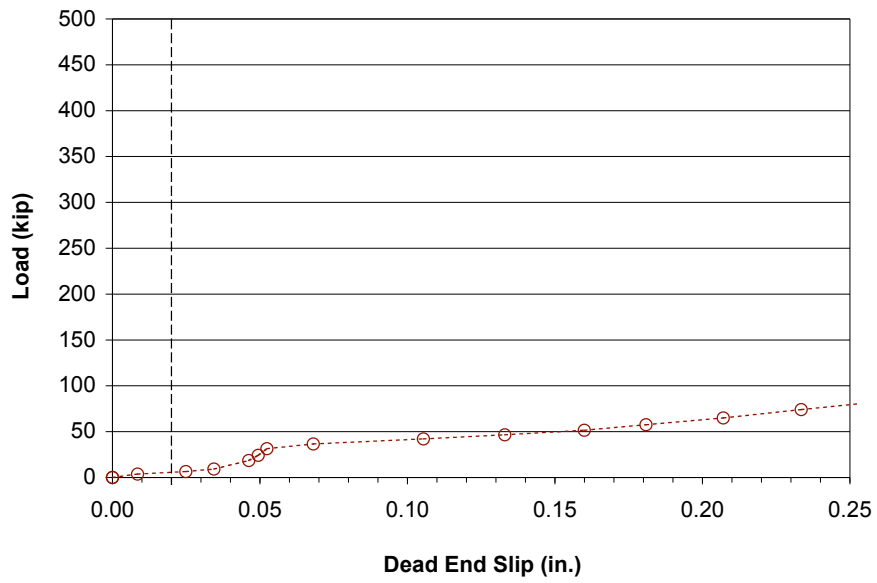


***Figure 5-68 Dead End Load-Slip Response for Specimen 1-HD-7.5°-2, Amplified Scale***

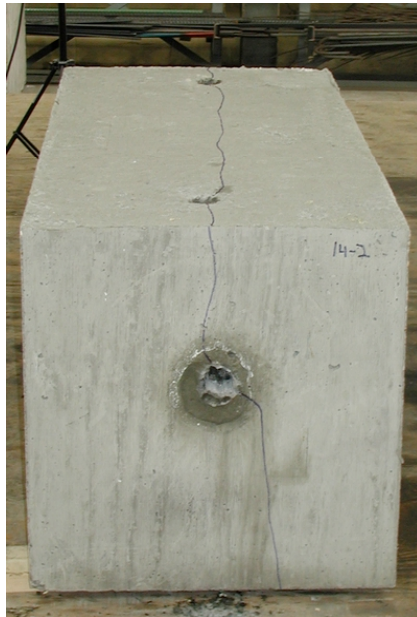


***Figure 5-69 Photo of Specimen 1-HD-7.5°-2 after Testing***

#### 5.2.3.6 2-HD-7.5°-1 (Lüthi)

Live end load-displacement and dead end load-slip response for 2-HD-7.5°-1 are shown in Figure 5-70. The figure indicates that a peak load of 293 kip was achieved, at which point a gradual reduction in resistance occurred. The dead end load-slip response is shown on an amplified scale in Figure 5-71. The figure indicates that dead end slip reached 0.02 in. at a load of 49.9 kip, and dead end slip began accumulating rapidly once the load reached this level.

This specimen and its companions, 2-HD-7.5°-2 and 2-HD-7.5°-3, behaved differently from any specimens with steel pipe or galvanized duct. Before failure eventually occurred at the tendon-grout interface, the slope of the load-displacement and load-slip plots increased, indicating an increased resistance to pullout. The cause of this behavior is not clear, but the behavior may be due to poor adhesion between the tendon and the grout as described in Section 5.2.3.4.

Significant cracking occurred at the initial peak load. Figure 5-72 shows the pattern of cracking observed in the specimen, with splitting cracks radiating out from the duct and across the top of the specimen to the live end. One crack on the side of the specimen extended approximately halfway to the live end.

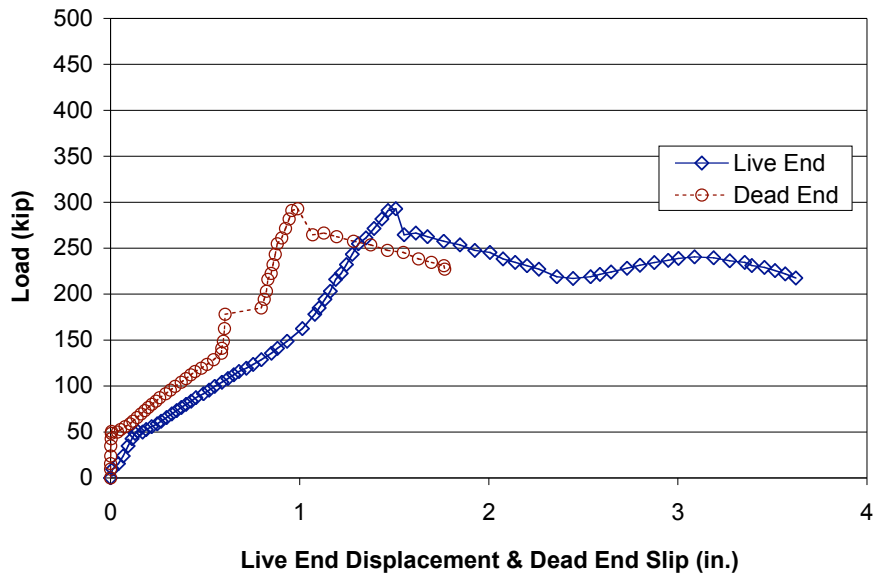


**Figure 5-70 Live End Load-Displacement and Dead End Load-Slip Response for Specimen 2-HD-7.5°-1**

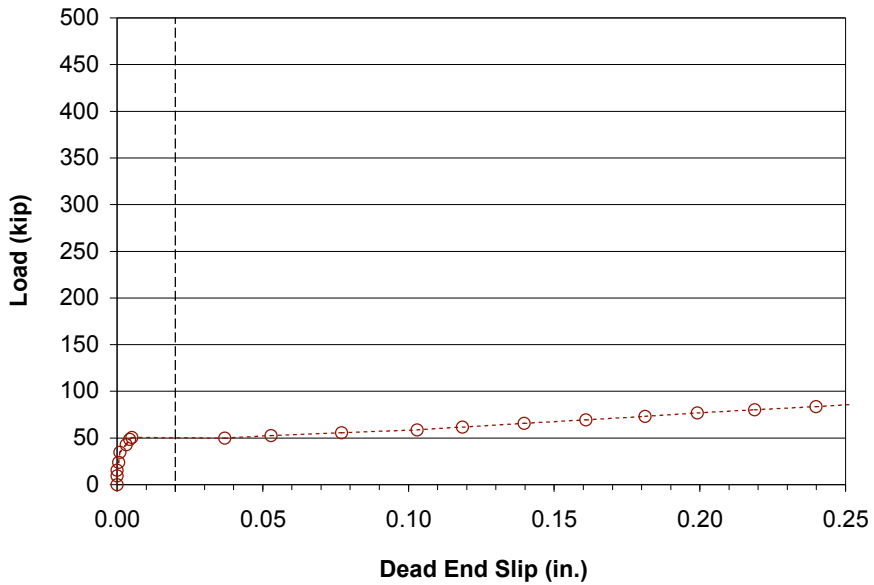


**Figure 5-71 Dead End Load-Slip Response for Specimen 2-HD-7.5°-1, Amplified Scale**



***Figure 5-72 Profile of Specimen 2-HD-7.5°-1 after Testing***

#### **5.2.3.7 2-HD-7.5°-2 (Lüthi)**

Live end load-displacement and dead end load-slip response for 2-HD-7.5°-2 are shown in Figure 5-73. The figure indicates that a peak load of 295 kip was achieved, at which point a reduction in resistance occurred. The dead end load-slip response is shown on an amplified scale in Figure 5-74. The figure indicates that dead end slip reached 0.02 in. at a load of 62.3 kip, and dead end slip began accumulating rapidly once the load reached this level.

This specimen and its companions, 2-HD-7.5°-1 and 2-HD-7.5°-3, behaved differently from any specimens with steel pipe or galvanized duct. Before failure eventually occurred at the tendon-grout interface, the slope of the load-displacement and load-slip plots increased, indicating an increased resistance

to pullout. The cause of this behavior is not clear, but the behavior may be due to poor adhesion between the tendon and the grout as described in Section 5.2.3.4.

Significant cracking occurred at the initial peak load. Figure 5-75 shows the pattern of cracking observed in the specimen, with splitting cracks radiating out from the duct and across the top of the specimen to the live end.

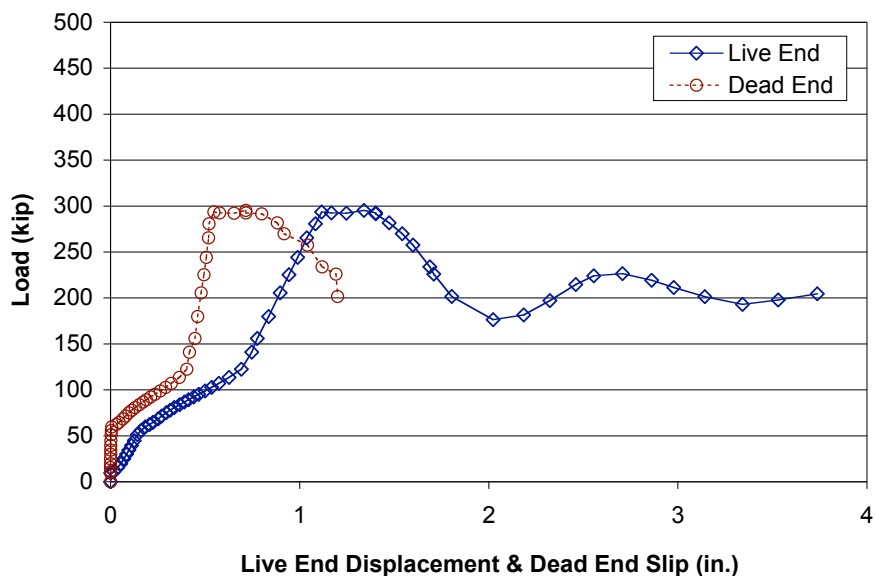


**Figure 5-73 Live End Load-Displacement and Dead End Load-Slip Response for Specimen 2-HD-7.5°-2**

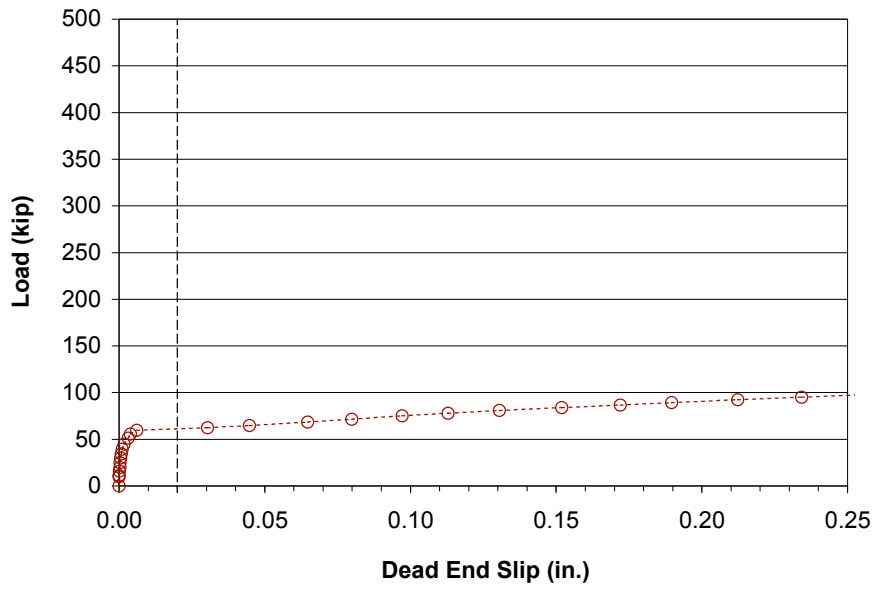


***Figure 5-74 Dead End Load-Slip Response for Specimen 2-HD-7.5°-2, Amplified Scale***



***Figure 5-75 Photo of Specimen 2-HD-7.5°-2 after Testing***

#### 5.2.3.8 2-HD-7.5°-3 (Lüthi)

Live end load-displacement and dead end load-slip response for 2-HD-7.5°-3 are shown in Figure 5-76. The figure indicates that a peak load of 268 kip was achieved, at which point a slight reduction in resistance occurred. The dead end load-slip response is shown on an amplified scale in Figure 5-77. The figure indicates that dead end slip reached 0.02 in. at a load of 78.5 kip, and dead end slip began accumulating rapidly once the load reached this level.

This specimen and its companions, 2-HD-7.5°-1 and 2-HD-7.5°-2, behaved differently from any specimens with steel pipe or galvanized duct. Before failure eventually occurred at the tendon-grout interface, the slope of the load-displacement and load-slip plots increased, indicating an increased resistance to pullout. The cause of this behavior is not clear, but the behavior may be due to poor adhesion between the tendon and the grout as described in Section 5.2.3.4.

Significant cracking occurred at the initial peak load. Figure 5-78 shows the pattern of cracking observed in the specimen, with one splitting crack radiating out from the duct and across the top of the specimen to the live end.

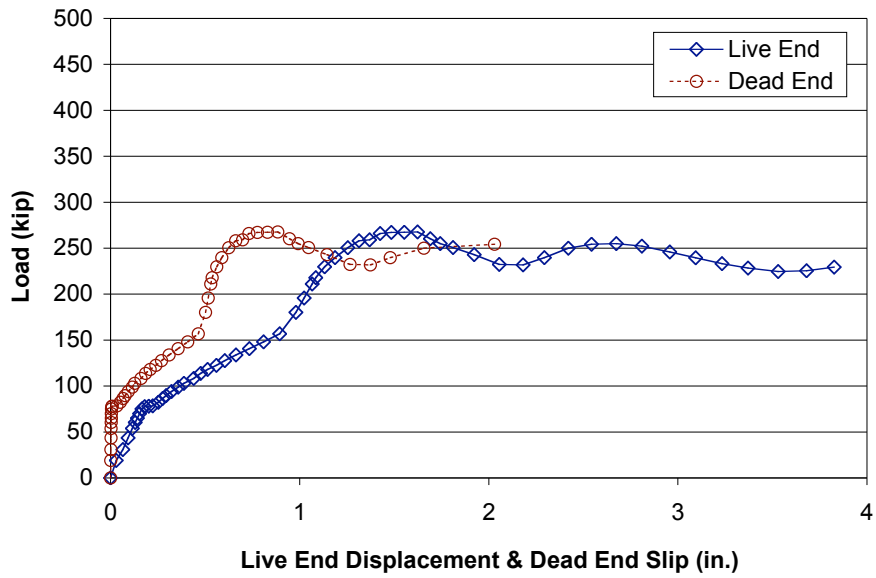


**Figure 5-76 Live End Load-Displacement and Dead End Load-Slip Response for Specimen 2-HD-7.5°-3**

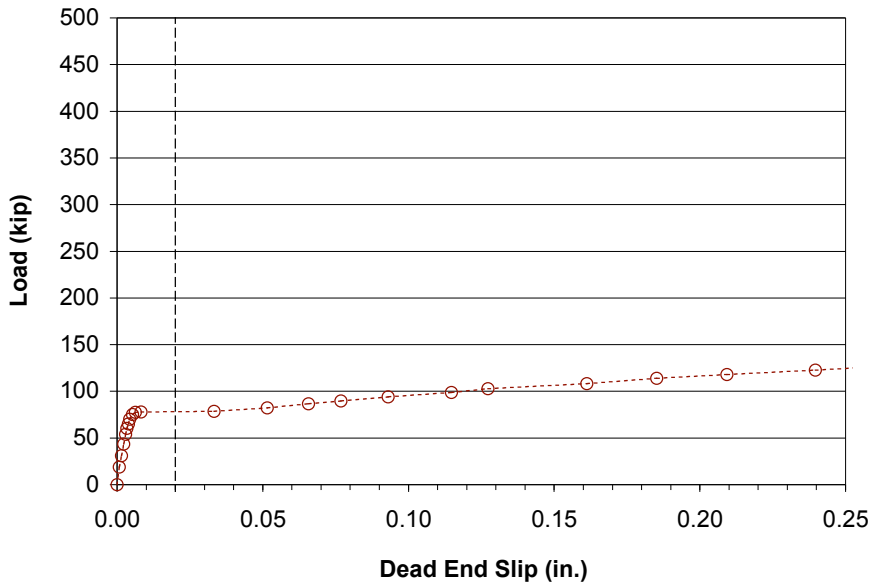


**Figure 5-77 Dead End Load-Slip Response for Specimen 2-HD-7.5°-3, Amplified Scale**





*Figure 5-78 Photo of Specimen 2-HD-7.5°-3 after Testing*

#### **5.2.3.9 1\*-HD-7.5°-1 (Lüthi)**

Live end load-displacement and dead end load-slip response for 1\*-HD-7.5°-1 are shown in Figure 5-79. The figure indicates that a peak load of 278 kip was achieved, at which point a significant reduction in resistance occurred. The dead end load-slip response is shown on an amplified scale in Figure 5-80. The figure indicates that dead end slip reached 0.02 in. at a load of 130 kip, and dead end slip began accumulating rapidly once the load reached approximately 90 kip.

Before failure eventually occurred at the tendon-grout interface, the slope of the load-displacement and load-slip plots decreased, indicating a decreased resistance to pullout. The cause of this behavior is not clear.

Significant cracking occurred at the initial peak load. Figure 5-81 shows the pattern of cracking observed in the specimen, with one splitting crack

radiating out from the duct and across the top of the specimen to the live end. An additional crack on the side of the specimen (not pictured) extended almost to the live end.

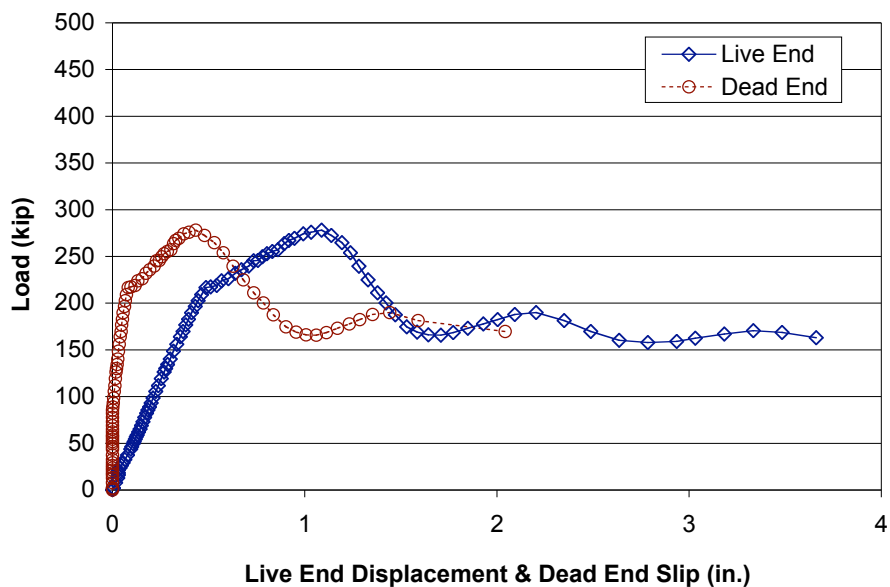


**Figure 5-79 Live End Load-Displacement and Dead End Load-Slip Response for Specimen 1\*-HD-7.5°-1**

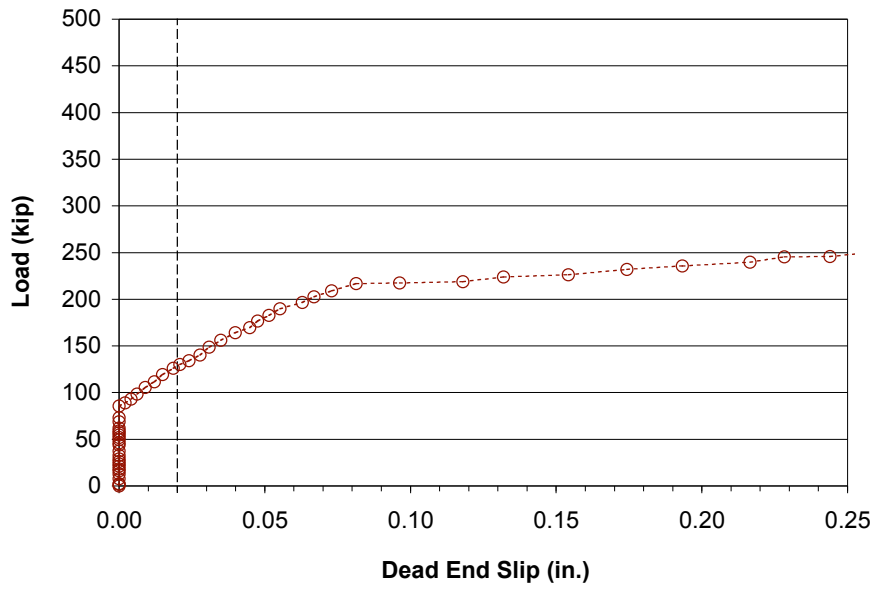


**Figure 5-80 Dead End Load-Slip Response for Specimen 1\*-HD-7.5°-1, Amplified Scale**



**Figure 5-81 Photo of Specimen 1\*-HD-7.5°-1 After Testing**

### 5.2.3.10 1\*-HD-7.5°-2 (Lüthi)

Live end load-displacement and dead end load-slip response for 1\*-HD-7.5°-2 are shown in Figure 5-82. The figure indicates that a peak load of 333 kip was achieved, at which point a reduction in resistance occurred. The dead end load-slip response is shown on an amplified scale in Figure 5-83. The figure indicates that dead end slip reached 0.02 in. at a load of 79.2 kip, and dead end slip began accumulating rapidly once this load was reached.

Failure occurred in this specimen at the tendon-grout interface. After the initial peak load was reached, the resistance dropped to approximately 230 kip and remained steady through large displacements.

Significant cracking occurred at the initial peak load. Figure 5-84 shows the pattern of cracking observed in the specimen, with splitting cracks radiating out from the duct and across the top of the specimen to the live end.

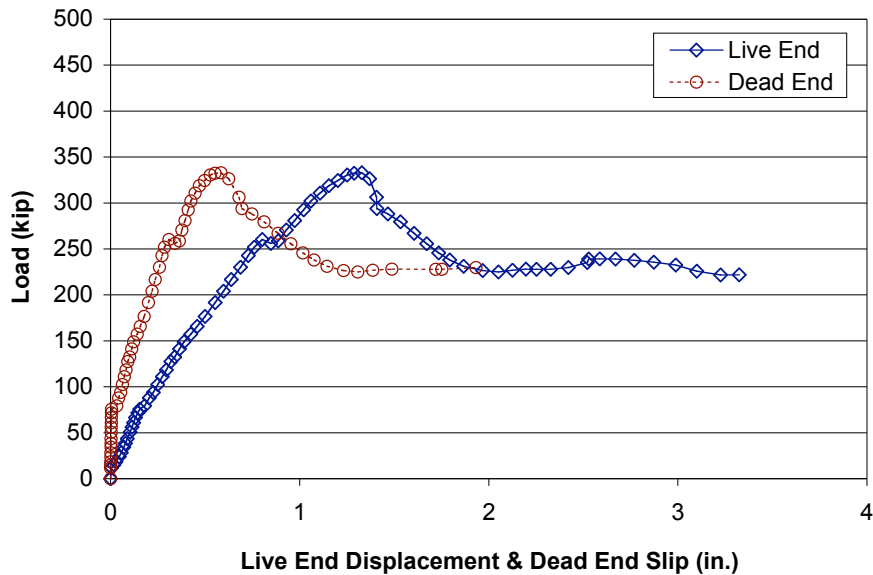


**Figure 5-82 Live End Load-Displacement and Dead End Load-Slip Response for Specimen 1\*-HD-7.5°-2**

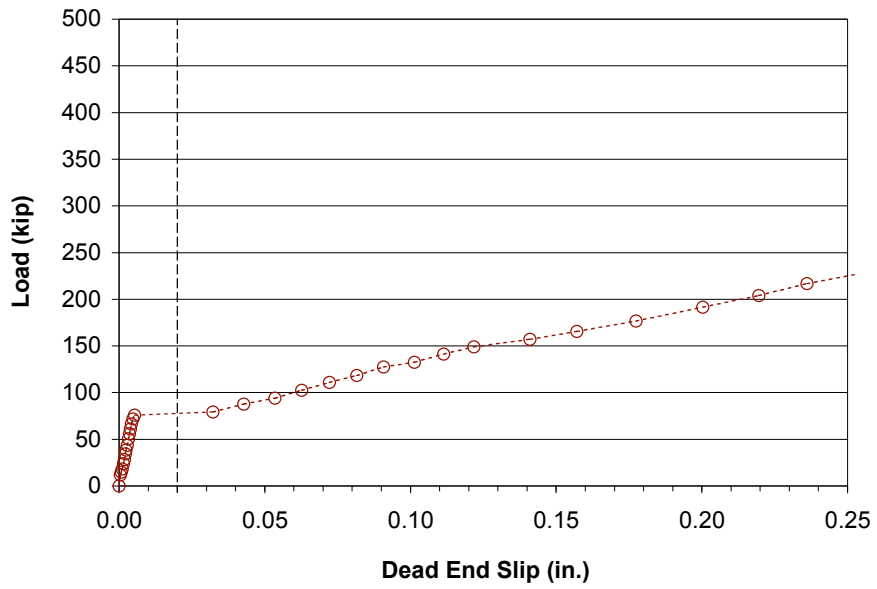


***Figure 5-83 Dead End Load-Slip Response for Specimen 1\*-HD-7.5°-2, Amplified Scale***



***Figure 5-84 Profile of Specimen 1\*-HD-7.5°-2 after Testing***

### 5.3 FRICTION TESTS

This section presents the results from all friction tests, which were originally reported in Icaza (2004). Seven tests were performed on each specimen. In most cases, these tests consisted of three tests with an unoiled tendon, followed by two tests with a new, freshly oiled tendon, and then two tests with the same oiled tendon one day later. In one case, as described in Section 5.3.1, seven tests with an unoiled tendon were performed.

One plot is included for each specimen which shows friction losses versus total load for all seven tests. Friction losses are expressed as a percentage of the total load and do not include hardware losses due to the tendon passing through the steel bearing plates and the steel chair used to hold the load cells. Hardware losses were subtracted from the total calculated losses so that final results would represent only those losses occurring inside the duct. Information on the determination of hardware losses can be found in Icaza (2004). While friction losses are shown over the entire load range, major interest is in the unshaded 350–400 kip range, corresponding to 70%–80% of the guaranteed ultimate tensile strength of the tendon. This load range is typical of most practical applications.

A naming scheme was used to distinguish among the various specimens. The scheme denotes strand surface condition, duct type, and tendon angle change as described below:

- A number denotes strand surface condition. The number “0” indicates the tendon was unoiled for all seven tests, “1” indicates the tendon was oiled with Citgo Trukut NC205 for four of the seven tests, and “2” indicates the tendon was oiled with NoxRust 703D for four of the seven tests.

- A two-letter combination indicates duct type. “SP” denotes a rigid steel pipe, “GD” denotes a galvanized duct, and “HD” denotes an HDPE duct.
- Total tendon angle change from one end of the duct to the other is given in degrees. An angle change of 90 degrees corresponds to specimens with a 10-ft radius of curvature; an angle change of 30 degrees corresponds to specimens with a 30-ft radius of curvature.

For example, specimen 2-HD-90° contained a tendon oiled with NoxRust 703D inside an HDPE duct, and the total tendon angle change was 90 degrees (i.e. the radius of curvature was 10 ft.).

### **5.3.1 Steel Pipe Specimens**

One specimen, 0-SP-90°, was tested 7 times with an unoiled tendon and then discarded. This series of tests deviated from the usual sequence of three tests with an unoiled tendon, two tests with a freshly oiled tendon, and two more tests after the oil had been given one day to dry. Results for specimen 0-SP-90° are presented first, followed by the results for specimens with a 10-ft radius of curvature (1-SP-90° and 2-SP-90°) and specimens with a 30-ft radius of curvature (1-SP-30° and 2-SP-30°).

#### ***5.3.1.1 0-SP-90°***

Friction loss measurements for specimen 0-SP-90° are shown in Figure 5-85. This specimen was the only one for which 7 tests with unoiled tendons were performed. Losses at high loads ranged from 29% to 35%, with an average loss of 32%. The data are highly scattered at low loads but converge at loads greater than 300 kip. Losses increased from the first to the third tests, then dropped to the lowest level in the fourth test before again increasing with each subsequent test.

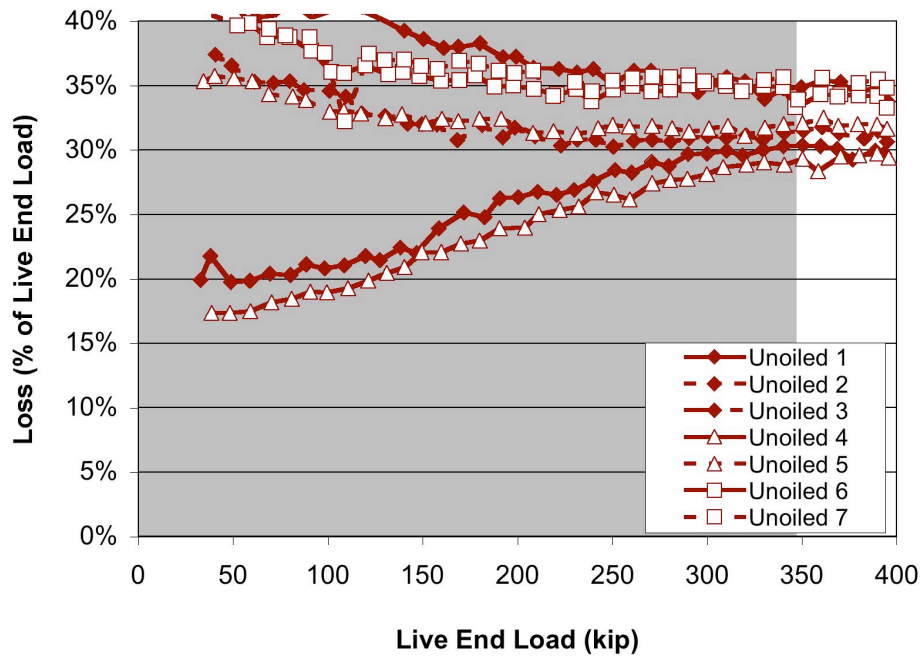


**Figure 5-85 Friction Losses for Specimen 0-SP-90°**

**5.3.1.2 1-SP-90°**

Friction loss measurements for specimen 1-SP-90° are shown in Figure 5-86. Losses for the unoiled tendon at high loads ranged from 29% to 36%, with an average loss of 33%. Average losses at high loads for the tendon with fresh oil were 27% and 30% for the first and second tests, respectively. Average losses at high loads for the tendon one day after oiling were approximately 34% for both tests. The data are highly scattered at low loads but begin converging at loads greater than 300 kip.



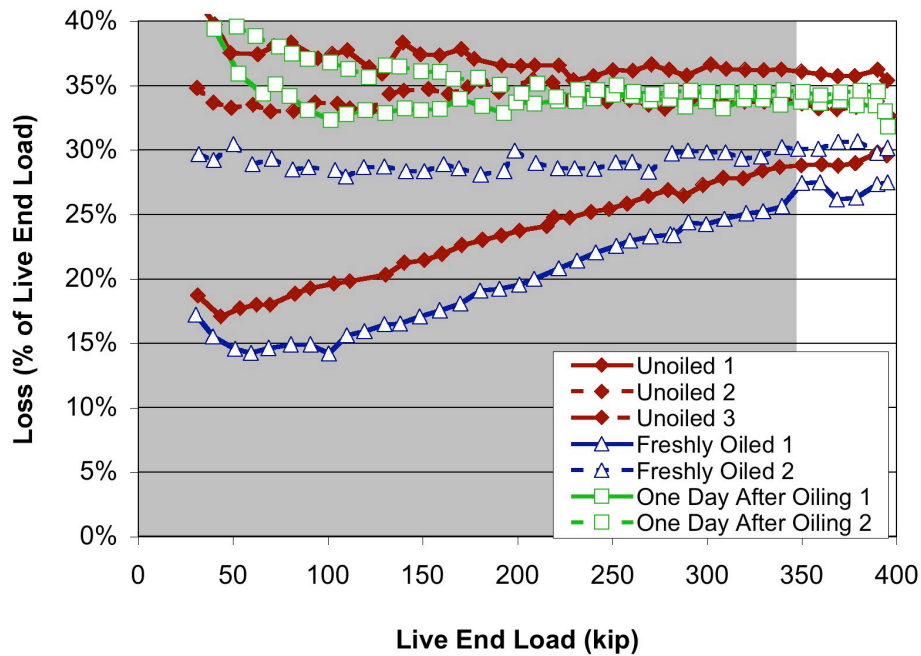


**Figure 5-86 Friction Losses for Specimen 1-SP-90°**

### 5.3.1.3 2-SP-90°

Friction loss measurements for specimen 2-SP-90° are shown in Figure 5-87. Losses for the unoiled tendon at high loads ranged from 28% to 32%, with an average loss of 30%. Average losses at high loads for the tendon with fresh oil were 21% and 25% for the first and second tests, respectively. Average losses at high loads for the tendon one day after oiling were 30% and 33% for the first and second tests, respectively. The data are relatively scattered at all load levels, though they are less scattered at higher loads.

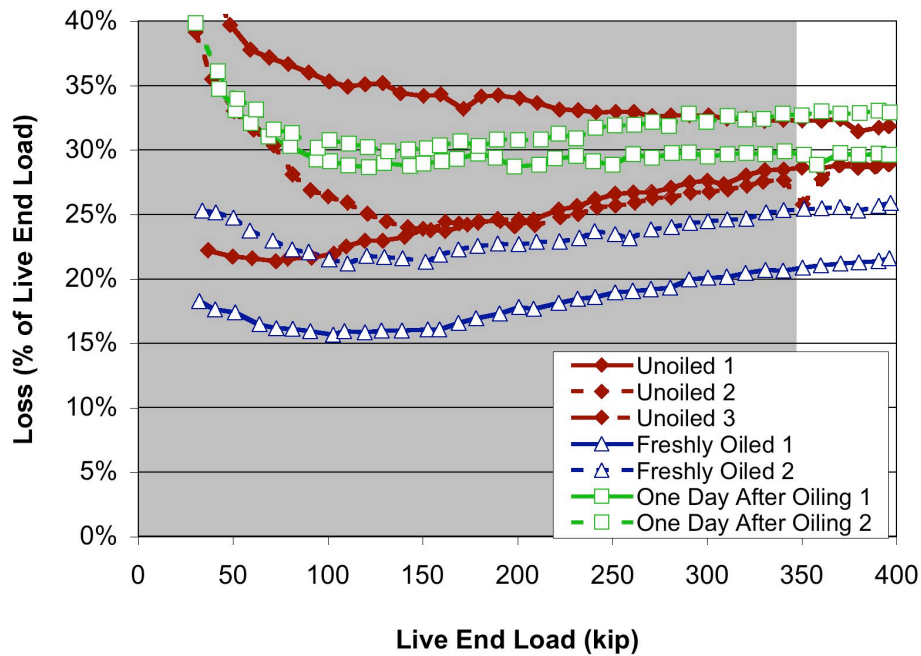


**Figure 5-87 Friction Losses for Specimen 2-SP-90°**

#### 5.3.1.4 1-SP-30°

Friction loss measurements for specimen 1-SP-30° are shown in Figure 5-88. Losses for the unoiled tendon at high loads were all approximately 16%. Average losses at high loads for the tendon with fresh oil were 13% and 12% for the first and second tests, respectively. Average losses at high loads for the tendon one day after oiling were approximately 14% for both tests. The data are somewhat scattered at low loads but converge at loads of greater than 300 kip.

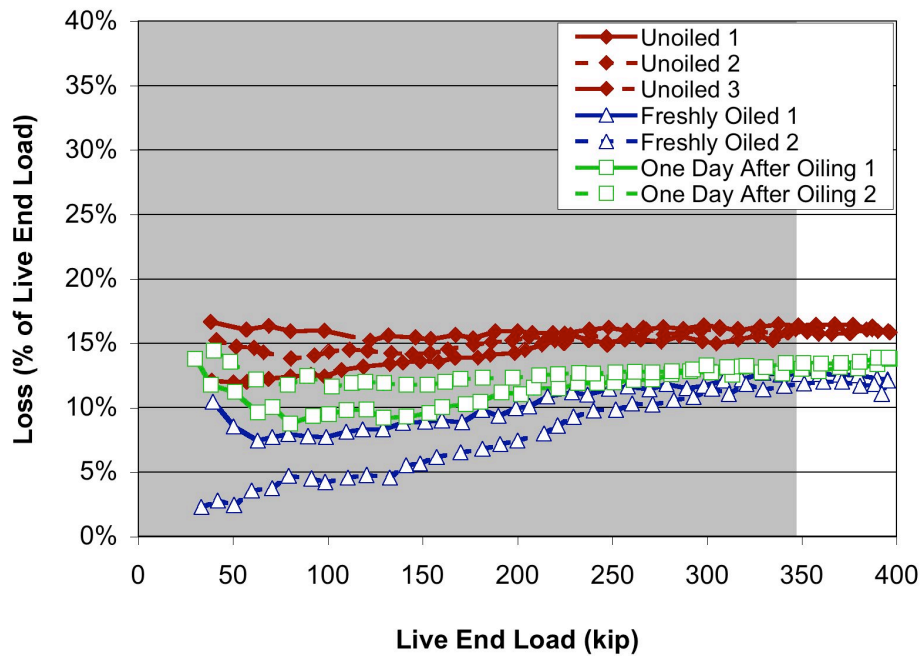


**Figure 5-88 Friction Losses for Specimen 1-SP-30°**

**5.3.1.5 2-SP-30°**

Friction loss measurements for specimen 2-SP-30° are shown in Figure 5-89. Losses for the unoiled tendon at high loads ranged from 13% to 14%, with an average loss of 13%. Average losses at high loads for the tendon with fresh oil were 8% for both tests. Average losses at high loads for the tendon one day after oiling were 9% and 10% for the first and second tests, respectively. The data are somewhat scattered at low loads but converge at loads of greater than 300 kip.

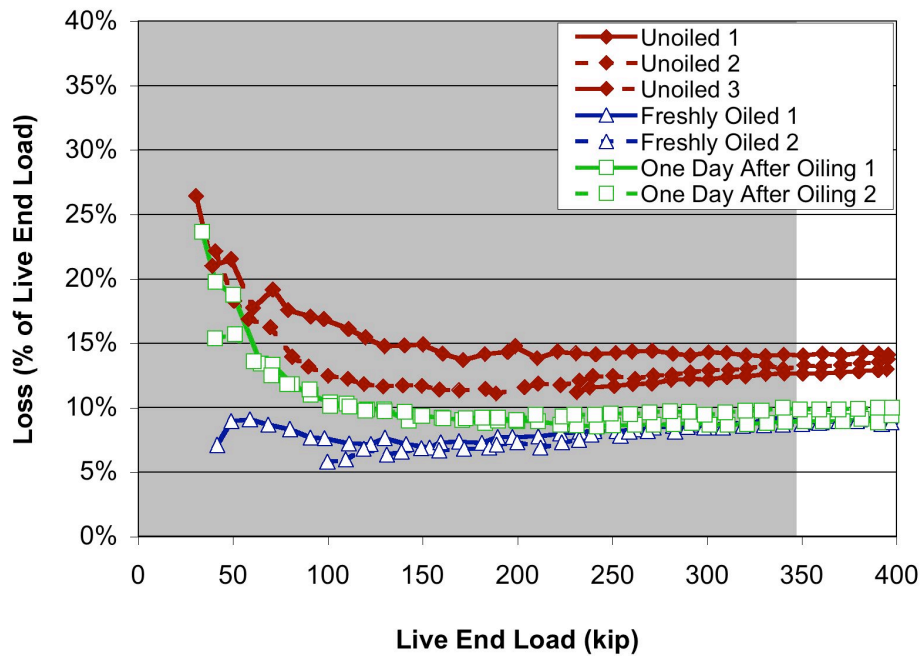


**Figure 5-89 Friction Losses for Specimen 2-SP-30°**

### 5.3.2 Galvanized Duct Specimens

Results are presented for specimens with a 10-ft radius of curvature (1-GD-90° and 2-GD-90°) and specimens with a 30-ft radius of curvature (1-GD-30° and 2-GD-30°). Unlike the steel pipe specimens, no specimen was prepared solely for testing with an unooled tendon.

#### 5.3.2.1 1-GD-90°

Friction loss measurements for specimen 1-GD-90° are shown in Figure 5-90. Losses for the unooled tendon at high loads ranged from 24% to 34%, with an average loss of 28%. Average losses at high loads for the tendon with fresh oil were 24% and 26% for the first and second tests, respectively. Average losses at high loads for the tendon one day after oiling were 29% for both tests. The data

are scattered at all load levels for unoiled and freshly oiled tendons; the data for tendons one day after oiling exhibit almost no scatter.

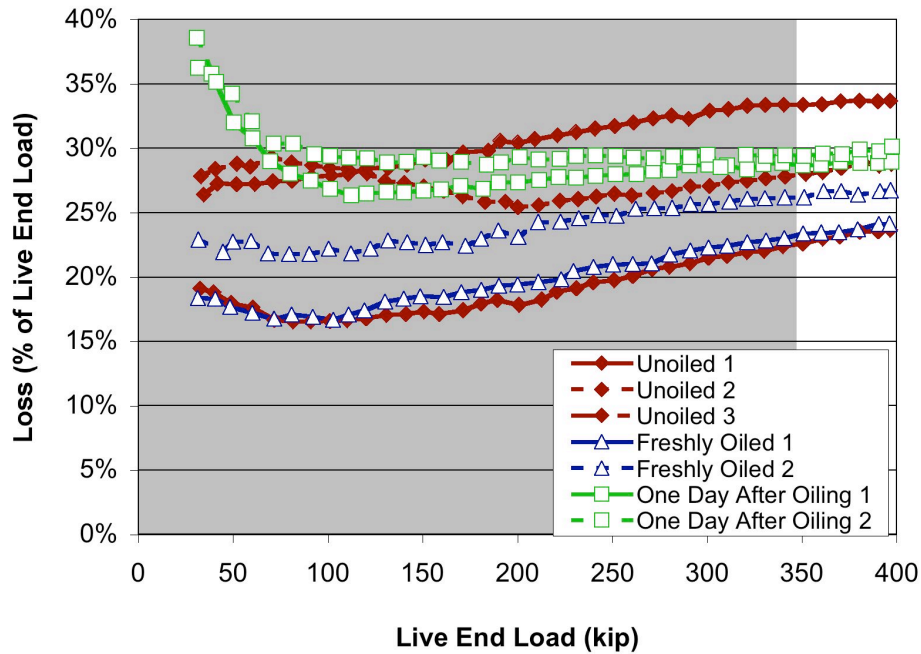


*Figure 5-90 Friction Losses for Specimen 1-GD-90°*

### 5.3.2.2 2-GD-90°

Friction loss measurements for specimen 2-GD-90° are shown in Figure 5-91. Losses for the unoiled tendon at high loads ranged from 25% to 30%, with an average loss of 28%. Average losses at high loads for the tendon with fresh oil were 25% and 28% for the first and second tests, respectively. Average losses at high loads for the tendon one day after oiling were 30% and 29% for the first and second tests, respectively. The data for the unoiled and freshly oiled tendons are scattered at all load levels; the data for tendons one day after oiling exhibit almost no scatter.

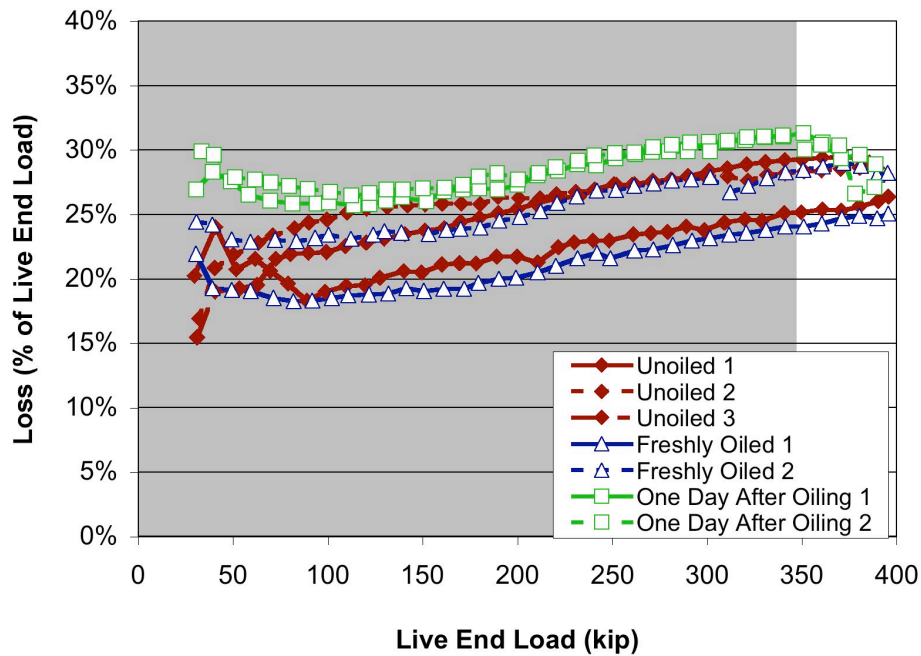


*Figure 5-91 Friction Losses for Specimen 2-GD-90°*

### 5.3.2.3 1-GD-30°

Friction loss measurements for specimen 1-GD-30° are shown in Figure 5-92. Losses for the unoiled tendon at high loads ranged from 8% to 10%, with an average of approximately 8.5%. Average losses at high loads for the tendon with fresh oil were approximately 8% for both tests. Average losses at high loads for the tendon one day after oiling were also approximately 8% for both tests. The data for all tests show almost no scatter.

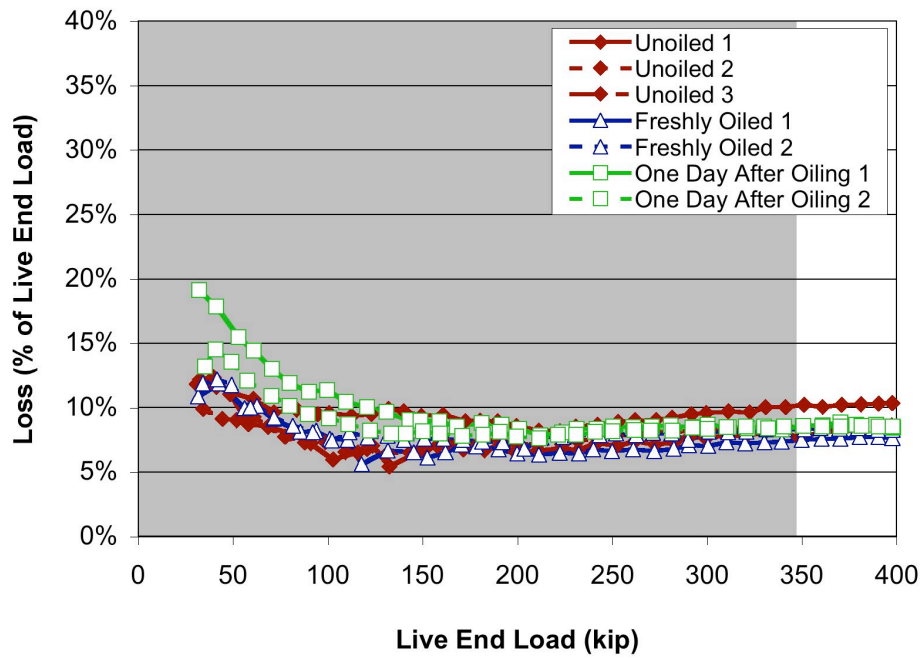


*Figure 5-92 Friction Losses for Specimen 1-GD-30°*

#### 5.3.2.4 2-GD-30°

Friction loss measurements for specimen 2-GD-30° are shown in Figure 5-93. Losses for the unoiled tendon at high loads ranged from 9% to 12%, with an average of 11%. Average losses at high loads for the tendon with fresh oil were 11% and 9% for the first and second tests, respectively. Average losses at high loads for the tendon one day after oiling were approximately 11% for both tests. The data for all tests show little scatter.

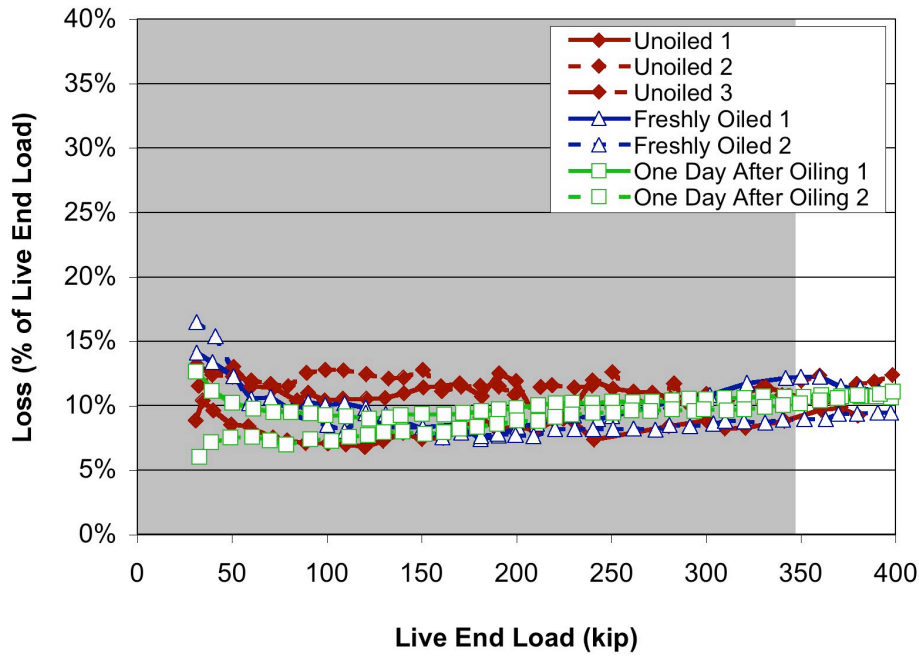


**Figure 5-93 Friction Losses for Specimen 2-GD-30°**

### 5.3.3 HDPE Duct Specimens

Results are presented for specimens with a 10-ft radius of curvature (1-HD-90° and 2-HD-90°) and specimens with a 30-ft radius of curvature (1-HD-30° and 2-HD-30°). Unlike the steel pipe specimens, no specimen was prepared solely for testing with an unoiled tendon.

#### 5.3.3.1 1-HD-90°

Friction loss measurements for specimen 1-HD-90° are shown in Figure 5-94. Losses for the unoiled tendon at high loads ranged from 17% to 19%, with an average of 18%. Average losses at high loads for the tendon with fresh oil were approximately 14% for both tests. Average losses at high loads for the tendon one day after oiling were 15% for the first test; losses in the second test were at



approximately 14% when the testing was stopped due to wire breakage, as explained below. The data show relatively little scatter, particularly at load levels above 250 kip.

Upon removal of the tendon from this specimen, the strands were found to be sharply kinked at the point where they passed through the bearing plate and into the ram, as was also true for specimen 1-HD-30°. A representative bent strand is shown in Figure 5-95. This kink was likely due to a misalignment of the bearing plate and the duct, causing wires to break at high loads during the last test. Friction losses for the unoiled tendons were approximately the same in this specimen and in 2-HD-90°; therefore the problem likely did not affect the test results. Once the load reached 320 kip in the second test one day after oiling, wires were breaking so rapidly that the load could not be increased, and the test was stopped.

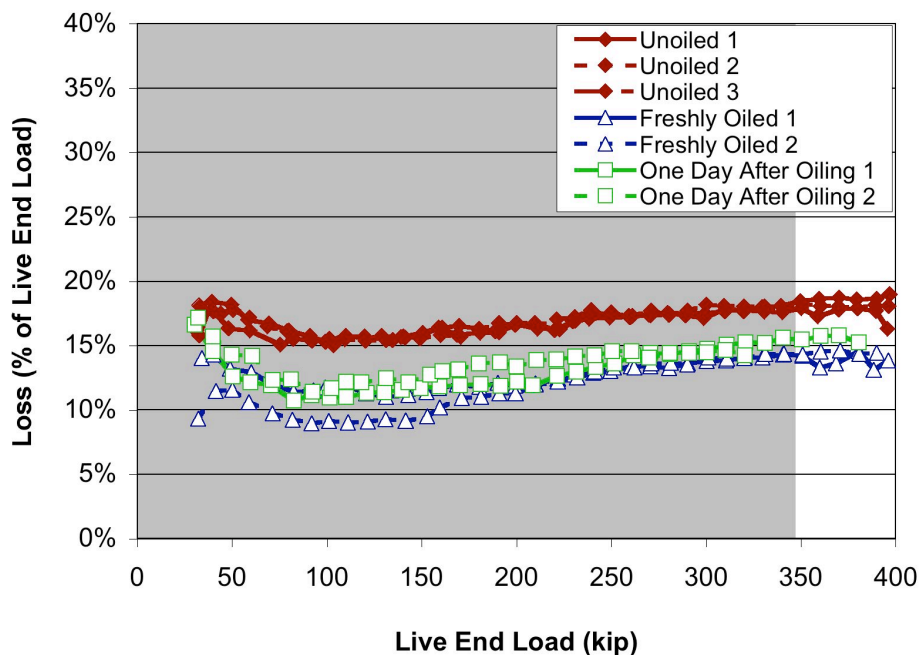


*Figure 5-94 Friction Losses for Specimen 1-HD-90°*



*Figure 5-95 Sharp Kink in Strand after Friction Testing*

### **5.3.3.2 2-HD-90°**

Friction loss measurements for specimen 2-HD-90° are shown in Figure 5-96. Losses for the unoiled tendon at high loads ranged from 17% to 18%, with an average of 18%. Average losses at high loads for the tendon with fresh oil were 15% and 14% for the first and second tests, respectively. Average losses at high loads for the tendon one day after oiling were 15% for both tests. The data are somewhat scattered at low loads but converged at load levels above 250 kip.

During the third test with the unoiled tendon, the load measured by one of the load cells dropped while increasing as expected for the other two load cells, likely due to some kind of problem with the electronic data acquisition equipment. The calculated losses for this test were therefore much higher than normal and were disregarded.

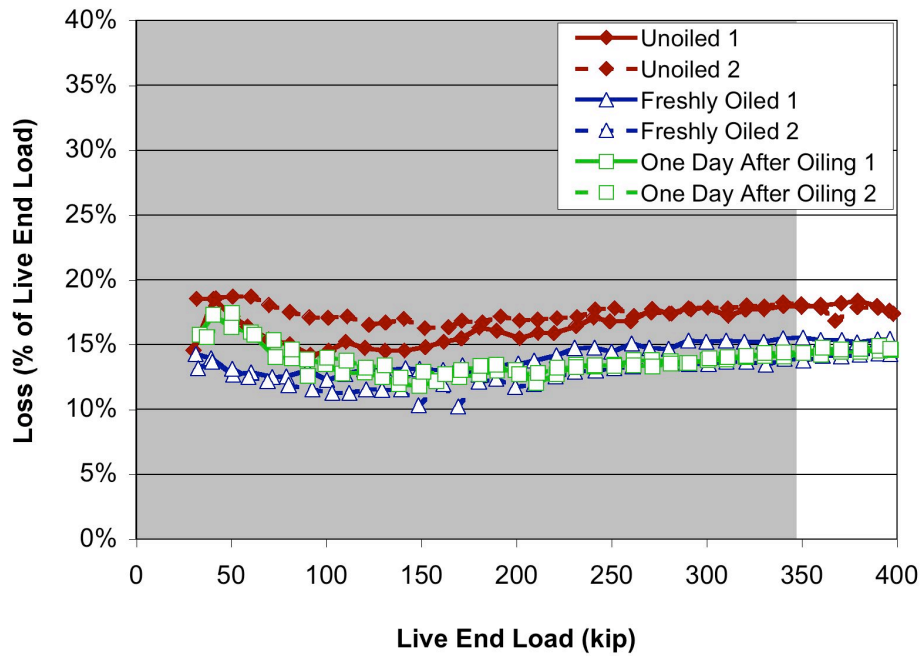


**Figure 5-96 Friction Losses for Specimen 2-HD-90°**

### 5.3.3.3 1-HD-30°

Friction loss measurements for specimen 1-HD-30° are shown in Figure 5-97. Losses for the unoiled tendon at high loads were all approximately 7%. Average losses at high loads for the tendon with fresh oil were 6% for both tests. Average losses at high loads for the tendon one day after oiling were also 6% for both tests. The data show little scatter at all load levels.

Upon removal of the tendon from this specimen, the strands were found to be sharply kinked at the point where they passed through the bearing plate and into the ram, as was also true for specimen 1-HD-90°. A representative bent strand is shown in Figure 5-95. This kink was likely due to a misalignment of the bearing plate and the duct, causing wires to break at high loads during the last test. Friction losses for the unoiled tendons were approximately the same in this

specimen and in 2-HD-30°; therefore the problem likely did not affect the test results. Despite wires breaking, the load did reach 400 kips, and a complete data set is still available for this set of tests.

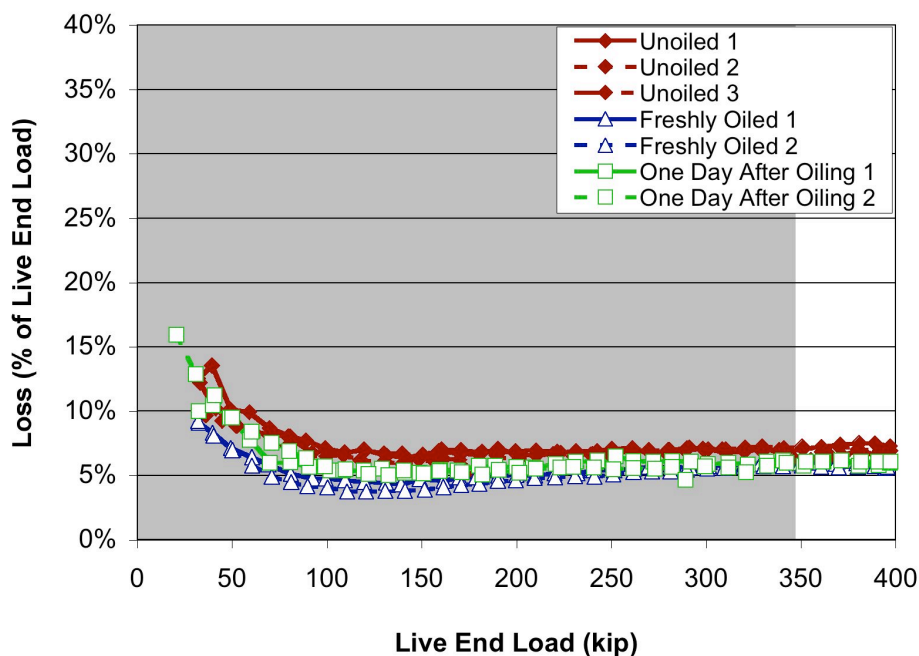


**Figure 5-97 Friction Losses for Specimen 1-HD-30°**

#### 5.3.3.4 2-HD-30°

Friction loss measurements for specimen 2-HD-30° are shown in Figure 5-98. Losses for the unoiled tendon at high loads were all slightly above 6%. Average losses at high loads for the tendon with fresh oil were slightly below 6% for both tests. Average losses at high loads for the tendon one day after oiling were slightly above 6% for both tests. The data show little scatter at all load levels.

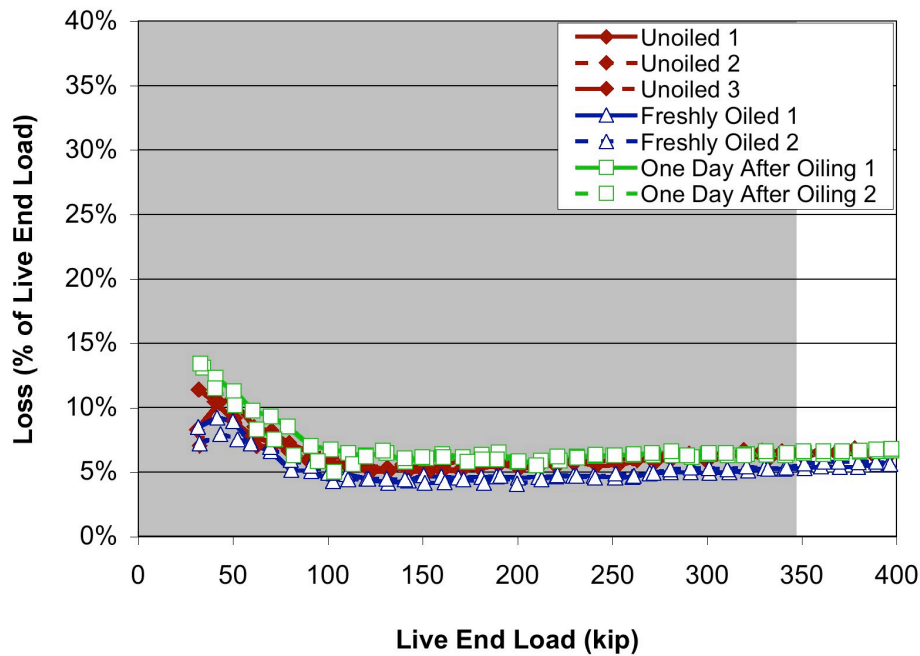


*Figure 5-98 Friction Losses for Specimen 2-HD-30°*

### 5.3.4 Duct Damage

After testing of all specimens with HDPE or galvanized ducts, the ducts were removed and cut open to inspect the damage caused by post-tensioning. The galvanized ducts are shown in Figure 5-99 through Figure 5-102: Figure 5-99 and Figure 5-100 show ducts with a 10-ft radius of curvature, while Figure 5-101 and Figure 5-102 show ducts with a 30-ft radius of curvature. HDPE ducts are shown in Figure 5-103 through Figure 5-106: Figure 5-103 and Figure 5-104 show ducts with a 10-ft radius of curvature, while Figure 5-105 and Figure 5-106 show ducts with a 30-ft radius of curvature. The damage along the cut edges was primarily caused by the jackhammer used to remove the ducts. The damage of interest is on the interior surfaces of the ducts and can be seen in the form of “grooves” caused by the bearing of the tendon against the duct. As can be seen when comparing

ducts with different radii of curvature, ducts with a 10-ft radius of curvature sustained more damage than ducts with a 30-ft radius of curvature. This trend is expected, since a smaller radius of curvature causes higher normal stresses on the surface of the duct. In all cases, however, the damage was not severe, nor was the integrity of the duct compromised.



*Figure 5-99 Duct from Specimen 1-GD-90° after Testing*



*Figure 5-100 Duct from Specimen 2-GD-90° after Testing*



*Figure 5-101 Duct from Specimen 1-GD-30° after Testing*



*Figure 5-102 Duct from Specimen 2-GD-30° after Testing*



*Figure 5-103 Duct from Specimen 1-HD-90° after Testing*





*Figure 5-104 Duct from Specimen 2-HD-90° after Testing*



*Figure 5-105 Duct from Specimen 1-HD-30° after Testing*



*Figure 5-106 Duct from Specimen 2-HD-30° after Testing*

## CHAPTER 6

### Comparison of Behavior and Effect of Variables

#### 6.1 INTRODUCTION

This chapter contains discussions of the corrosion test results from Pennsylvania State University presented Chapter 3 and the bond and friction test results from the University of Texas at Austin presented in Chapter 5. The discussions of bond and friction test results include comparisons based on duct type and strand surface condition. In the case of the friction tests, comparisons are also made based on radius of curvature. Recommendations for implementation and further research are provided in shaded boxes throughout the chapter.

#### 6.2 CORROSION TESTS

This section contains a brief summary of the corrosion test results for the two oils used in large-scale testing, Trukut NC205 and NoxRust 703D.

Single-strand specimens were exposed to three different environments and given a corrosion rating on a scale of 1-7 every four weeks for a total of six months. Specimens were placed either outdoors, in a controlled temperature and humidity chamber, or in a 5% NaCl solution. Corrosion ratings were assigned after visual inspection of the specimens according to the rating system given in Table 6-1. A rating of 4 or less was required for any candidate oil to be considered for large-scale testing.

Average corrosion test results at the end of six months are presented in Table 6-2. Both oils received ratings of less than 4 in all environments. As expected, corrosion damage was most severe for specimens stored in the NaCl solution. In all three environments, specimens oiled with 703D performed slightly

better than specimens oiled with NC205, receiving average ratings between 0.1 and 1.0 points lower.

**IMPLEMENTATION:** *Both emulsifiable oils used in this test program, Trukut NC205 and NoxRust 703D, provide adequate temporary corrosion protection for post-tensioned tendons. NoxRust 703D performed slightly better in this test program than Trukut NC205.*

**Table 6-1 Rating System for Corrosion Tests**

Rating	Description
1	As received from manufacturer and completely clean from any corrosion products.
2	No signs of corrosion at any level or small spots of rust.
3	Small blisters, superficial but widely spread corrosion, pitting is unusual.
4	Small blisters, uniform corrosion or initial signs of wide pitting in centralized areas.
5	Large blisters, trail of blisters does not exceed 2 in., deep and wide pitting is visible, corrosion products and pitting do not affect more than 50% of the steel area.
6	Large blisters, trail of blisters along the strand exceeds 2 in., deep and wide pitting cover most of the strand surface, corrosion products and pitting affect over 50% of the steel surface, and several forms of corrosion are present simultaneously.
7	High levels of corrosion with visible large areas of steel lost.

**Note:** Rating system is precise to  $\pm 0.5$  (i.e. borderline specimens can receive a rating of 2.5, 3.5, etc.)

**Table 6-2 Corrosion Test Results, Trukut NC205 and NoxRust 703D**

<b>Oil</b>	<b>Environment</b>	<b>Final Corrosion Rating (Average)</b>
NC205	outdoor exposure	3.0
	controlled temperature and humidity	3.0
	5% NaCl solution	3.8
703D	outdoor exposure	2.0
	controlled temperature and humidity	2.7
	5% NaCl solution	3.7

### **6.3 BOND TESTS**

This section makes comparisons to illustrate the effect of the variables discussed in Chapter 4 based on the data presented in Chapter 5. Comparisons are first made among duct types and then among strand surface conditions.

Two failure criteria are used for discussion in this chapter: peak load and load at 0.02 in. dead end slip. The peak load criterion is used to gauge strength, and the slip criterion is used to gauge serviceability. Because proper crack width control depends on good bond behavior, high levels of slip could be associated with poor serviceability in a post-tensioned member. A value of 0.02 in. as the limiting dead end slip was chosen as representative of the transition point from linear to non-linear slip in uncoiled specimens (Diephuis 2004). This value is larger than the ASTM A 981-97 limiting value of 0.01 in. for single-strand pullout testing but smaller than the North American Strand Producers Association recommended value of 0.1 in. (Salcedo 2003).

Data in this section are presented primarily in the form of load-displacement plots which show a band of values which enclose all data points for the multiple specimens tested. This approach helps show “average” behavior while also indicating the level of scatter present in the data. A table containing all bond test results, including calculated bond stresses, is given in Appendix A.

### **6.3.1 Comparisons among Duct Types**

The effect of duct type on bond capacity can be assessed by comparing live end load-displacement behavior for specimens with the same strand surface condition but different duct types. As is clearly shown in Figure 6-1 through Figure 6-3, peak loads achieved for specimens with galvanized ducts were consistently higher than peak loads achieved for specimens with HDPE ducts, which in turn were much higher than peak loads achieved for the smooth steel pipe specimens. Figure 6-1 shows live end load-displacement behavior for specimens with uncoiled tendons. For this strand surface condition, the average peak loads for specimens with HDPE duct and galvanized pipes were 22% and 77% lower, respectively, than the average peak load for specimens with galvanized ducts. The figure also shows the importance of providing studs or shear connectors on the outside of galvanized steel pipes. Although the shear studs did eventually fail in these experiments, the specimens with studded pipes had a higher capacity after initial failure than those without studs. Figure 6-2 shows live end load-displacement behavior for specimens with tendons oiled with NC205. For this strand surface condition, the average peak loads for specimens with HDPE duct and galvanized pipes were 26% and 92% lower, respectively, than the average peak load for specimens with galvanized ducts. Figure 6-3 shows live end load-displacement behavior for specimens with tendons oiled with 703D. For this strand surface condition, the average peak loads for specimens with HDPE duct and galvanized pipes were 39% and 86% lower, respectively, than the average peak load for specimens with galvanized ducts.

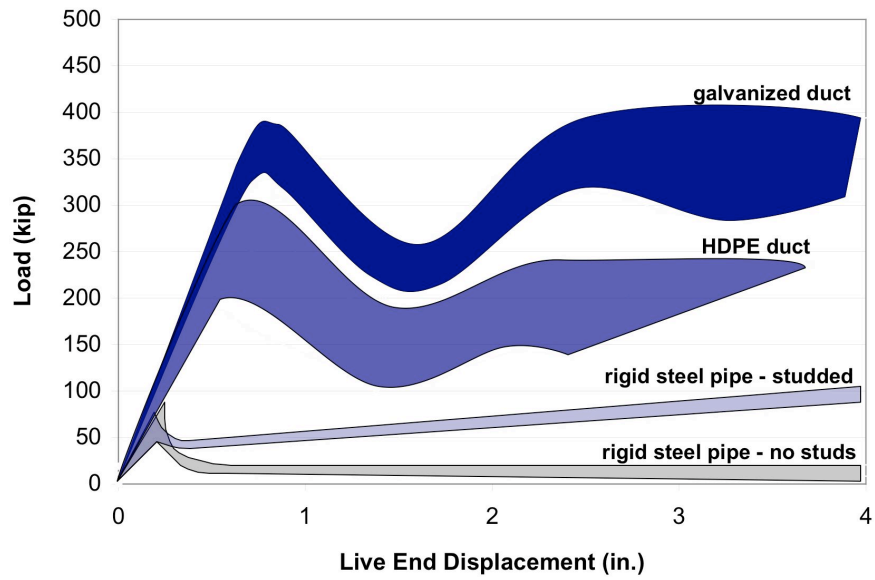


**Figure 6-1 Live End Load-Displacement Behavior, Uncoiled Tendons**

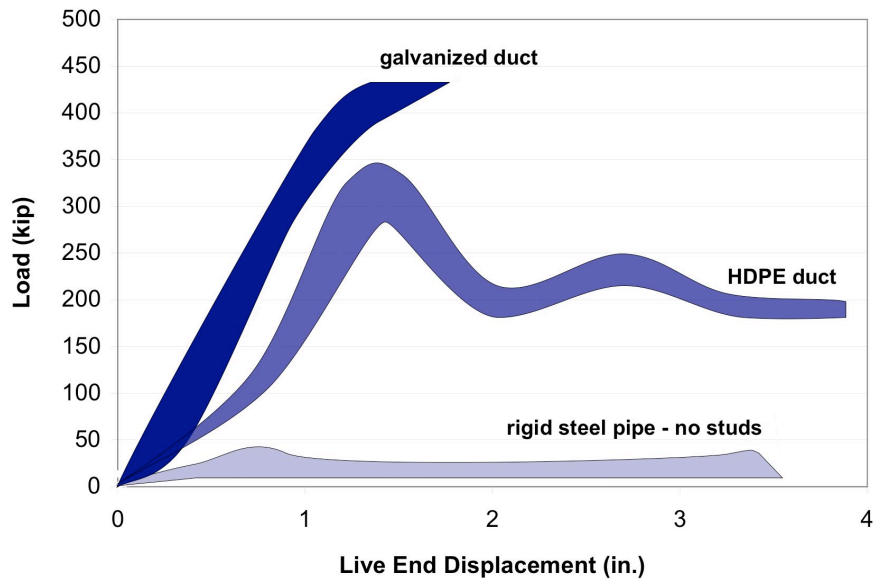


**Figure 6-2 Live End Load-Displacement Behavior, Tendons Oiled with NC205**

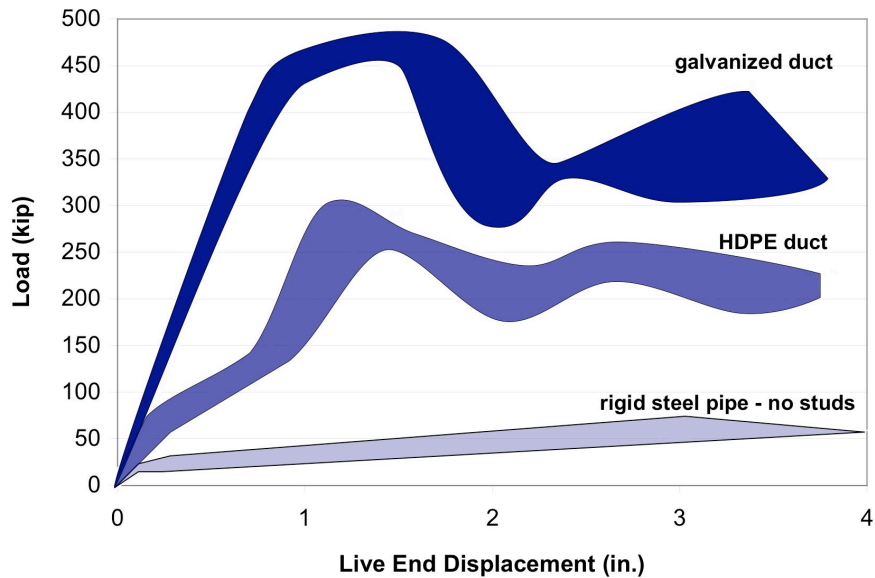


**Figure 6-3 Live End Load-Displacement Behavior, Tendons Oiled with 703D**

These results indicate that galvanized ducts provide considerably better development than HDPE ducts, on the order of 20% to 40%. Galvanized ducts therefore allow bonded tendons to be developed in shorter lengths than HDPE ducts.

**IMPLEMENTATION:** *Bond stresses in HDPE duct specimens were found to be 20% to 40% lower than in galvanized duct specimens for unoiled and oiled tendons, respectively. Designers using HDPE ducts in place of galvanized ducts must take these lower stresses into account and provide bonded lengths sufficient to develop the tendons.*

The relatively poor performance of the specimens with smooth steel pipes was due to failure at the grout-duct or duct-concrete interface. This failure differed from the failure observed in specimens with corrugated ducts, which



typically occurred at the tendon-grout interface. In early tests, no attempts were made to anchor the pipe into the concrete. Failure generally occurred at the duct-concrete interface, and the entire pipe began pulling out of the specimen. A similar problem has recently been observed with deviators in segmental concrete bridges in Florida, where measures to better anchor the deviators are being considered (Nickas 2005). In this test program, two specimens were constructed each with 4 studs, 2 in. in length, welded to the underside of the pipes. These studs prevented initial failure at the duct-concrete interface but did not result in higher peak loads. Initial failure for the specimens with shear studs occurred at the grout-duct interface, and the entire grout plug began pulling out of the specimen.

Two important conclusions can be drawn from these steel pipe specimen results. First, proper anchorage must be provided to ensure that deviators do not slip relative to the concrete. Second, bond stresses at the tendon-grout interface are generally not what controls behavior if the inside surface of the duct is smooth. Only very low bond stresses were developed between the grout and the steel pipe. For this reason, further discussion of bond results will focus only on specimens with corrugated galvanized or HDPE ducts.

**IMPLEMENTATION:** *Shear connectors or shear studs should be used for anchorage purposes on the outside of smooth steel deviator pipes.*

### **6.3.2 Comparisons among Strand Surface Conditions**

This section contains three major comparisons: a general comparison between unoiled and oiled tendons, a comparison between tendons oiled with NC205 and those oiled with 703D, and a comparison between tendons grouted 2 days and 10 days after oiling.

### ***6.3.2.1 Unoiled Tendons versus Oiled Tendons***

Somewhat surprisingly, specimens with oiled tendons generally exhibited peak load behavior similar to or better than that of specimens with unoiled tendons. Live end load-displacement plots, which show peak loads, are shown for specimens with galvanized ducts in Figure 6-4 and for specimens with HDPE ducts in Figure 6-5. For specimens with galvanized ducts, the average peak loads for NC205 and 703D specimens were actually 20% and 28% higher, respectively, than the average peak load for unoiled specimens. For specimens with HDPE ducts, the average peak loads for NC205 and 703D specimens were 15% and 1% higher, respectively, than the average peak load for unoiled specimens. One possible explanation for the increase in peak load capacity for oiled specimens is that the oil, by destroying adhesion between the tendon and the grout, allowed the tendon to slip relative to the grout at low loads. This slippage may have initially helped relieve some of the splitting pressure which eventually caused the specimens to crack and the load to drop. Mechanical interlock would therefore be the primary source of resistance, rather than bond stresses.

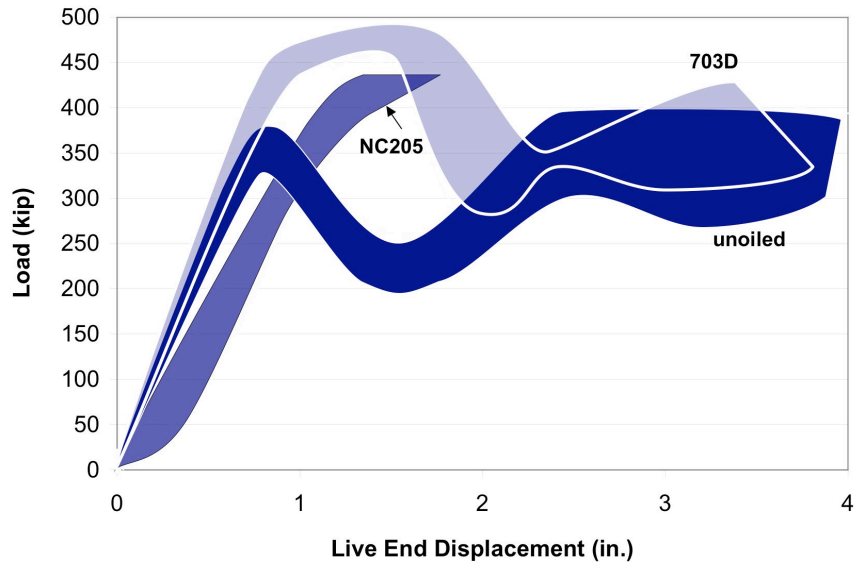


**Figure 6-4 Live End Load-Displacement Behavior, Galvanized Duct**

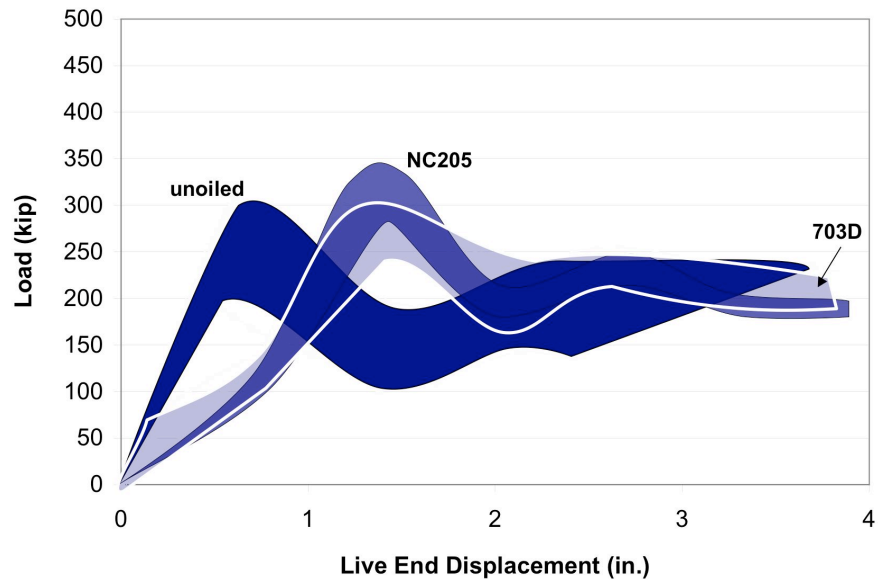


**Figure 6-5 Live End Load-Displacement Behavior, HDPE Duct**

Specimens with oiled tendons experienced high levels of dead end slip at low loads. Dead end slip behavior is shown for specimens with galvanized ducts in Figure 6-6 and for specimens with HDPE ducts in Figure 6-7. For specimens with galvanized ducts, the average loads at a dead end slip of 0.02 in. for NC205 and 703D specimens were 78% and 13% lower, respectively, than the average failure load due to slip for unoiled specimens. In the case of the 703D specimens, however, the data are highly scattered at a dead end slip of 0.02 in. This scatter is indicated in Figure 6-6 by the large width of the band as it crosses the dotted line. For specimens with HDPE ducts, the average peak loads for NC205 and 703D specimens were 92% and 75% lower, respectively, than the average failure load due to slip for unoiled specimens.

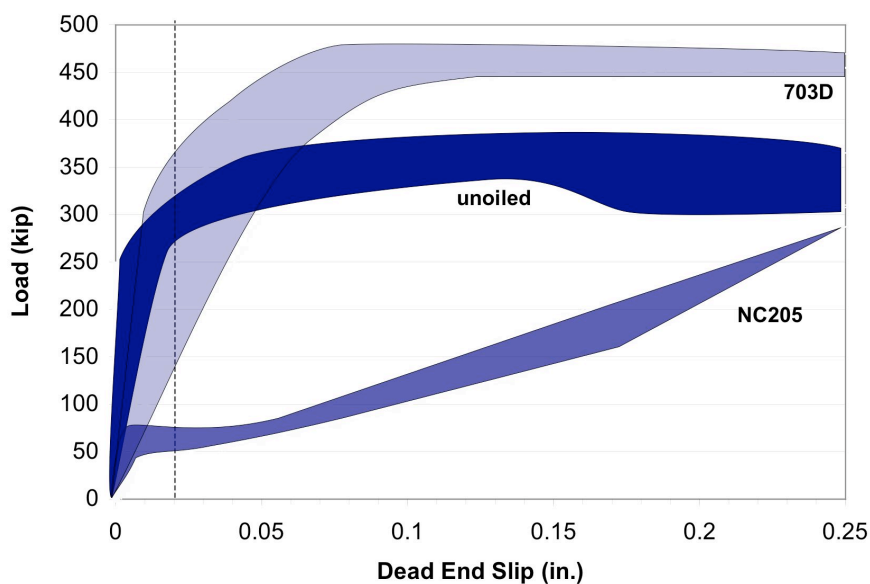


**Figure 6-6 Dead End Load-Slip Behavior, Galvanized Duct**

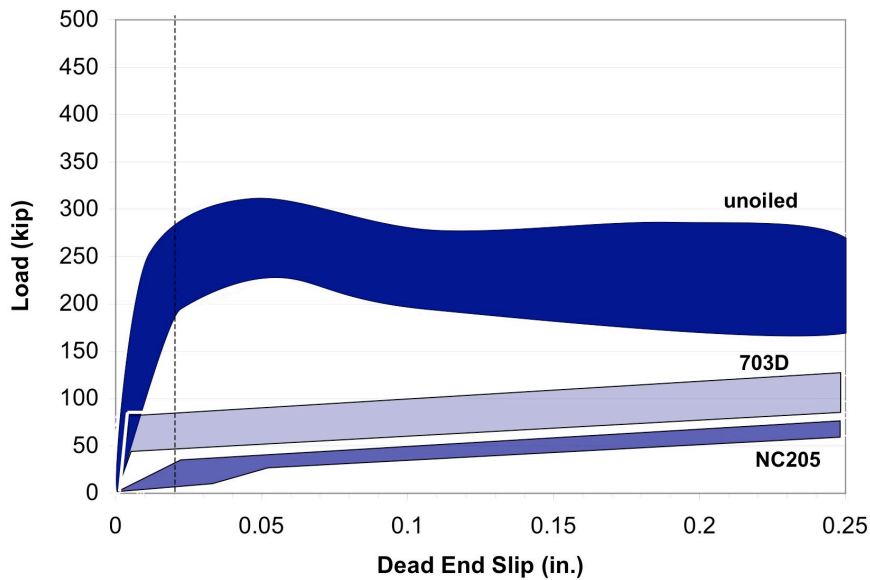


**Figure 6-7 Dead End Load-Slip Behavior, HDPE Duct**

Direct comparisons of peak loads and failure loads based on dead end slip are shown for specimens with galvanized ducts in Figure 6-8 and for specimens with HDPE ducts in Figure 6-9. For unoiled specimens, the failure loads based on peak load and dead end slip were within 20%. For oiled specimens, the figures show no change or slight increases in capacity compared with unoiled specimens. However, the figures clearly show greatly reduced bond for oiled specimens based on dead end slip. As shown in Figure 6-8, the average failure load based on dead end slip for specimens with galvanized ducts and unoiled tendons was 18% lower than the average peak load. In comparison, the average failure loads based on dead end slip for NC205 and 703D specimens were 85% and 44% lower, respectively, than the average peak loads. The dead end slip data for specimens with galvanized ducts and tendons oiled with 703D, however, are highly scattered at a dead end slip of 0.02 in., as shown in Figure 6-6. Because of this significant variability, the 44% figure cannot be reported with much confidence. The data for

HDPE specimens, shown in Figure 6-9, exhibit a similar trend and are more consistent. The average failure load based on dead end slip for specimens with uncoiled tendons was 9% lower than the average peak load. The average failure loads based on dead end slip for NC205 and 703D specimens were 94% and 78% lower, respectively, than the average peak loads.

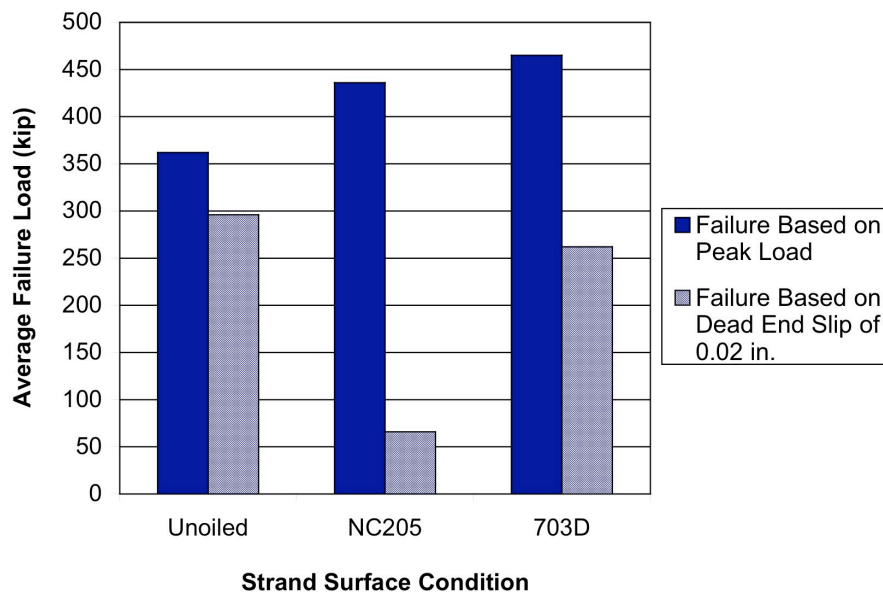


***Figure 6-8 Average Failure Loads, Galvanized Ducts***

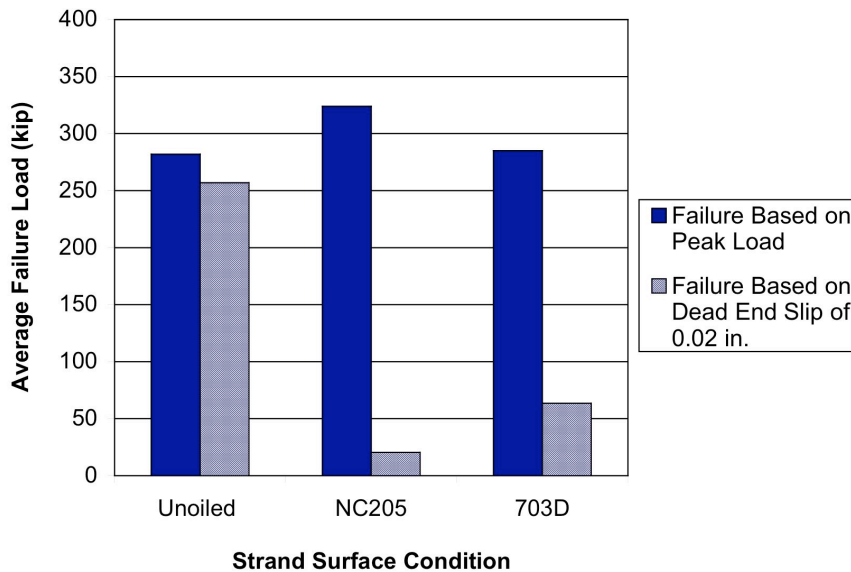


**Figure 6-9 Average Failure Loads, HDPE Ducts**

Based on these data, emulsifiable oils can be used as temporary corrosion protection for grouted post-tensioning tendons without being flushed. This recommendation is made for two main reasons. First, the strength of the bond specimens in this test program did not decrease when tendons were coated with oil. In fact, in most cases the peak load was higher for specimens with oiled tendons than specimens with uncoiled tendons. Second, although specimens with oiled tendons often experienced high levels of dead end slip at low loads, such slip behavior would only be significant if the post-tensioned member were cracked. If the member is cracked, then poor bond could result in wider cracks, creating serviceability problems. However, in many types of post-tensioned construction, cracking should not occur under service loads. For example, in segmental applications, no tensile stresses are permitted under service loads, and therefore the members should not be cracked. For cast-in-place construction, where some tensile stresses are allowed, cracks could be wider for members with

oiled tendons than for members with unoiled tendons. However, in cast-in-place construction, supplementary mild steel reinforcement for crack control could easily be provided.

**IMPLEMENTATION:** *Emulsifiable oils used as temporary corrosion protection in grouted post-tensioned construction do not need to be flushed with water. In cases where cracking might occur under service loads, the oil may cause cracks to widen, but the strength of the member will not be affected. Such cracking would not be expected in segmental construction and could easily be controlled in cast-in-place construction with supplementary mild reinforcement.*

#### **6.3.2.2 NC205 versus 703D**

Live end load-displacement behavior and peak loads for NC205 and 703D specimens were fairly similar. Live end load-displacement behavior for galvanized duct specimens is shown in Figure 6-4. The average peak load for NC205 specimens was only 6% lower than the average peak load for 703D specimens, although large displacements could not be achieved for the NC205 specimens due to wire breakage at the peak load. Live end load-displacement behavior for HDPE duct specimens is shown in Figure 6-5. The average peak load for NC205 specimens was 14% higher than the average peak load for 703D specimens, and post-peak behavior was similar in both cases.

Failure due to slip occurred at higher loads for 703D specimens than for NC205 specimens. Dead end load-slip behavior for galvanized duct specimens is shown in Figure 6-6. The average failure load due to slip for 703D specimens was almost three times the value for NC205 specimens but still 13% lower than the



value for unoiled specimens. However, as previously noted, the dead end data for 703D specimens are highly scattered at a dead end slip of 0.02 in. These results are therefore not reported with as much confidence as the data for HDPE duct specimens, which were more consistent. Dead end load-slip behavior for HDPE duct specimens is shown in Figure 6-7. The average failure load due to slip for 703D specimens was more than twice the value for NC205 specimens but still 75% lower than the value for unoiled specimens.

Based on these data, both of the oils used in this test program are acceptable for use in the field. Peak loads were similar for NC205 and 703D specimens. On average, 703D specimens exhibited slightly better slip performance than NC205. However, as previously discussed, peak load and overall load-displacement behavior are of primary concern for most post-tensioned applications under service loads.

**IMPLEMENTATION:** *The two emulsifiable oils used in this test program, Trukut NC205 and NoxRust 703D, are both acceptable for use based on the results of bond tests.*

### **6.3.2.3 NC205, Freshly Oiled versus 10 Days Drying Time**

Peak loads for specimens with fresh and dried oil were fairly similar, though specimens with fresh oil tended to have larger live end displacements at a given load compared with specimens with dried oil. Live end load-displacement behavior for galvanized duct specimens is shown in Figure 6-10. The average peak load for specimens with fresh oil was only 9% lower than the average peak load for specimens with dried oil, although large displacements could not be achieved for the specimens with fresh oil due to wire breakage at the peak load. The figure indicates that specimens with fresh oil experienced slightly greater live

end displacements at given loads than unoiled specimens, shown in the figure as a flatter initial slope. Specimens with dried oil, however, experienced live end displacements similar to those of unoiled specimens. Live end load-displacement behavior for HDPE duct specimens is shown in Figure 6-11. The average peak load for specimens with fresh oil was 6% higher than the average peak load for specimens with dried oil, and post-peak behavior was similar in both cases. Specimens with fresh oil experienced significantly greater live end displacements at given loads than unoiled specimens, shown in the figure as a flatter initial slope. Specimens with dried oil, however, experienced live end displacements similar to those of unoiled specimens.

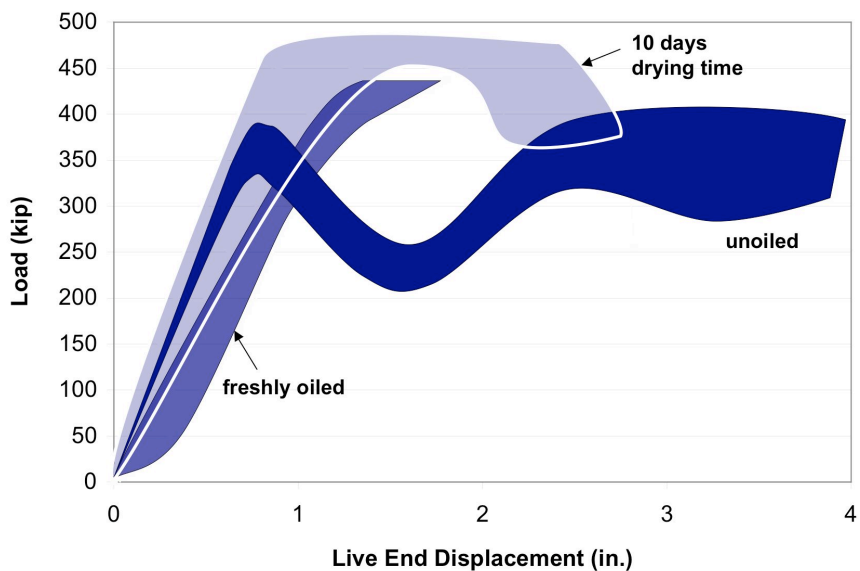


**Figure 6-10 Live End Load-Displacement Behavior, Galvanized Duct, Tendon Oiled with NC205**

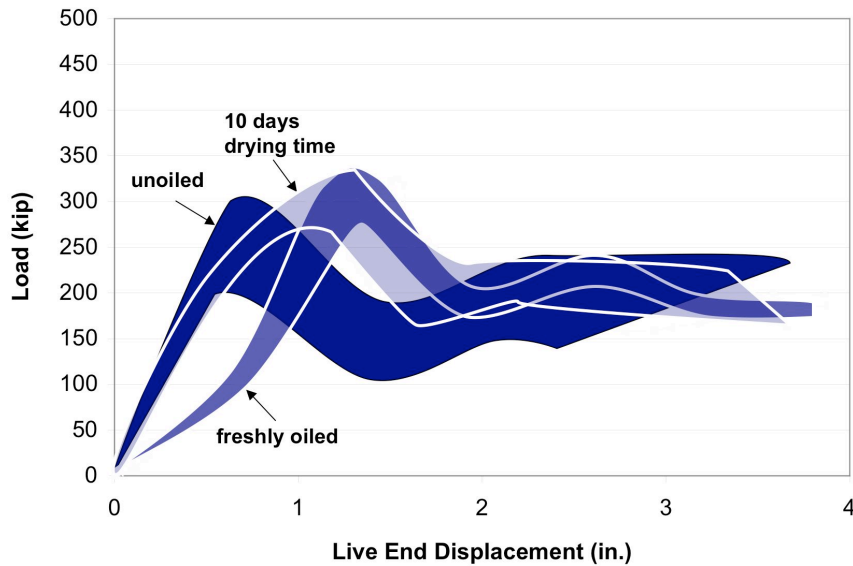


***Figure 6-11 Live End Load-Displacement Behavior, HDPE Duct, Tendon Oiled with NC205***

Failure due to slip occurred at substantially higher loads for specimens with dried oil than for specimens with fresh oil. Dead end load-slip behavior for galvanized duct specimens is shown in Figure 6-12. The average failure load due to slip for specimens with dried oil was almost twice the value for specimens with fresh oil but still 36% lower than the value for unoiled specimens. However, as previously noted, the dead end data for 703D specimens are highly scattered. These results are therefore not reported with as much confidence as the data for HDPE duct specimens, which were more consistent. Dead end load-slip behavior for HDPE duct specimens is shown in Figure 6-13. The average failure load due to slip for specimens with dried oil was more than four times the value for specimens with fresh oil but still 59% lower than the value for unoiled specimens. Specimens with fresh oil experienced significantly greater dead end displacements at given loads than unoiled specimens, shown in the figure as a

flatter initial slope. Specimens with dried oil, however, experienced dead end displacements similar to those of unoiled specimens.

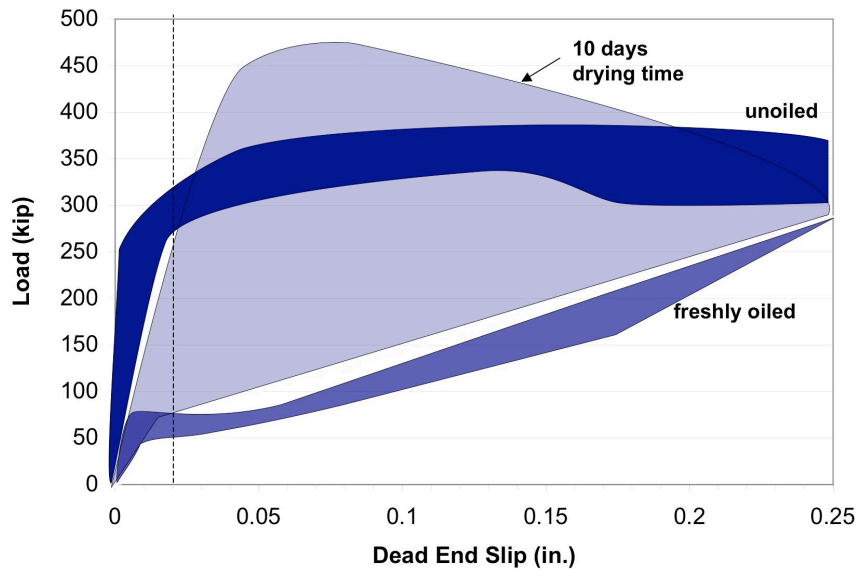


***Figure 6-12 Dead End Load-Slip Behavior, Galvanized Duct, Tendon Oiled with NC205***

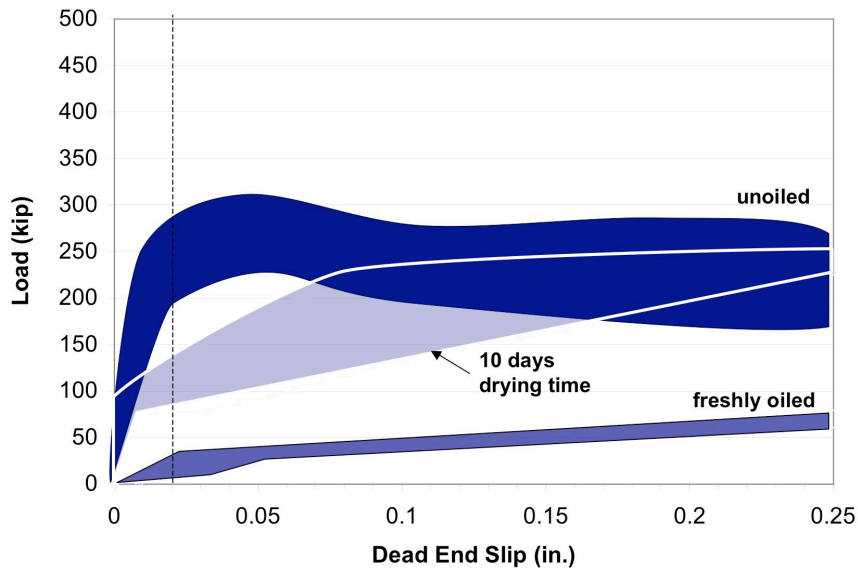


**Figure 6-13 Dead End Load-Slip Behavior, HDPE Duct, Tendon Oiled with NC205**

Because similar peak loads were achieved with fresh and dried oil, allowing emulsifiable oils to dry prior to grouting is not necessary. Slip performance was slightly better with dried oil at both the live and dead ends, but strength is of greater concern than slip behavior.

**IMPLEMENTATION:** *Post-tensioning tendons may be grouted when the oil is still fresh. Allowing the oil to dry will improve slip behavior but has no effect on strength.*

#### 6.4 FRICTION TESTS

This section makes comparisons to illustrate the effect of the variables discussed in Chapter 4 based on the data presented in Chapter 5. Comparisons are first made among radii of curvature and duct types and then among strand surface

conditions. All of the information here is a summary of the comparisons presented in Icaza (2004).

The results in Chapter 5 were presented as percent load loss from the live end to the dead end. This loss is due to curvature friction losses, wobble friction losses, and losses due to the testing hardware used at the anchorages. Wobble friction losses were assumed to be negligible in comparison with curvature friction losses. This assumption was based on the specimens' large angle changes (30 and 90 degrees) and relatively short length (less than 16 ft), as well as the fact that the specimens were carefully constructed in a laboratory. Using the recommended wobble and friction coefficients in AASHTO of 0.0002 and 0.15, respectively, the predicted losses for specimens with galvanized ducts and an angle change of 30 degrees are as follows:

$$P_B = P_A e^{-(\mu\theta + KL)}$$

$$P_B = P_A (e^{-\mu\theta})(e^{-KL})$$

$$P_B = P_A (e^{-0.15 \cdot 30 \cdot \pi / 180})(e^{-0.0002 \cdot 15.71})$$

$$P_B = P_A (0.924)(0.996) = P_A (0.920)$$

In this example, the wobble loss of 0.4% is more than an order of magnitude smaller than the friction loss of 7.6% and therefore can be neglected. Hardware losses were measured as described in Chapter 3 and were subtracted from the total losses to give only the losses due to curvature friction.

A table containing all friction test results, including calculated friction coefficients, is given in Appendix A.

#### 6.4.1 Comparisons among Radii of Curvature and Duct Types

Comparisons among specimens with different radii of curvature and duct types are made based on all tests performed with uncoiled tendons. These test results are presented as average load losses in Figure 6-14 and as average friction coefficients in Figure 6-15.

The data from this test program indicate that radius of curvature has no significant effect on the friction coefficient. Total load losses were higher for specimens with the tighter, 10-ft radius of curvature, which is expected because of the greater angle change. The friction coefficient, however, should be independent of the radius of curvature, since the effects of angle change are accounted for in calculations only with the  $\frac{1}{R}$  term. As shown in Figure 6-15, the friction coefficients calculated for specimens with the same duct type were virtually identical for both radii of curvature. In the case of the steel pipe specimens, the friction coefficient was higher for the 30-ft radius of curvature, while for the galvanized duct specimens, the opposite was true. In both cases, the scatter was larger than the difference between the values. In the case of the HDPE specimens, the same friction coefficient was calculated for 10-ft and 30-ft radius of curvature specimens.

Although the friction coefficient is independent of radius of curvature, the data show that duct type does have a significant effect on the friction coefficient. As shown in Figure 6-15, the average friction coefficients calculated for steel pipe, galvanized duct, and HDPE duct were 0.26, 0.20, and 0.12, respectively. Using the galvanized duct specimens as a base case, the friction coefficient for the steel pipe specimens was 30% higher, and the coefficient for the HDPE duct specimens was 40% lower.

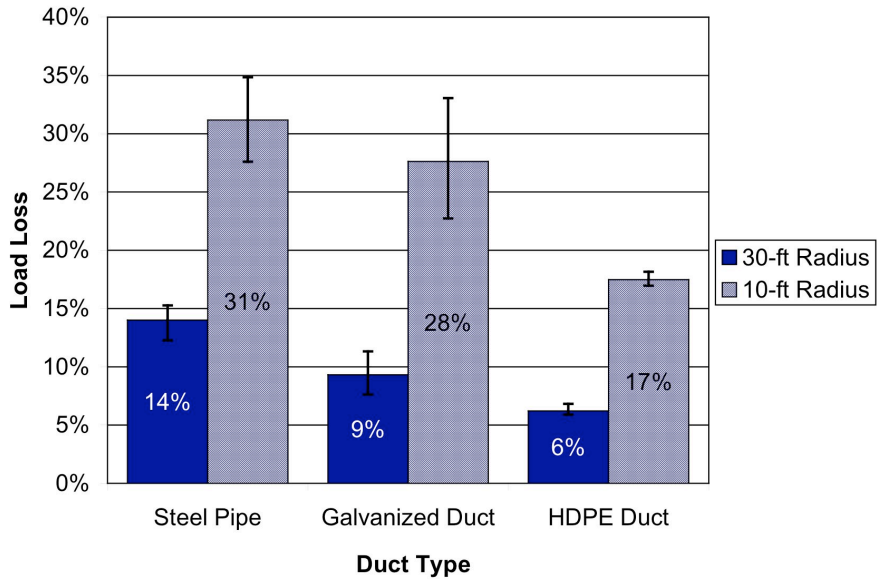


**Figure 6-14 Average Load Loss, Uncoiled Tendons**

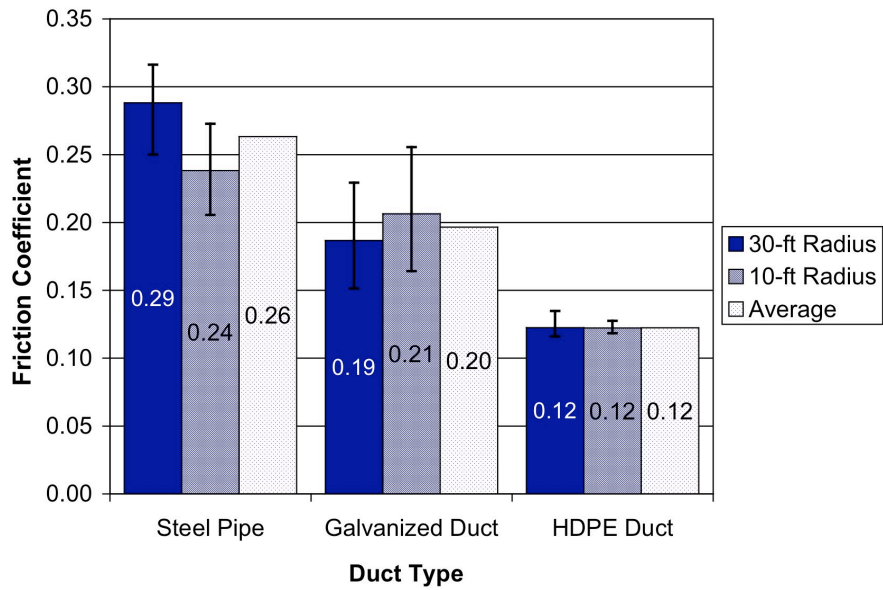


**Figure 6-15 Average Friction Coefficients, Uncoiled Tendons**



## **6.4.2 Comparisons among Strand Surface Conditions**

This section contains three major comparisons: a general comparison between unoiled and oiled tendons, a comparison between tendons oiled with NC205 and those oiled with 703D, and a comparison between tendons stressed immediately after oiling and those stressed one day after oiling.

### ***6.4.2.1 Unoiled Tendons versus Oiled Tendons***

As expected, lubricating the tendons caused a decrease in the calculated friction coefficient. However, the extent of the friction coefficient reduction in this test program was largely dependent on duct type. Figure 6-16 shows the average reduction in friction coefficient for specimens with freshly oiled tendons of all duct types and radii of curvature. As shown in the figure, oiling had the most significant effect for specimens with steel pipes, with an average friction coefficient reduction of 20% for specimens with a 30-ft radius of curvature and 32% for specimens with a 10-ft radius of curvature. Oiling was somewhat less effective in specimens with HDPE ducts. The average friction coefficient reduction was 17% for specimens with a 30-ft radius of curvature and 22% for specimens with a 10-ft radius of curvature. Oiling had the smallest effect on the friction coefficient in specimens with galvanized ducts. The average friction coefficient reduction was 7% for specimens with a 30-ft radius of curvature and 10% for specimens with a 10-ft radius of curvature.

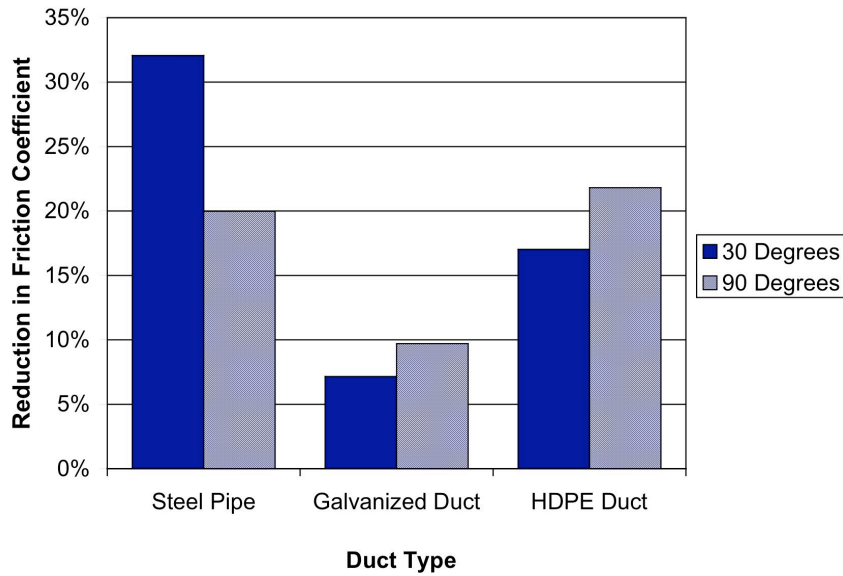


***Figure 6-16 Reduction in Friction Coefficient, Freshly Oiled Tendons (Average Reduction for Both Oils)***

#### **6.4.2.2 NC205 versus 703D**

Overall, tendons oiled with NC205 experienced less friction loss than tendons oiled with 703D. The average reductions in friction coefficient for freshly oiled tendons are shown in Figure 6-17, and the same data for tendons one day after oiling are shown in Figure 6-18. For the freshly oiled specimens, oil NC205 reduced the friction coefficient between 12% and 28%, with an average of 19%. Oil 703D reduced the friction coefficient between 2% and 36%, with an average of 17%. Although the average reductions in friction coefficients were similar for the two oils, the tendons oiled with NC205 behaved more consistently than those oiled with 703D. The data for specimens tested one day after oiling are highly scattered and make any definitive conclusions difficult to draw. In many cases, the calculated friction coefficient was actually higher than that calculated for the

unoiled tendons, which is shown in Figure 6-18 as a negative reduction in the friction coefficient. Average friction coefficients for NC205 specimens one day after oiling were less than the average for unoiled tendons in four of six specimen types. For 703D specimens one day after oiling, only two of six specimen types had an average friction coefficient less than that for unoiled tendons.

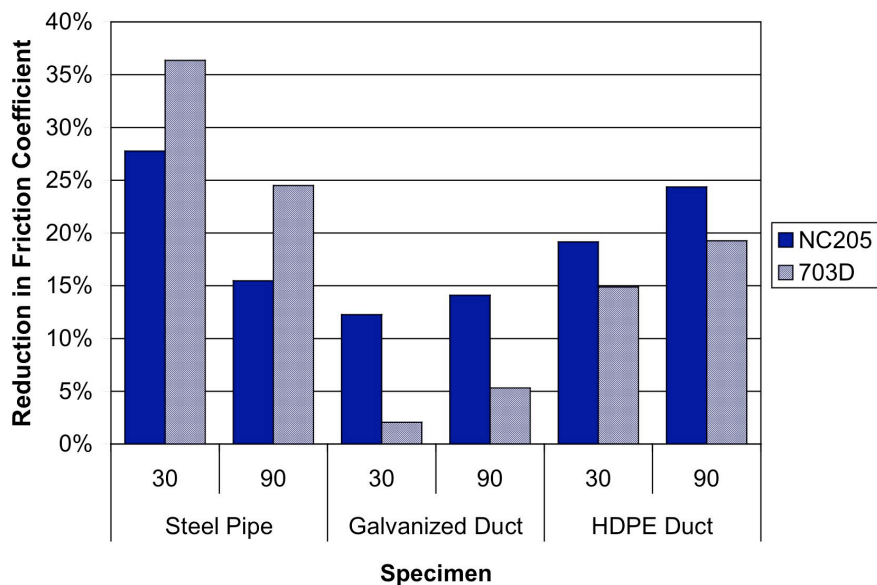


*Figure 6-17 Reduction in Friction Coefficient, Freshly Oiled Tendons*

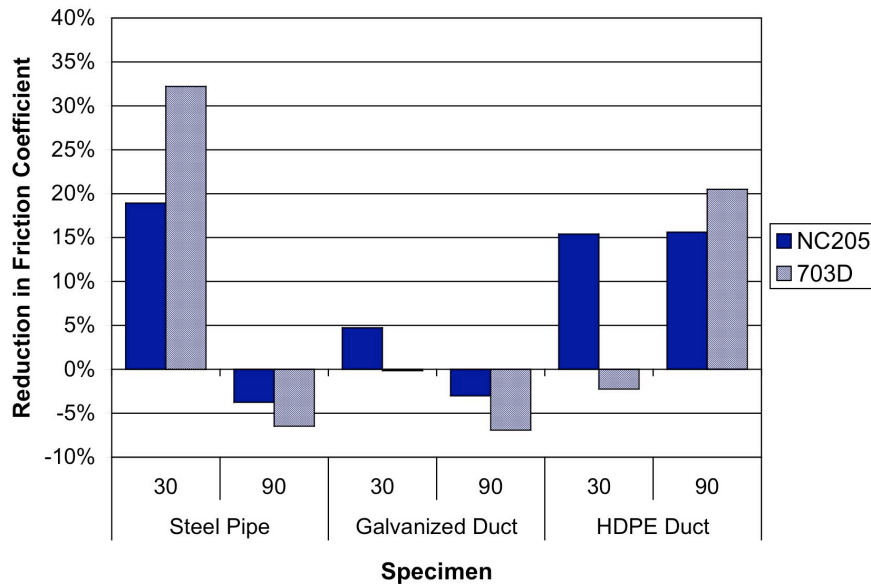


**Figure 6-18 Reduction in Friction Coefficient, One Day after Oiling**

#### **6.4.2.3 Freshly Oiled versus One Day after Oiling**

In all but one case, oil allowed to dry for one day was less effective in reducing friction losses than fresh oil. Figure 6-19 shows the reduction in friction coefficient for specimens both freshly oiled and one day after oiling. (In all cases the friction coefficient is compared to the coefficient calculated for unoiled tendons.) The 10-ft radius of curvature specimen with an HDPE duct and oiled with 703D was the only one to have a greater reduction in the friction coefficient one day after oiling. If a reduction in the friction coefficient of 5% or less is considered insignificant, then seven of the 12 oiled specimens had no change in the friction coefficient one day after oiling. Three of those seven specimens were oiled with NC205, and four were oiled with 703D. Oil NC205 could also be considered slightly better at reducing friction losses than oil 703D after one day's drying time because fewer NC205 specimens exhibited an increase in the friction

coefficient one day after oiling. As shown in Figure 6-19, two NC205 specimens are associated with negative values, as opposed to four 703D specimens.

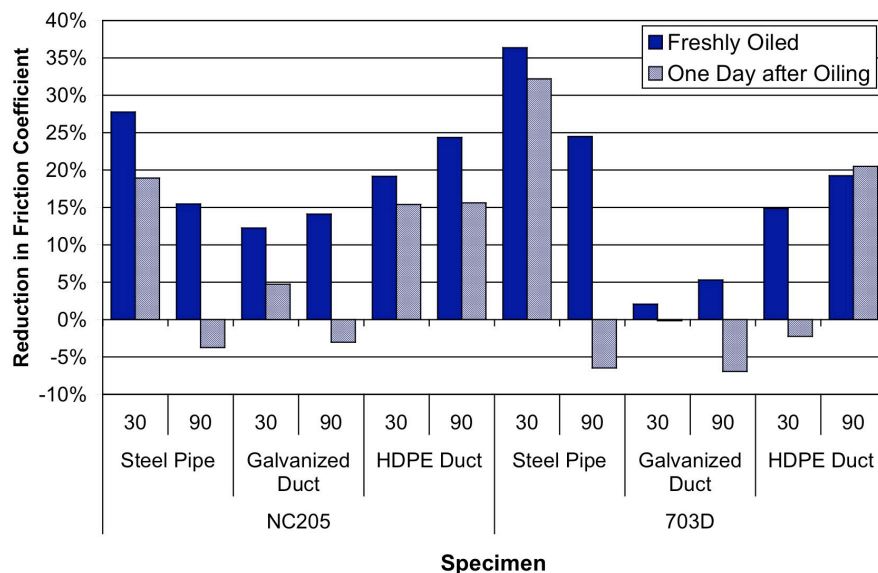


**Figure 6-19 Reduction in Friction Coefficient, Freshly Oiled Tendons versus One Day after Oiling**

These data provide some limited insight into the effect of drying time on friction losses, but many potentially important factors were not accounted for in this testing program. For example, ambient conditions such as temperature and relative humidity may affect the behavior and characteristics of emulsifiable oils in different ways over time. This research shows that fresh oil is the most effective in reducing friction losses, but more detailed information about how these oils' effectiveness changes over time would require further study.

### 6.4.3 Comparison of Results with Current Design Values and Previous Research

This section first compares the friction coefficients calculated for various duct types and uncoiled tendons to values recommended by ACI, AASHTO, and PTI. Comparisons are then made among friction coefficient reductions for oiled tendons calculated in this test program and in previous research projects.

The average friction coefficients based on tests performed with uncoiled tendons were 0.26, 0.20, and 0.12 for steel pipes, galvanized ducts, and HDPE ducts, respectively. As shown in Table 6-3, the calculated friction coefficients for steel pipe and galvanized duct are in agreement with current recommended values, but the coefficient for HDPE ducts is significantly less. For steel pipe, the AASHTO-recommended friction coefficient of 0.25 is the only available suggested value and is in close agreement with the value of 0.26 found in this research. For galvanized ducts, all recommended values fall in the range of 0.15-0.25, which again agrees closely with the value of 0.20 found in this research. ACI recommends this value for design but still allows use of values between 0.16 and 0.24. The results for HDPE ducts, however, differ substantially from AASHTO recommendations. Results from this testing program indicate an average friction coefficient of 0.12, almost 50% less than the AASHTO value of 0.23. The AASHTO value is also about 30% higher than the value reported in NCHRP Project 4-15. Given these results, a friction coefficient of 0.15 for HDPE ducts would likely be a conservative value for use in design.

**IMPLEMENTATION:** *Additional data on friction losses in HDPE ducts should be compiled from field measurements. The current AASHTO-recommended friction coefficient of 0.23 is overly conservative compared with the value of 0.12 found in this program.*

**Table 6-3 Comparison of Friction Coefficients to Recommended Values**

	Steel Pipe	Galvanized Duct	HDPE Duct
ACI	-	0.16 – 0.24 (0.20 <sup>a</sup> )	-
AASHTO	0.25 <sup>b</sup>	0.15 – 0.25 <sup>c</sup>	0.23
PTI	-	0.15 – 0.25	-
NCHRP Project 4-15	-	0.23	0.18
Current Research	0.26	0.20	0.12

<sup>a</sup> Recommended for design.  
<sup>b</sup> Lubrication will probably be required.  
<sup>c</sup> A friction coefficient of 0.25 is appropriate for 12-strand tendons. A lower coefficient may be used for larger tendon and duct sizes.

Although the two oils used in this research program had not been tested previously, the average reductions in the friction coefficient for NC205 and 703D were similar to values found in previous research, as shown in Table 6-4. Reductions found in TxDOT Project 1264 with large-scale specimens ranged from 8% to 25%. The average values of 19% and 17% for NC205 and 703D, respectively, fall within this range. Of all the values reported in Table 6-4, only five are below 14%. A 15% reduction in the friction coefficient is therefore conservatively recommended when fresh lubrication is used. However, since the reductions in friction coefficient in this test program were consistently below 15% for galvanized ducts, this reduction is only recommended for steel pipes and HDPE ducts. In addition, this reduction should only be taken if an oil is approved for use after demonstrating a reduction in the friction coefficient of 14% or more in tests similar to those performed in this research program or in TxDOT Project 1264.

**Table 6-4 Reduction in Friction Coefficients Compared to Previous Research**

		<b>Oil</b>	<b>Reduction in Friction Coefficient</b>
Owens and Moore			No Reduction
TxDOT Project 1264	Small Scale	Visconorust 8415E	17%
		Dromus B	17%
		Unocal 10	14%
		Unocal MS	14%
		Texaco Soluble D	27%
		Rust-veto FB20	0%
		Hocut 737	-9%
		Hocut 4284	18%
		Nalco 6667	12%
	Wright 502	21%	
	Large Scale	Texaco Soluble D	19%
		Wright 502 (monolithic)	25%
		Wright 502 (segmental)	15%
		Hocut 4284	17%
Dromus B		8%	
Current Research		NC205	19%
		703D	17%

**IMPLEMENTATION:** *A 15% reduction in the friction coefficient can be used with steel pipes or HDPE ducts and approved oils if the tendon is stressed immediately after oiling. Both emulsifiable oils used in this test program, Trukut NC205 and NoxRust 703D, are approved for this application.*

#### **6.4.4 Duct Damage**

This section has been excerpted directly from Icaza (2004).

Evaluation of the inside surfaces of the ducts after stressing, presented in Chapter 5, showed no significant damage in either the HDPE ducts or the galvanized steel ducts. AASHTO currently limits the radius of curvature for HDPE ducts to 30 ft. The limit set by AASHTO for either steel pipes or



galvanized steel ducts is 10 ft. Therefore, it is possible that the minimum radius of curvature for HDPE ducts could be reduced from 30 ft to 10 ft. However, this recommendation applies only when the sole concern is damage to the inside of the duct due to stressing. Other considerations should be taken into account, such as the possibility of tendon breakouts on the interior face of horizontally curved members, concrete splitting and crushing from radial stresses on the inside of sharply curved tendons, and fracture of wires in sharp bends.

**IMPLEMENTATION:** *No significant damage to HDPE ducts was observed, even with a 10-ft radius of curvature. AASHTO currently limits the radius of curvature for HDPE ducts to 30 ft or greater. A reduction of the limiting radius of curvature for HDPE ducts is possible based on damage to the inside of the duct. However, other factors should be considered before changing this limit.*

#### **6.4.5 Example of Practical Implications**

This section has been excerpted from Icaza (2004).

In the previous sections, the data from the tests performed in this study were analyzed and compared to the findings of previous research and to the recommendations by ACI, AASHTO, and PTI. The objective of this section is to illustrate the practical implications of these findings. This objective will be accomplished by the use of examples.

Assume that one is to design a post-tensioned girder. Following the standard practice, galvanized steel ducts are to be used. Therefore, the assumed coefficient of friction in this case would be 0.20.

Consider the hypothetical case in which the designer is trying to decide whether to use external tendons (bonded at discrete deviators) or internal tendons,

and that the total angle change and tendon length are the same for both cases. If external tendons are used, then the coefficient of friction must be increased to 0.25, because steel pipes are used at deviators instead of galvanized steel ducts. If the designer cannot tolerate this increase in friction, she may use lubrication to reduce the coefficient for the steel pipe by 15% to 0.21. In that case, the coefficient is similar to that of the galvanized steel duct.

However, if the decision is made to use internal tendons, and the estimated friction losses are still too large, the designer can replace the galvanized steel ducts with HDPE ducts. This change would reduce the friction coefficient to 0.15. Further reduction, to a coefficient of 0.13, is possible if both HDPE ducts and lubrication are used.

The effect of the coefficient of friction on the actual percent load loss depends on the total angle change in the tendon. The relationship between these quantities is shown by the equation of friction loss:

$$PL = 1 - e^{-\mu \theta}$$

This equation is presented graphically in Figure 6-20, where the coefficient of friction is plotted against percent load loss for a given total angle change. The figure shows that for small angle changes, the percent load loss is almost independent of the coefficient of friction in the range of practical values, whereas at high angle changes, the coefficient of friction becomes more important.

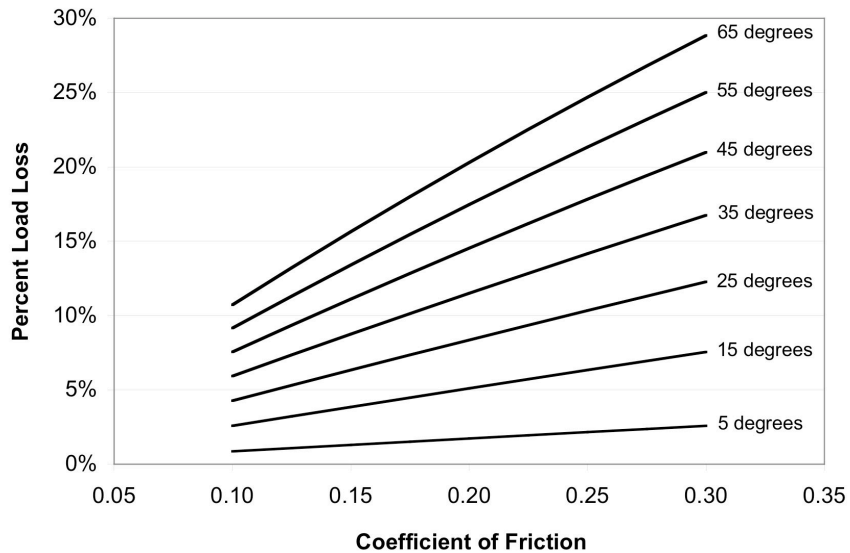


**Figure 6-20 Relationship among Total Angle Change, Coefficient of Friction, and Percent Load Loss**

Assume that a symmetrical post-tensioned girder (half of which is shown in Figure 6-21) is to be stressed from both ends. Half of the girder has a total angle change of 58.4 degrees. If galvanized steel ducts are used, then assuming a coefficient of friction of 0.20 and a wobble coefficient of  $0.0002 \text{ ft}^{-1}$  gives a percent load loss of 22.0% to the middle of the girder. Assuming that the tendon is stressed to 80% of its tensile capacity, the post-tensioning force at the live end is 929 kips, and 725 kips at the middle.

If HDPE ducts are used, the coefficient of friction would be 0.15 and the load loss 17.9%. However, a reduction of 4% in the load loss (from 22.0% loss to 17.9%) will not have a significant effect on the design. Four percent in the area of a twenty-strand tendon is less than the area of a single strand, and no strand may be removed. Therefore, reducing the coefficient of friction from 0.20 to 0.15 has no effect in this case.

However, if both HDPE ducts and lubrication are used, the coefficient of friction would be 0.128 and the load loss 16.0%. A six percent reduction in the area of a twenty-strand tendon is 1.2 times the area of a single strand. If 19 strands are used instead of 20, then 80% of the tensile strength is 882 kips, and the load at the dead end is 741 kips. In this case the tendon force at the dead end is higher than what it was when galvanized steel ducts and uncoiled tendons are used. Saving one strand means saving 448 ft, or 302 lb of steel. A reduction of 36% in the friction coefficient leads to a reduction of five percent in the required steel area, assuming the same size strand is to be used.

Tendon: twenty 0.6 strands Grade 270

Area: 4.3 in<sup>2</sup>

Total Length: 448 ft

Wobble Coefficient: 0.0002 ft<sup>-1</sup>

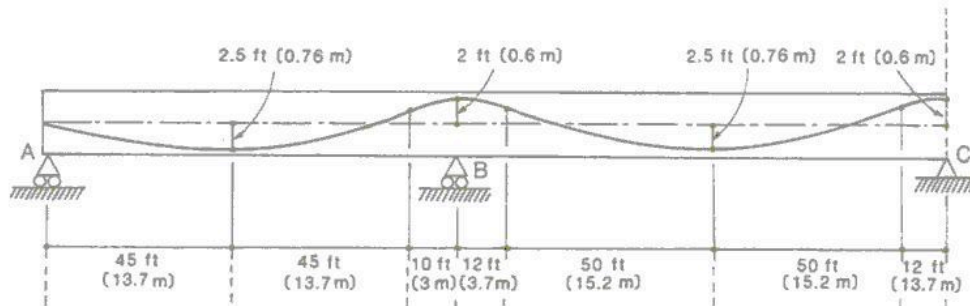


**Figure 6-21 Example of Friction Loss Calculations (Collins and Mitchell 1997)**

## **CHAPTER 7**

### **Summary and Conclusions**

#### **7.1 SUMMARY OF PROJECT OBJECTIVES AND TEST PROGRAM**

The research presented in this thesis was part of The University of Texas at Austin, Center for Transportation Research Project 0-4562: “Effect of Emulsifiable Oils Used as Temporary Corrosion Protection in Grouted Post-Tensioned Tendons, and Investigation of Alternate Corrosion Resistant Post-Tensioning Systems.” This thesis contains the full results of the first phase of the project, which investigated the effects of emulsifiable oils on bond behavior and friction losses in multi-strand post-tensioned tendons.

Emulsifiable oils have been used to reduce friction losses in post-tensioned tendons as well as to provide temporary corrosion protection during the period of time between tendon stressing and grouting. Prior to grouting, the ducts were sometimes flushed with water to remove the oil, and compressed air was used to remove water from the ducts. In addition to environmental problems related to disposal of the flushing water, voids in the grout were found in a number of ducts which had been flushed in this manner. In response to these problems, Project 0-4562 investigated the effect of emulsifiable oils on corrosion, bond, and friction in unflushed ducts.

Initial tests for this project were performed under the supervision of Dr. Andrea Schokker by Salcedo (2003) at Pennsylvania State University. Nineteen emulsifiable oils that are currently available on the market were chosen for initial tests. Corrosion tests were performed over the course of six months using individual strands in three environments: outdoor exposure, a controlled

temperature and humidity chamber, and a 5% NaCl solution. In addition, single-strand pullout tests were performed as a preliminary indication of the oils' effect on bond strength.

Based on the results of these initial tests, two oils were chosen for large-scale tests at the University of Texas at Austin: Citgo Trukut NC205 and Daubert NoxRust 703D. All tests were performed with 12-strand tendons, which are representative of a typical tendon size used in post-tensioned applications. Three duct types were used for both bond and friction tests: rigid steel pipes, such as those used in deviator blocks; corrugated galvanized ducts; and corrugated HDPE ducts. Bond tests, performed by Diephuis (2004) and the author, were monotonic pullout tests of tendons grouted inside simply supported concrete beams. Tendons were either unoiled or oiled with one of the two chosen oils. Most oiled specimens were grouted two days after oiling, though some specimens were grouted ten days after oiling to determine whether drying time affects bond behavior. Friction tests were performed by Icaza (2004) using curved concrete specimens with either a 10-ft or 30-ft radius of curvature. Tests were performed with tendons unoiled, freshly oiled, and one day after oiling.

Conclusions based on corrosion tests, large-scale bond tests, and large-scale friction tests are presented in the next three sections, respectively. Overall recommendations are then presented, and directions for future research are suggested.

## **7.2 CORROSION TEST CONCLUSIONS**

Corrosion test conclusions are based on the average rating (1-7) given to specimens treated with each of the emulsifiable oils selected for preliminary testing. A lower number indicates less corrosion damage, and a rating of 4 or

below in all three environments was selected as the criterion for “acceptable” performance.

Because oils were only considered for large-scale testing if they met this minimum standard, both Trukut NC205 and NoxRust 703D provide adequate temporary corrosion protection for post-tensioned tendons. NoxRust 703D performed slightly better in all three environments than Trukut NC205. Average ratings for Trukut NC205 specimens outdoors, in the controlled temperature and humidity chamber, and in the NaCl solution were 3.0, 3.0, and 3.8, respectively. Average ratings for NoxRust 703D were 2.0, 2.7, and 3.7, respectively.

### **7.3 BOND TEST CONCLUSIONS**

Bond test conclusions are based primarily on two failure criteria. The first criterion is peak load, which indicates the ultimate strength of the specimen. The second criterion is a limiting value of dead end slip, which in this test program was set at 0.02 in. This criterion is related to serviceability rather than strength. High levels of dead end slip at low loads indicate poor bond between the tendon and grout. Because good bond is required for effective crack width control, high levels of slip could lead to serviceability problems if a member is already cracked. However, in many post-tensioned applications, members are designed such that cracking will not occur under service loads. For example, in segmental applications, tensile stresses are not permitted under service loads, and therefore cracking can only occur in overload situations. In cast-in-place construction, tensile stresses are allowed, but additional mild steel can easily be provided for crack control. Therefore, although slip behavior is of interest, peak load is the primary basis for recommendations.

Peak loads for specimens with galvanized ducts were 20% to 40% higher than peak loads for specimens with HDPE ducts. These results were consistent for

all strand surface conditions. Galvanized ducts therefore allow bonded tendons to be developed in shorter lengths than HDPE ducts.

Peak loads for specimens with rigid steel pipes were 70% to 90% lower than peak loads for specimens with galvanized or HDPE ducts, given the same strand surface condition. This poor behavior was due to failure at the interface of the concrete and the smooth steel pipe. The pipe often pulled out of the specimen as a rigid body before failure could occur at the tendon-grout interface, as was desired for these bond tests. Shear studs welded to the outside of the pipes prevented this type of failure, but peak loads were still low due to failure at the grout-duct interface. In cases where the pipe did not pull out of the concrete, the entire grout plug typically pulled out of the pipe.

For specimens with corrugated galvanized or HDPE ducts, peak loads were actually higher for specimens with oiled tendons than specimens with unoiled tendons. The average peak load for specimens with galvanized ducts and tendons oiled with Trukut NC205 was 20% higher than for galvanized duct specimens with unoiled tendons. For specimens with HDPE ducts and tendons oiled with Trukut NC205, the average peak load was 15% higher than for HDPE duct specimens with unoiled tendons. In the case of NoxRust 703D, specimens with oiled tendons and galvanized ducts had an average peak load 28% higher than galvanized duct specimens with unoiled tendons. Specimens with oiled tendons and HDPE ducts had approximately the same peak load as HDPE duct specimens with unoiled tendons.

While peak load behavior was unchanged or improved for specimens with oiled tendons, these specimens tended to exhibit high levels of dead end slip at low loads. “Failure” using a slip criterion was defined as the load at 0.02 in. of dead end displacement. For specimens with unoiled tendons, failure based on slip was typically 10% to 20% lower than the peak load. For NC205 specimens, the



average failure loads based on slip were 85% and 94% lower than the average peak loads for galvanized and HDPE ducts, respectively. For 703D specimens, the average failure loads based on slip were 44% and 78% lower than the average peak loads for galvanized and HDPE ducts, respectively.

Giving the oil 10 days to dry instead of the typical two days did not change peak loads significantly. The additional drying time did, however, increase failure loads based on slip. For galvanized duct specimens, the average failure load based on slip for specimens with dried oil was almost twice the value for specimens with fresh oil but still 36% lower than the value for unoiled specimens. For HDPE duct specimens, the average failure load based on slip for specimens with dried oil was more than four times the value for specimens with fresh oil but still 59% lower than the value for unoiled specimens.

#### **7.4 FRICTION TEST CONCLUSIONS**

Friction tests were conducted to determine the effects of duct type and strand surface condition on friction losses. Results were compiled primarily in the form of friction coefficients rather than total load loss, since the friction coefficient should be independent of specimen size and curvature.

The measured friction coefficients for each of the three duct types were found to be independent of radius of curvature. This result was expected, since the effects of curvature are accounted for in calculations separately from the friction coefficient.

Measured friction coefficients for unoiled tendons in rigid steel pipes and corrugated galvanized ducts generally agreed with design values suggested by AASTHO, ACI and PTI. The average friction coefficient for rigid steel pipes found in this research was 0.26, less than 5% higher than the AASHTO-recommended value of 0.25. The average friction coefficient for galvanized ducts

found in this research was 0.20, which coincides exactly with the ACI-recommended value. AASHTO and PTI both recommend values between 0.15 and 0.25.

The measured friction coefficient for unoiled tendons in HDPE ducts was 0.12, almost 50% lower than the AASHTO-recommended value. Based on these results as well as the results of a previous study conducted by the National Cooperative Highway Research Program (NCHRP), the AASHTO value appears overly conservative.

Tendons which were lubricated with oil and stressed immediately after oiling experienced lower friction losses than unoiled tendons. Oiling caused the greatest reductions in the friction coefficient for steel pipe specimens, on the order of 20% to 30%. Reductions for HDPE duct specimens were smaller but still significant, on the order of 20%. Reductions for galvanized ducts specimens were the least significant, on the order of 10%.

The average reduction in the friction coefficient for specimens of all duct types and tendons oiled with NC205 was 19%. The average reduction for specimens of all duct types and tendons oiled with 703D was 17%, though these data were more scattered than the data for NC205 specimens.

For tendons stressed one day after oiling, the data were highly scattered. In half of the specimens, the friction coefficient was actually higher for these tendons than for tendons with no oil. These results clearly indicate that dried oil is less effective in reducing friction losses than fresh oil, but detailed conclusions about the effect of time on these oils cannot be drawn based on these tests.

Inspection of the galvanized ducts and HDPE ducts after testing revealed minimal damage to the inside walls of the ducts, even for specimens with a tight, 10-ft radius of curvature.

## 7.5 RECOMMENDATIONS

Based on corrosion test results, the following recommendation is made:

- Both emulsifiable oils used in this test program, Trukut NC205 and NoxRust 703D, provide adequate temporary corrosion protection for post-tensioned tendons. NoxRust 703D performed slightly better in this test program than Trukut NC205.

Based on bond test results, the following recommendations are made:

- Bond stresses in HDPE duct specimens were found to be 20% to 40% lower than in galvanized duct specimens for unoiled and oiled tendons, respectively. Designers using HDPE ducts in place of galvanized ducts must take these lower stresses into account and provide bonded lengths sufficient to develop the tendons.
- Shear connectors or shear studs should be used for anchorage purposes on the outside of smooth steel deviator pipes.
- Emulsifiable oils used as temporary corrosion protection in grouted post-tensioned construction do not need to be flushed with water. In cases where cracking might occur under service loads, the oil may cause cracks to widen, but the strength of the member will not be affected. Such cracking would not be expected in segmental construction and could easily be controlled in cast-in-place construction with supplementary mild reinforcement.
- The two emulsifiable oils used in this test program, Trukut NC205 and NoxRust 703D, are both acceptable for use based on the results of bond tests.
- Post-tensioning tendons may be grouted when the oil is still fresh. Allowing the oil to dry will improve slip behavior but has no effect on strength.

Based on friction test results, the following recommendations are made:

- Additional data on friction losses in HDPE ducts should be compiled from field measurements. The current AASHTO-recommended friction coefficient of 0.23 is overly conservative compared to the value of 0.12 found in this program.
- A 15% reduction in the friction coefficient can be used with steel pipes or HDPE ducts and approved oils if the tendon is stressed immediately after oiling. Both emulsifiable oils used in this test program, Trukut NC205 and NoxRust 703D, are approved for this application.
- No significant damage to HDPE ducts was observed, even with a 10-ft radius of curvature. AASHTO currently limits the radius of curvature for HDPE ducts to 30 ft or greater. A reduction of the limiting radius of curvature for HDPE ducts is possible based on damage to the inside of the duct. However, other factors should be considered before changing this limit.

## **7.6 SUGGESTIONS FOR FUTURE RESEARCH**

Further research related to grouted tendons could be performed to determine the effect, if any, of emulsifiable oils on grout strength.

As described in the previous section, there is also a need for additional data to be collected and analyzed regarding the friction coefficient for unlubricated tendons in HDPE ducts. If the findings of this research are corroborated, the friction coefficient for HDPE ducts may be significantly decreased.

## APPENDIX A

### Large-Scale Test Results

*Table A-1 Bond Test Results*

Specimen	Peak Load Failure Interface	Peak Load (kip)	Load at 0.02 in. Slip (kip)	Maximum Bond Stress (psi)			Bond Stress at 0.02 in. Slip (psi)		
				Duct-Concrete	Grout-Duct	Tendon-Grout	Duct-Concrete	Grout-Duct	Tendon-Grout
0-SP-7.5 <sup>o</sup> -1	Duct-Concrete	67.1	NA	138	159	317	NA	NA	NA
0-SP-7.5 <sup>o</sup> -2	Duct-Concrete	89.1	NA	183	211	422	NA	NA	NA
0-SP-7.5 <sup>o</sup> -3	Grout-Duct	64.1	58.9	131	152	303	121	139	278
0-SP-7.5 <sup>o</sup> -4	Grout-Duct	54.0	54.0	111	128	256	111	128	256
1-SP-7.5 <sup>o</sup> -1	Multiple	39.3	4.6	80.5	92.9	186	9.4	11	22
1-SP-7.5 <sup>o</sup> -2	Grout-Duct	32.9	4.5	67.4	77.8	156	9.2	11	21
2-SP-7.5 <sup>o</sup> -1	Grout-Duct	75.5	18.9	155	178	357	38.7	44.7	89.4
2-SP-7.5 <sup>o</sup> -2	Grout-Duct	58.5	14.6	120	138	277	29.9	34.5	69.1
0-GD-7.5 <sup>o</sup> -1	Tendon-Grout	382	307	864	946	1810	694	761	1450
0-GD-7.5 <sup>o</sup> -2	Tendon-Grout	345	276	780	855	1630	624	684	1310
0-GD-7.5 <sup>o</sup> -3	Tendon-Grout	360	306	814	892	1700	692	758	1450
1-GD-7.5 <sup>o</sup> -1	No Pullout	434	77.3	981	1080	2050	175	192	366
1-GD-7.5 <sup>o</sup> -2	No Pullout	437	54.3	988	1080	2070	123	135	257
2-GD-7.5 <sup>o</sup> -1†	No Pullout	436	100	986	1080	2060	226	248	473
2-GD-7.5 <sup>o</sup> -2	Tendon-Grout	481	269	1090	1190	2280	608	666	1270
2-GD-7.5 <sup>o</sup> -3	Tendon-Grout	455	150	1030	1130	2150	339	372	710
2-GD-7.5 <sup>o</sup> -4	Tendon-Grout	460	368	1040	1140	2180	831	912	1740
1*-GD-7.5 <sup>o</sup> -1	Tendon-Grout	473	79.7	1070	1170	2240	180	197	377

**Table A-1 (Cont.) Bond Test Results**

Specimen	Peak Load Failure Interface	Peak Load (kip)	Load at 0.02 in. Slip (kip)	Maximum Bond Stress (psi)			Bond Stress at 0.02 in. Slip (psi)		
				Duct-Concrete	Grout-Duct	Tendon-Grout	Duct-Concrete	Grout-Duct	Tendon-Grout
1*-GD-7.5 <sup>o</sup> -2	No Pullout	480	298	1090	1190	2270	674	738	1410
0-HD-7.5 <sup>o</sup> -1	Tendon-Grout	228	196	519	565	1080	446	486	927
0-HD-7.5 <sup>o</sup> -2	Tendon-Grout	311	288	708	771	1470	655	714	1360
0-HD-7.5 <sup>o</sup> -3	Tendon-Grout	307	287	698	761	1450	653	711	1360
1-HD-7.5 <sup>o</sup> -1	Tendon-Grout	322	34.3	732	798	1520	780	85.0	162
1-HD-7.5 <sup>o</sup> -2	Tendon-Grout	325	6.5	739	805	1540	15	16	31
2-HD-7.5 <sup>o</sup> -1	Tendon-Grout	293	49.9	667	726	1390	114	124	236
2-HD-7.5 <sup>o</sup> -2	Tendon-Grout	295	62.3	671	731	1400	142	154	295
2-HD-7.5 <sup>o</sup> -3	Tendon-Grout	268	78.5	610	664	1270	179	194	371
1*-HD-7.5 <sup>o</sup> -1	Tendon-Grout	278	130	632	689	1320	296	322	615
1*-HD-7.5 <sup>o</sup> -2	Tendon-Grout	333	79.2	757	825	1580	180	196	375

† Behavior not consistent with three other tests; data disregarded.

**Table A-2 Friction Test Results – Average Total Load Loss, Kip**

Specimen	Test						
	Unoiled 1	Unoiled 2	Unoiled 3	Freshly Oiled 1	Freshly Oiled 2	One Day after Oiling 1	One Day after Oiling 2
1-SP-30°	15.8	16.1	16.3	12.5	11.8	13.2	13.6
2-SP-30°	12.8	13.4	14.1	9.0	8.8	9.0	9.9
0-SP-90°	29.9	31.2	34.8	29.3*	32.0*	34.1*	34.9*
1-SP-90°	29.1	33.3	35.8	27.0	30.2	33.5	34.0
2-SP-90°	28.8	28.1	32.0	21.2	25.5	29.5	32.9
1-HD-30°	6.6	7.0	7.3	5.8	5.7	5.9	6.1
2-HD-30°	6.6	6.4	6.4	5.5	5.7	6.5	6.7
1-HD-90°	18.7	18.1	17.5	13.8	14.4	15.5	-
2-HD-90°	18.0	17.6	-	15.4	14.1	14.4	14.7
1-GD-30°	8.1	8.5	10.2	7.6	8.3	8.6	8.5
1-GD-90°	9.6	11.8	10.6	11.7	9.2	10.7	10.6
2-GD-30°	23.2	28.5	33.6	23.7	26.5	28.8	29.7
2-GD-90°	25.6	28.5	29.3	24.6	28.5	29.9	28.9

\*Tendon was not oiled in these tests.

**Table A-3 Friction Test Results – Average Percent Load Loss (Curvature Friction Only)**

Specimen	Test						
	Unoiled 1	Unoiled 2	Unoiled 3	Freshly Oiled 1	Freshly Oiled 2	One Day after Oiling 1	One Day after Oiling 2
1-SP-30°	14.8	15.1	15.3	11.5	10.8	12.2	12.6
2-SP-30°	12.3	12.9	13.6	8.5	8.3	8.5	9.4
0-SP-90°	29.4	30.7	34.3	28.8*	31.5*	33.6*	34.4*
1-SP-90°	28.1	32.3	34.8	26.0	29.2	32.5	33.0
2-SP-90°	28.3	27.6	31.5	20.7	25.0	29.0	32.4
1-HD-30°	6.1	6.5	6.8	5.3	5.2	5.4	5.6
2-HD-30°	6.1	5.9	5.9	5.0	5.2	6.0	6.2
1-HD-90°	18.2	17.6	17.0	13.3	13.9	15.0	-
2-HD-90°	17.5	17.1	-	14.9	13.6	13.9	14.2
1-GD-30°	7.6	8.0	9.7	7.1	7.8	8.1	8.0
2-GD-30°	9.1	11.3	10.1	11.2	8.7	10.2	10.1
1-GD-90°	22.7	28.0	33.1	23.2	26.0	28.3	29.2
2-GD-90°	25.1	28.0	28.8	24.1	28.0	29.4	28.4

\*Tendon was not oiled in these tests.



**Table A-4 Friction Test Results – Average Friction Coefficient**

Specimen	Test						
	Unoiled 1	Unoiled 2	Unoiled 3	Freshly Oiled 1	Freshly Oiled 2	One Day after Oiling 1	One Day after Oiling 2
1-SP-30°	0.306	0.313	0.316	0.232	0.218	0.248	0.257
2-SP-30°	0.250	0.264	0.280	0.171	0.166	0.170	0.189
0-SP-90°	0.222	0.234	0.267	0.216*	0.241*	0.260*	0.268*
1-SP-90°	0.210	0.248	0.273	0.192	0.220	0.250	0.255
2-SP-90°	0.212	0.206	0.241	0.148	0.184	0.218	0.249
1-HD-30°	0.119	0.129	0.135	0.105	0.102	0.106	0.110
2-HD-30°	0.120	0.116	0.116	0.097	0.102	0.119	0.122
1-HD-90°	0.128	0.123	0.118	0.091	0.096	0.104	-
2-HD-90°	0.123	0.120	-	0.102	0.093	0.096	0.097
1-GD-30°	0.151	0.160	0.195	0.141	0.156	0.162	0.160
2-GD-30°	0.182	0.229	0.203	0.226	0.175	0.206	0.204
1-GD-90°	0.164	0.209	0.256	0.168	0.192	0.212	0.220
2-GD-90°	0.184	0.209	0.216	0.176	0.209	0.222	0.213

\*Tendon was not oiled in these tests.

## References

1. American Association of State Highway and Transportation Officials, "Guide Specifications for Design and Construction of Segmental Concrete Bridges," 2nd Edition, 1999.
2. American Association of State Highway and Transportation Officials, "Standard Specification for Highway Bridges," 17th Edition, 2002.
3. American Concrete Institute Committee 318, "Building Code Requirements for Structural Concrete (ACI 318-02) and Commentary (ACI 318R-02)," 2002.
4. American Segmental Bridge Institute, "2002 Grouting Certification training Manual," Phoenix, AZ, 2002.
5. American Segmental Bridge Institute, "Interim Statement on Grouting Practices," Phoenix, AZ, 2000.
6. Anderson, A. R. and Anderson R. G., "An Assurance Criteria for Flexural Bond in Pretensioned Hollow Core Units," ACI Journal, Proceedings Vol. 73, No. 8, August 1976.
7. Barnes, R. W., Grove, J. W., and Burns, N. H., "Experimental Assessment of Factors Affecting Transfer Length," ACI Structural Journal, Vol. 100, No. 6, November/December 2003.
8. Braverman, F., "Pull-Out Tests of Prestressing Strands Grouted Inside Smooth-Wall Steel Ducts," Master's Report, The University of Texas at Austin, 1985.
9. Carter, L. L., "Deviator Behavior in Externally Post-Tensioned Bridges," Master's Thesis, The University of Texas at Austin, 1987.
10. Collins, M. P., and Mitchell, D., "Prestressed Concrete Structures," 1<sup>st</sup> Edition, 1997.
11. Construction Industry Research and Information Association, "Prestressed Concrete – Friction Losses During Stressing," Report 74, 1987.

12. Cordes, H., Schütt, K., Trost, H., "Großmodellversuche zur Spanngliedreibung, Deutscher Ausschuss für Stahlbeton," Berlin, 1981
13. Davis, R. T., "Friction Losses in Segmental Bridge Tendon," Master's Thesis, The University of Texas at Austin, 1993.
14. Davis, R. T., Tran, T. T., Breen, J. E., and Frank, K. H., "Reducing Friction Losses in Monolithic and Segmental Bridge Tendons," Research Report 1264-2, Center for Transportation Research, Bureau of Engineering Research, The University of Texas at Austin, 1993.
15. Diephuis, J. R., "Factors Affecting Bond in Multi-Strand Post-Tensioning Tendons Including the Effect of Emulsifiable Oils," Master's Thesis, The University of Texas at Austin, 2004.
16. Ferguson, P. M., Breen, J.E., and Thompson, J.N., "Pullout Tests on High Strength Reinforcing Bars," Journal of the American Concrete Institute, Vol. 62, No. 8, August 1965.
17. fib, "Corrugated Plastic Ducts for Internal Bonded Post-Tensioning," Federation International du beton (fib) Technical Report Bulletin No. 7, January 2000.
18. Freyermuth, C. L., "Status of the Durability of Post-Tensioning Tendons in the United States," Durability of Post-Tensioning Tendons, fib-IABSE Technical Report, Bulletin 15, Workshop 15-16 November 2001, Ghent, Belgium, 2001.
19. Ganz, H. R., "Recent Developments in the Protection of Prestressing Steels," Proceeding of the 1<sup>st</sup> fib Congress: Concrete Structures in the 21<sup>st</sup> Century, Session 7, Osaka, Japan, 2002.
20. Hagenberger, M. J., "Consideration of Strand Fatigue for Load Rating Prestressed Concrete Bridges," Ph.D. Dissertation, The University of Texas at Austin, 2004.
21. Hanson, N. W. and Kaar, P. H., "Flexural Bond Tests of Pretensioned Prestressed Beams," ACI Journal, Vol. 30, No. 7, January 1959.
22. Icaza Aguirre, J. J., "Factors Affecting Friction Losses in Multi-Strand Post-Tensioning Tendons Including the Effect of Emulsifiable Oils," Master's Thesis, The University of Texas at Austin, 2004.

23. Janney, J. R., "Nature of Bond in Pre-Tensioned Prestressed Concrete," ACI Journal, Vol. 25 No. 9, May 1954.
24. Karr, P. H., Lafrugh, R. W., and Mass, M. A., "Influence of Concrete Strength on Strand Transfer Length," PCI Journal, Vol. 8, No. 5, October 1963.
25. Kittleman, W. M., Davis, R. T., Hamilton, H. R., Frank, K. H., and Breen, J. E., "Evaluation of Agents for Lubrication and Temporary Corrosion Protection of Post-Tension Tendons," Research Report 1264-1, Center for Transportation Research, Bureau of Engineering Research, The University of Texas at Austin, 1993.
26. Kittleman, W.M., "Evaluation of Emulsifiable Oils for Lubrication and Temporary Corrosion Protection of Seven-Wire Strand," Master's Thesis, The University of Texas at Austin, 1992.
27. Laldji, S. and Young, A. G., "Bond Between Steel Strand and Cement Grout in Ground Anchorages," Magazine of Concrete Research, Vol. 40, No. 143, June 1988.
28. Losinger, AG. (VSL International), "Zugversuche an Felsanker E 6-52," Berne, Switzerland, December 1977.
29. Nickas, W., "Florida DOT Efforts toward Improving Post-Tension Durability," Seminar given at The University of Texas at Austin, February 2005.
30. Osborne, W. R., "Bond Performance of Grouted Untensioned Multi-Strand Bundles During Pullout Tests," Master's Report, The University of Texas at Austin, 1986.
31. Perenchio, W. F., Fraczek, J., Pfeifer, D. W., "Corrosion Protection of Prestressing Systems in Concrete Bridges," Report 313, Transportation Research Board, National Research Council, 1989.
32. Pielstick, B. H., "Grouting of Segmental Post-Tensioned Structures in America," Proceedings of the 1<sup>st</sup> fib Congress: Concrete Structures in the 21<sup>st</sup> Century, Session 8, Osaka, Japan, 2002.

33. Poston, R. W., and West, J. S., "North American Strategies for Improving Bonded Post-Tensioned Concrete Construction," Durability of Post-Tensioning Tendons, fib-IABSE Technical Report, Bulletin 15, Workshop 15-16 November 2001, Ghent, Belgium, 2001.
34. Post-Tensioning Institute, "Post-Tensioning Manual," Fifth Edition, 1990.
35. Post-Tensioning Institute, "Specification for Grouting of Post-Tensioned Structures," 2000.
36. Radloff, B. J., "Bonding of External Tendons at Deviators," Master's Thesis, The University of Texas at Austin, 1990.
37. Russell, B. W., and Burns, N. H., "Measurement of Transfer Lengths on Pretensioned Concrete Elements," Journal of Structural Engineering, Vol. 123, No. 5, May 1997.
38. Salas, R. M., "Accelerated Corrosion Testing, Evaluation and Durability Design of Bonded Post-Tensioned Concrete Tendons," Ph.D. Dissertation, The University of Texas at Austin, 2003.
39. Salcedo Rueda, E., "Effects of Emulsifiable Oils Used as Temporary Corrosion Protection in Grouted Post-Tensioning Tendons," Master's Thesis, Pennsylvania State University, 2003.
40. Salcedo Rueda, E., Schokker, A. J., Kreger, M. E., and Breen, J. E., "Bond and Corrosion Studies of Emulsifiable Oils Used for Corrosion Protection in Post-Tensioned Tendons," PTI Journal, Vol. 2, No. 1, January 2004.
41. Salmons, J. and McCrate, T., "Bond Characteristics of Untensioned Prestressing Strand," PCI Journal Vol. 22, No. 1, Jan-Feb 1977.
42. Schokker, A. J., Koester, B. D., Breen, J. E., and Kreger, M. E., "Development of High Performance Grouts for Post-Tensioned Structures," Research Report 1405-2, Center for Transportation Research, Bureau of Engineering Research, The University of Texas at Austin, December 1999.
43. Schupack, M. and Johnston, D.W., "Bond Development Length Tests of a Grouted 54 Strand Post-Tensioning Tendon," ACI Journal, Vol. 71 No. 10, October 1974.

44. Tourneur, S., "Prestressing: 60 Years of Innovation," Compact Disc: The French Technology of Concrete, The 1<sup>st</sup> fib Congress 2002, Osaka, Japan.
45. Tran, T. T., "Reducing Friction Loss for Post-Tensioned Tendons in Monolithic Girders," Master's Thesis, The University of Texas at Austin, 1992.
46. Trost, H., Cordes, H., and Hagen, H., "Auswirkungen des Verbundverhaltens Zwischen Spannglied und Einpressmörtel Bei Verwendung Von Spanngliedern Mit Über 1500 Kn Zulässiger Spannkraft," Technischen Hochschule Aachen, July 1978.
47. Trost, H., Cordes, H., Thormahlen, U., and Hagen, H., "Verbundfestigkeit von Spanngliedern und ihre Bedeutung für Ribbilung und Ribbreitenbeschränkung," Deutscher Ausschuss für Stahlbeton, Heft 310, W. Ernst and Sohn, Berlin, West Germany, 1980.
48. Vos, E. and Reinhardt, H. W., "Bond Stress-Slip Behavior of Deformed Bars, Plain Bars, and Strands Under Impact Loading," Bond in Concrete, Ed. P. Bartos, Applied Science Publishers, London, 1982.
49. VSL International, "Considerations Concernant le Dimensionnement et L'arrangement de la Zone de Scellement du Tirant."
50. Woodward, R., "Durability of Post-Tensioned Tendons on Road Bridges in the UK," Durability of Post-Tensioned Tendons, fib-IABSE Technical Report, Bulletin 15, Workshop 15-16 November 2001, Ghent (Belgium), 2001.

## VITA

Tanya Lüthi was born in Upper Saddle River, New Jersey on 21 October 1977, to Ernst Lüthi and Rosalie (Scaturro) Lüthi. She graduated from Northfield Mount Hermon School in Northfield, Massachusetts in the spring of 1996. Entering Princeton University the following fall, she earned a Bachelor of Arts degree summa cum laude in politics in the spring of 2000. She entered the graduate school of The University of Texas at Austin in January of 2003.

Permanent Address: 32 Ware Road

Upper Saddle River, NJ 07458

This thesis was typed by the author.